BRNO UNIVERSITY OF TECHNOLOGY
VYSOKÉ UČENÍ TECHNICKÉ V BRNĚ

FACULTY OF MECHANICAL ENGINEERING
FAKULTA STROJNÍHO INŽENÝRSTVÍ

INSTITUTE OF MATERIALS SCIENCE AND ENGINEERING
ÚSTAV MATERIÁLOVÝCH VĚD A INŽENÝRSTVÍ

PROCESSING AND PROPERTIES OF 1D AND 2D BORON NITRIDE NANOMATERIALS REINFORCED GLASS COMPOSITES

PŘÍPRAVA A VLASTNOSTI KOMPOZITŮ SE SKELNOU MATRICÍ S DISPERZÍ (VÝZTUŽÍ) 1D A 2D NANOČÁSTIC NITRIDU BÓRU

DOCTORAL THESIS
DIZERTAČNÍ PRÁCE

AUTHOR — Ing. Richa Saggar
AUTOR PRÁCE

SUPERVISOR — prof. Ing. Ivo Dlouhý, CSc.
ŠKOLITEL

BRNO 2016

Abstract

Glasses and ceramics offer several unique characteristics over polymers or metals. However, they suffer from a shortcoming due to their brittle nature, falling short in terms of fracture toughness and mechanical strength. The aim of this work is to reinforce borosilicate glass matrix with reinforcements to increase the fracture toughness and strength of the glass. Boron nitride nanomaterials, i.e. nanotubes and nanosheets have been used as possible reinforcements for the borosilicate glass matrix. The tasks of the thesis are many fold which include:

1. Reinforcement of commercially derived and morphologically different (bamboo like and cylinder like) boron nitride nanotubes in borosilicate glass with the concentration of 0 wt%, 2.5 wt% and 5 wt% by ball milling process. Same process was repeated with reinforcing cleaned boron nitride nanotubes (after acid purification) into the borosilicate glass with similar concentrations.

2. Production of boron nitride nanosheets using liquid exfoliation technique to produce high quality and high aspect ratio nanosheets. These boron nitride nanosheets were reinforced in the borosilicate glass matrix with concentrations of 0 wt%, 2.5 wt% and 5 wt% by ball milling process.

The samples were consolidated using spark plasma sintering. These composites were studied in details in terms of material analysis like thermo-gravimetric analysis, detailed scanning electron microscopy and transmission electron microscopy for the quality of reinforcements etc.; microstructure analysis which include the detailed study of the composite powder samples, the densities of bulk composite samples etc; mechanical properties which include fracture toughness, flexural strength, micro-hardness, Young's modulus etc. and; tribological properties like scratch resistance and wear resistance.

Cleaning process of boron nitride nanotubes lead to reduction in the Fe content (present in boron nitride nanotubes during their production as a catalyst) by ~54%. This leads to an improvement of ~30% of fracture toughness measured by chevron notch technique for 5 wt% boron nitride nanotubes reinforced borosilicate glass. It also contributed to the improvement of scratch resistance by ~26% for the 5 wt% boron nitride nanotubes reinforced borosilicate glass matrix.

On the other hand, boron nitride nanosheets were successfully produced using liquid exfoliation technique with average length was ~0.5 μm and thickness of the nanosheets was between 4-30 layers. It accounted to an improvement of ~45% for both fracture toughness and flexural strength by reinforcing 5 wt% of boron nitride nanosheets. The wear rates reduced by ~3 times while the coefficient of friction was reduced by ~23% for 5 wt% boron nitride nanosheets reinforcements.

Resulting improvements in fracture toughness and flexural strength in the composite materials were observed due to high interfacial bonding between the boron nitride nanomaterials and borosilicate glass matrix resulting in efficient load transfer. Several toughening and strengthening mechanisms like crack bridging, crack deflection and significant pull-out were observed in the matrix.

It was also observed that the 2D reinforcement served as more promising candidate for reinforcements compared to 1D reinforcements. It was due to several geometrical advantages like high surface area, rougher surface morphology, and better hindrance in two dimensions rather than just one dimension in nanotubes.

All obtained results and mechanisms are discussed in details in the work below providing scope for future work in the end of the thesis.

Keywords: Boron nitride nanosheets; Boron nitride nanotubes; Borosilicate glass; Nanocomposite; Mechanical properties; Tribological properties.

Bibliographic citation

SAGGAR, R. *Processing and Properties of 1D and 2D Boron Nitride Nanomaterials Reinforced Glass Composites.* Brno: Vysoké učení technické v Brně, Fakulta strojního inženýrství, 2017. 124 s. Vedoucí dizertační práce prof. Ing. Ivo Dlouhý, CSc.

Acknowledgements

I would like to offer my sincere gratitude to my PhD supervisor prof. Ivo Dlouhý for his continuous guidance, support and motivation to carry out the work. His deep insight in the subject helped me to fulfil my tasks with precision.

I would also like to thank Dr. Zdeněk Chlup, Dr. Luca Bertolla, Martina Halasová and other members of Brittle Fracture Group who helped with stimulating ideas and discussions as well as for providing support during experimental work.

A special thanks to my father Mr. S.K. Saggar, mother Mrs. Gayatri Saggar and my entire family for helping me become what I am today and constantly boosting my morale to complete the tasks and letting me fulfil my dreams to attain a PhD degree.

I am grateful to Dr. Jiří Buršík and Dr. Pavla Roupcová, Institute of Physics of Materials, Czech Republic, for helping in TEM and XRD studies of BNNSs. I would also like to acknowledge Professor Dušan Galusek from Vitrium Laugaricio, Joint Glass Centre of Institute of Inorganic Chemistry, Slovakia, for help in measurement of density of the BNNSs. I want to show my gratitude to Dr. Harshit Porwal, Queen Mary University of London, UK for the help in conducting ultrasonication of suspensions and SPS for production of bulk composite samples as well as for characterizations like zeta-potential, TGA etc. Also I would like to acknowledge Dr. Jan Balko, Institute of Materials Research, Slovak Academy of Sciences, Košice, Slovak Republic for helping in tribological tests and Dr. Peter Tatarko for helpful discussions.

Additionally, I would like to thank European Union's Seventh Framework Programme managed by Research Executive Agency REA–Marie Curie action, GlaCERCo GA 264526 and Czech Science Foundation (project number: 14-11234S) for funding and support for this research work.

Declaration

I hereby confirm that I am the sole author of the written work here enclosed and that I have compiled it in my own words. The work was made under the supervision of prof. Ing. Ivo Dlouhý, CSc.

Brno..... .....

Ing. Richa Saggar

Institute of Materials Science and Engineering
Faculty of Mechanical Engineering
Brno University of Technology
and
Institute of Physics of Materials
Academy of Science of the Czech Republic
Brno

saggar@ipm.cz; saggar.richa@gmail.com

Table of Contents

Chapter 1 - Introduction

Composites play a significant role in vast areas of applications. Composites constitute of two or more components (matrix and reinforcements) having different set of characteristics. The individual characteristics of the components determine the properties of the processed composite. Composites bear, in general, superior properties compared to its individual constituting components. Various naturally occurring composites have been known to exist, e.g. wood is a naturally occurring composite with the constituents being, cellulose fibres as reinforcement contributing to the tensile strength to the composite and lignin as a matrix responsible for higher stiffness. Bone structure is another example formed by collagen fibres embedded in apatite mineral matrix[1]. The naturally occurring composites acted as a motivation for engineered composites in which researchers had the possibility of tailoring the properties of the composites according to required applications.

Broadly composites can be classified into three categories: ceramic matrix composites (CMC), metal matrix composites (MMC) and polymer matrix composites (PMC) on the basis of type of matrix used in the composites. The properties of the different matrix composites are mentioned in Fig. 1.1. The study of naturally occurring composites by researchers lead to onset of fabrication of polymer matrix composites in late 1940s which further stimulated the growth of more complicated metal and ceramics matrices based composites. Though the physical properties of polymers matrix, metal matrix and ceramic matrix composites are similar in terms of strength and toughening, however, there is a vast difference in terms of chemical interactions between in the matrix and the reinforcements, e.g. the interactions at the interfaces or in general the fabrication process of these composites. The fabrication and interactions in CMCs and MMCs are far more complex compared to PMCs.

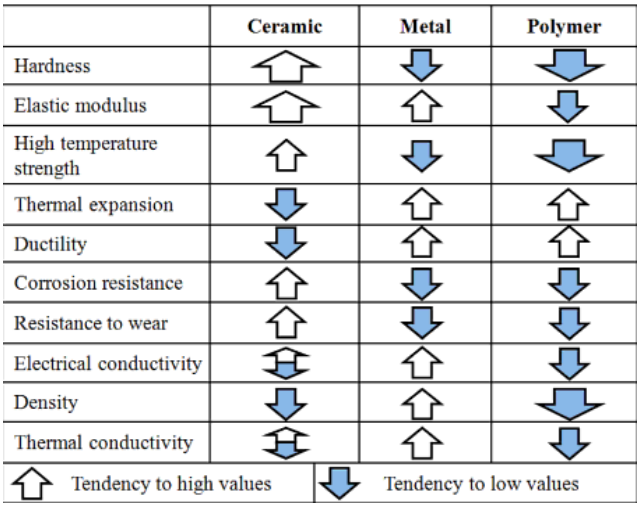

Fig. 1.1: Comparison of the properties of Ceramics, Metals and Polymers[2]

Some preliminary advantages of composites over individual constituents were higher stiffness, higher strength, lower weight etc. which was not achievable by individual constituents by themselves[3]. The manipulation of the microstructure during the processing stages of the composite irrespective of the type of matrix used can efficiently alter the properties of the composites for achieving desirable set of characteristics for specific applications. The properties of the reinforcements, their relative concentrations in the matrix and their geometries act as the key factors influencing the properties of the composites.

As far as CMCs are concerned, various forms of CMCs are known to exist, e.g. fibres reinforced, whiskers reinforced, platelets reinforced, particulates reinforced and layered CMCs. CMCs are advantageous over monolithic materials because in spite of using brittle reinforcements like fibres, they are tougher due to several supportive phenomena occurring because of the reinforcements which help in crack arresting or deflection. This increases their toughness by delaying the failure of material. Recent advancements have been made in the field of nanostructured CMCs. Nanostructured CMCs refer to reinforcement of ceramic matrix incorporated with nanosized fillers (at least one dimension is in the range of 0-100 nm). These reinforcements have been observed to influence the properties of the composite to a much greater extent compared to micro sized reinforcements[4-6]. Nanostructured CMCs can be broadly classified into zero dimensional (0D), one dimensional (1D) and two dimensional (2D)

nanocomposites. This recent advancements in the field of CMCs have improved the mechanical properties of the composites to many folds[6-8].

Present work focuses on the applications of 1D and 2D boron nitride nanosized reinforcements in the borosilicate glass matrix to study their effect on the mechanical properties of the glass based nanocomposite in comparison to monolithic glass. The thesis is organized into eight chapters. Chapter 2 provides detailed literature review about production, processing and properties of glass ceramics composites and ceramic matrix composites. Chapter 3 mentions about the aims of the thesis which have been worked upon. Chapter 4 deals with processing of the boron nitride nanotubes (BNNT) as well as the effect of reinforcing different concentrations and different morphologies of BNNT on the borosilicate glass (BS). Chapter 5 focuses on the preparation and characterization of Boron nitride nanosheets (BNNS) as well as processing and study of mechanical properties of BNNS reinforced BS composites. In chapter 6, detailed discussion about the comparison of effect of 1D and 2D reinforcements in glass matrices is presented. Chapter 7 provides the summary and conclusion for the work. Chapter 8 suggests the prospects future work that can be done in this field.

Chapter 2 – Literature Review and Theoretical Background

2.1. Glass and Glass Ceramic Matrix Composites

Glasses and Glass Ceramics are presently being used for diverse applications due to their properties like high stiffness, strength and stability at high temperatures. There applications range from being used as transparent glass panels for architectural, automobile and aerospace applications to their use in glass optic fibres for telecommunication. They are also used in chemical industries for containers which are corrosion resistant and have some other applications in electrical/electronic industries. Glasses offer several lucrative features which promote their use in the form of matrices for composites[9] :

1. They possess moderate range of Young's modulus and the fillers can thus provide significant increase in the Young's modulus. The reinforcement with higher difference between the Young's modulus with the matrix, if judiciously selected, can lead to effective load transfer which is not applicable in the case of polycrystalline matrices.

2. Softening of glass at high temperatures leading to viscous flow providing ease for introducing the reinforcements without any damage to the matrix is one of the key advantages to glass matrix composites which are not applicable in polycrystalline ceramics. It is due to this characteristic that high density glass composites can be achieved during sintering as the viscous flow helps in removal of residual porosity at high temperatures/pressures.

3. It is easier to engineer the chemical composition of glasses. Even small amount of change can lead to drastic change in properties like coefficient of thermal expansion which can in turn effect the interaction of the matrix with the

reinforcement. It is possible to introduce certain compositions which may lead to formation of glass ceramic matrices, i.e. the glassy phase is densified further to produce small crystalline phases which can enhance the thermal stability of the composites.

4. Use of these matrices can provide chemical stability to the fillers. Additionally, these matrices are cost-effective, i.e. the raw materials for producing a glass or the processes for glass melting are easily available and well established.

5. Glass matrices are free of grain, sub-grain boundaries and similar defects in their microstructure. Due to this feature, the glass matrices act as a good model material for investigation of real reinforcement effects of fillers.

However glass matrices suffer from the main drawback of being highly brittle and with extremely low fracture toughness and they usually have catastrophic failure. The reason for the brittle nature of the matrix is due to presence of defects which act as stress concentrators which affect the matrix properties due to lack of stress relieving mechanisms. Efforts have been made by the researchers to use reinforcements that can effectively increase the toughness of these glass and glass ceramic matrix composites[10]. The reinforcements used for glass matrix are long and/or short fibres[11], particulates and platelets, whiskers reinforcement[12], laminates or layered reinforcements[13], nanomaterials[14] etc.

2.1.1. Fibre Reinforced Glass and Glass Ceramic Composites

Fibres were used as reinforcements initially in silicate glass in the beginning of 1970s[15,16]. Fibres can enhance the properties of the matrix if the constituting materials, their relative concentrations, orientation of the fibres as well as the fabrication methods are judiciously selected[17,18]. Damage of fibres by processing methods as well as the bonding of fibres to the matrix also affects the properties of the composites. The interest in fibre reinforced glass/glass-ceramics was developed because these composites illustrate properties like high strength, toughness, reliability and corrosion resistance and are favourable for high temperature applications[19]. Basically fibre reinforcements help in strengthening of the matrix if the modulus of the fibre is much higher than

matrix and if the matrix is able to transfer its tensile stresses to the fibres. Coefficient of thermal expansion must be also carefully controlled to avoid formation of high residual stresses in the matrix.

Fibres can be classified into continuous fibres (oxide and non-oxide fibres) as well as discontinuous fibres (whiskers or short fibres). Fig. 2.1 depicts the different forms of fibre reinforced composites. The impact of the strength of continuous fibres on the strength of a glass matrix having no internal stresses can be estimated by rule of mixture, while assuming that the strain affects the individual components equally. Depending on which components fails first, the strength of the composite can be given by equation 2.1[10]:

$$\sigma_c = \sigma_{f_u} V_f + \sigma_m V_m$$

or,

$$\sigma_c = \sigma_{m_u} V_m + \sigma_f V_f \,. \qquad (2.1)$$

Where, σ_c is the strength of continuous fibre reinforced composite, σ_{f_u} is ultimate failure strength of fibre, V_f is the volume fraction of the fibre, σ_m is the matrix stress at fibre failure strain and V_m is the volume fraction of the matrix; σ_{m_u} is ultimate failure strength of fibre.

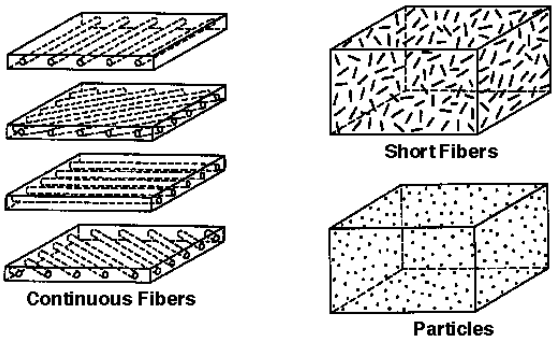

Fig. 2.1: Types of fibre reinforced composites

However, for discontinuous fibres, the orientation of the fibres is very important. The fibres oriented parallel to the tensile axis would lead to higher strength of the matrix compared to randomly oriented discontinuous fibres reinforced into the matrix.

The bonding between the fibres and matrix plays a pivotal role in determining the mechanical properties of the composite[20]. Weaker bonding facilitates effective relaxation mechanisms of the matrix. The crack interaction with the weakly bonded fibres present the matrix leads to pull-out of these fibres which acts as one of the key toughening mechanism also enabling relaxation of the matrix. Crack deflection is also commonly identified phenomena observed for fibre reinforced glass matrix composites (GMCs). Additionally, coefficient of thermal expansion for matrix and fibres play a crucial role in determining the stress-strain distribution post fabrication in the composite.

In earlier works, the use of fibres lead to increase in toughness on the expense of strength as the long fibres acted as stress concentrators which lead to weakening of otherwise strong matrix. However in the later phases, use of unidirectional carbon fibre reinforced glass lead to exceptionally high strength, toughness and fatigue resistance. Sambell et al. showed an increase in the strength of Pyrex glass from 100 MNm^{-2} to 680 MNm^{-2} by introducing 40 vol% of carbon fibres[16]. Use of carbon fibres limited the scope of applications to low temperatures due to being susceptible to oxidation at higher temperature. However, use of alumina fibres overcame the drawback of oxidation at higher temperatures but the increase in strength and toughness of these composites was comparatively much lower than carbon fibres. The SiC fibres (Nicalon) have gained attention due to their unique combination of properties where they are able to withstand high temperatures while rendering high increase in the strength and toughness of the matrices[21]. Under optimized fabrication condition Nicalon fibre / borosilicate glass matrix composite attained unique set of properties including fracture toughness on the level of 27 $MPam^{1/2}$ [22]. Oxide fibres have also gained limelight as they are even more stable against oxidation than Nicalon fibres. Amongst them Nextel fibres are one of the highly investigated ones[19].

Whiskers are special class of short crystalline fibres having high aspect ratio (10-100) with dimensions ranging up to 100 mm in length and 0.1-10 μm in thickness. As reinforcements, they are very strong but they easily undergo mechanical damage and due to this reason are limited to ≤ 1500 MPa. They may also be considered in some

cases as particles with high aspect ratio[23]. SiC whiskers have been most studied in terms of application for various glass and glass ceramic matrices[22,24].

2.1.2. Particulate Reinforced Glass and Glass Ceramic Composites

Traditionally, particulates have been used as fillers in ceramics to increase to an extent, the high temperature strength of the ancient ceramics so as to retain the shape during firing, as they were one of the easily available and cheap fillers. Post 1960s, studies to refine the coarse microstructures begun which ultimately lead to pore free, small grained, high strength (several hundred MPa) ceramics. These reinforcements do not provide considerable increase in fracture toughness or strength to glass ceramic composites but are used widely because of being cheaper and the processing required for particulate based composites is easier than for other shaped fillers.

Additionally, they impart isotropic properties to the matrix and are less toxic in nature. In literature, most of the work has been focused on the use of particulate systems for increasing the mechanical properties of the composites[25], however, they have also been used to improve other functional properties like thermal diffusivity, thermal conductivities[26], thermal shock and resistance to erosion[27] for the composites. Various forms of particles have been used as fillers, e.g. calcium carbonate, feldspar, clay, silica, graphite etc. Recently, diamond particles have been used in borosilicate glass to exploit their properties for application in high temperature devices, cutting tools etc[28]. Alumina platelets in borosilicate glass matrix affect the fracture surface roughness and thanks to this shielding/toughening mechanism corresponding toughness enhancement has been observed[29].

2.1.3. Layered/Laminate Glass Ceramic Composites

Composites with sandwich like structure have been observed to display augmented properties compared to monolithic materials (Fig. 2.2)[13,30]. Layered composites consist of multilayers of monolithic materials having different functional properties resulting in formation of composite materials with desired enhanced properties. Layered composites essentially have augmented affect in their mechanical properties. Use of layers with different properties like composition or thermal

coefficient of expansion lead to strengthening of the composites[31]. GMCs and CMCs with heterogeneous microstructures though have high toughness and resistance to damage but the use of heterogeneous phases lead to reduction in strength and wear resistance of these composites. The use of layered ceramics or laminates can be advantageous in such cases as they do not only provide higher wear resistance and strength due to outermost interacting homogenous layer but intrinsically they improve the toughness due to underlying heterogeneous layered structure. Laminated glass ceramic composites were initially used in polymer/glass security panels and for glazing applications[32]. Seal et al. have investigated soda lime glass layers with polymers showing raise in the loads applied for failure of the composite as well as large failure displacement of material[33]. Metal and Bioglass® multilayer composites have been used in biological applications showing very high magnitude of strength and fracture toughness over pure Bioglass® material[34,35]. Recently glass ceramic multilayered composites have found their applications in microelectronics industry[36] as they offer highly preferable characteristics including thermal, electrical as well as mechanical properties[37]. Layered or laminated glass ceramic composites have found many applications armour materials[38]. Oxide glasses find its applications in automobiles, aircraft wind-shields and bullet proof glass. In bullet proof glasses, the oxide glass is sandwiched between layers of thermoplastic material, performing different roles for the protection purposes[39].

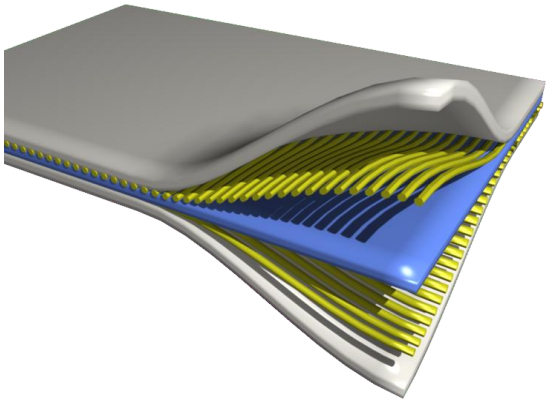

Fig. 2.2: Laminated glass ceramic composite

2.1.4. Nanocomposites

In the past decades, researchers have started considering nanomaterials as possible reinforcements for the composite matrices. Due to the high aspect ratio of nanomaterials, nanocomposites offer better properties then conventional bulk sized filler reinforced composites. The high surface to volume ratio of interacting surfaces between nanosized reinforcements and the matrix lead to observation of significant improvement in functional properties of the composites even by using very low amount of reinforcements. Conventional composites suffered through a drawback of using high loading concentration of fillers in order to achieve similar properties as achieved by smaller concentrations of nanofillers. This makes the processing and the final composite product becomes very costly for the industrial application. Use of nano reinforcements can aid the interaction between the matrix and reinforcement to be high, leading to higher enhancement in the properties of the composite compared to similar loading for fibre fillers[40].

The nanosized reinforcements can be classified into zero dimensional (0D; nanoparticles), one dimensional (1D; nanotubes, nanorods etc.) and two dimensional (2D; nanosheets, thin films etc.) as shown in Fig. 2.3.

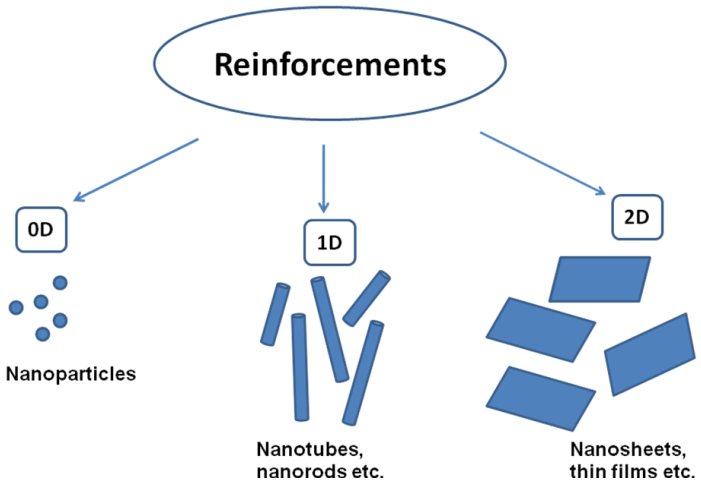

Fig. 2.3: Types of reinforcements used in nanocomposites

2.1.4.1. 0D nanocomposites

0D nanocomposites are defined as composites in which the reinforcements used are confined in all the three dimensions in nano range, i.e. all the dimensions are ≤ 100 nm. They mainly constitute of nanoparticles mainly produced by sol-gel technique[41,42]. The initiation of this concept was done by Niihara et al. in 1991 in order to improve the mechanical properties of structural ceramic composites by using SiC nanoparticles for Al_2O_3, MgO and Si_3N_4[4]. The processing routes involved in the preparation of 0D nanocomposites are powder processing[43], sol-gel processing[44,45], polymer precursor route (in-situ preparation of nanoparticles by incorporating the precursors in polymer matrix)[46] and gas phase pyrolysis[47]. Some of these methods would be discussed in details in the later sections of the thesis. These composites have found their applications in various fields.

Mota et al. reported bioactive glass nanoparticle reinforced in chitosan forming membranes for dental applications as they enhance the stiffness of chitosan and improve their wettability[48]. Enhancement in the mechanical, physical and thermal properties have been reported due to the reduction of nanoparticle size in polymer nano-composites[49]. They also have been used as effective reinforcement in polycrystalline alumina matrix[4].

However, the main drawback for these reinforcements is their agglomeration at high concentrations due to high surface energy of the nanoparticles and they have comparatively lesser surface area for interaction with the matrix compared to other nanofillers like 1D and 2D nanomaterials[50]. To realize their complete potential, measures have to be taken effectively for their uniform dispersion in the matrix and therefore processing is the essential challenge to be considered while preparation of 0D nanocomposites. In literature, though they have mainly been used as a reinforcement to improve the mechanical properties glasses and ceramics but as a mechanical reinforcement they do not provide complete justice to crack defence mechanism due to the geometric limitations of the particles.

2.1.4.2. 1D nanocomposites

1D nanocomposites are defined as composites in which the reinforcements used are having any one dimension confined in nano regime (≤ 100 nm). A considerable amount of research has been done on 1D reinforcement based nanocomposites. Amongst them, Carbon Nanotubes (CNT) has been one of the leading candidates as they offer several multifunctional properties to the glass composites including high aspect ratio, high Young's modulus (1300 GPa), high tensile strength (20-63 GPa), higher electrical conductivity (10^7 S/m) and high thermal conductivity (1800-6000 W/mK). Due to these properties, researchers have been actively using them as a reinforcement in enhancing the electrical and thermal properties of polymeric nanocomposites[51,52] and glass ceramics[53].

In context to mechanical properties, CNT have shown some potential in the toughening of glass and ceramic matrices[6,53,54,55,56]. 1D nanofillers like nanotubes possess, in general, geometrical advantage over nanoparticles as they are able to hinder the crack propagation in a direction perpendicular to the length of the nanotubes. Amongst the most common toughening mechanisms of the multiwalled CNTs are crack bridging as well as pull-out or telescoping out of individual nanotubes of multiwalled nanotubes which help the matrix to relax against induced stresses. The reinforcement of barium aluminosilicate glass by 10 vol% CNT produced 143% increase in fracture toughness in the composite[55]. However, CNT face a major challenge of agglomeration and entanglement, making it difficult to realize their actual potential which they possess once de-agglomerated in the matrices[57]. Additionally, processing of CNT based composites is a large complication for fabrication of such composites as CNTs suffer from degradation at high sintering temperatures or longer durations[58].

2.1.4.2.1. Boron Nitride Nanotubes

Recently, researchers have started to consider using boron nitride nanotubes (BNNTs)[59] as a new possible competent candidate for 1D reinforcement, as they possess similar properties to CNTs. They were initially produced by Chopra et al. by arc-discharge process in 1995 [59]. BNNTs structure is analogous to hexagonal comb structure present in CNTs in which adjacent carbon atom are replaced by B and

N atoms[60,61] (Fig. 2.4(a))[62]. In simpler terms, BNNTs are formed by rolling the single layer of boron nitride sheet similar to rolling of graphene sheet to form CNTs. BNNTs can be single walled or multi walled but occurrence of single walled BNNTs is rather typical. Unlike, covalent C-C bond of CNT, B-N bonds are partially ionic in nature. Various researchers have reported that the distance between the layers in hexagonal multi walled BNNTs ≥ 0.333 nm. The BNNTs support three chiralities according to the direction of rolling of boron nitride atomic layers: zig zag, arm chair and helical (Fig. 2.4(b)). Most of the single walled BNNTs occur in zig zag chirality as most common configuration. They are crystalline in nature due to exactly same ordered layout of the multiwalled nanotubes while CNTs can have rotational disordering which provides them different helicities[63].

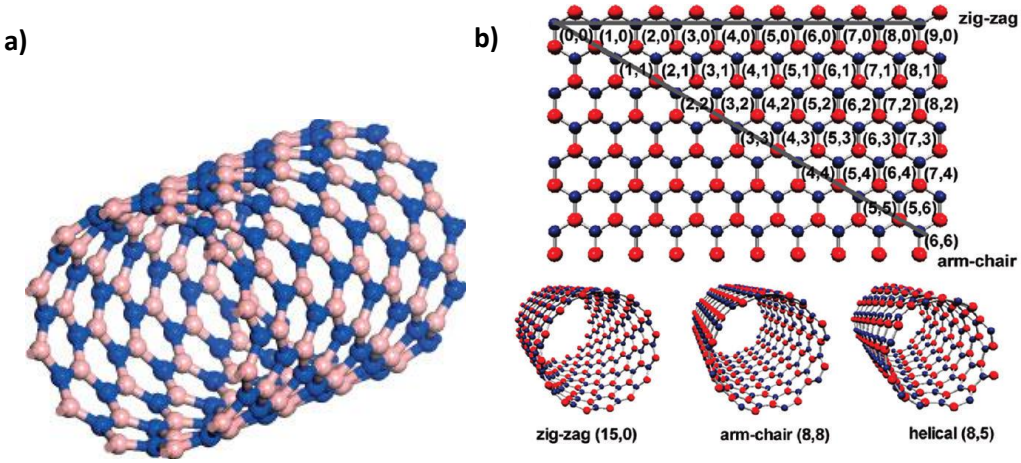

Fig. 2.4: a) Model of BNNT structure with adjacent boron and nitrogen atoms[62] ; b) Chiralities of single walled BNNTs indicating their (n,m) indices for rolling direction[63]

BNNTs are electrically insulating with a high band gap of 5.5 eV, independent of their chirality or morphology[64]. BNNTs exhibit comparable stiffness[62], elastic modulus[65,66], yield strength[67] and thermal conductivity[68,69] to CNTs due to their prevailing structure being similar to them. They also show a very high tensile strength of ~30 GPa like in CNTs[70]. However, individual BNNTs have been reported to withstand comparatively higher external tensile load than CNTs[71] and they are also considered better shock absorbing surfaces than CNTs[72]. They are additionally advantageous over CNTs as they can withstand higher temperatures without oxidising up to 950 °C and hence are considered chemically inert[62]. Owing to these features, BNNTs might actually

have more benefits over CNTs. Due to these properties, they have been investigated in different matrices like metals[73], polymers[74,75], biomaterials[76], glasses[8,77,78] and ceramics[79,80,81] to enhance the mechanical and thermal properties of the matrices. Bansal et al. reported an increase of 90% of strength and 35% of fracture toughness with reinforcing 4 wt% of BNNT in barium calcium aluminosilicate glass[8]. They reported the primary reason for improvement of mechanical properties was due to large amount of pull-out of BNNTs observed in the matrix as shown in Fig. 2.5.

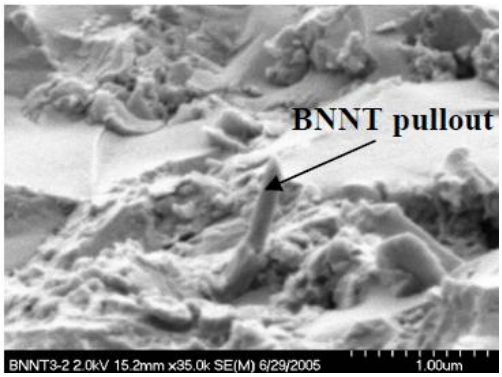

Fig. 2.5: Pull-out of BNNTs from barium calcium aluminosilicate glass observed by Bansal et al.[8]

The key factors governing the properties of 1D nanocomposites are:

1. Uniform (randomly oriented) dispersion of 1D reinforcement through the matrix for complete utilization of the properties.

2. In terms of mechanical properties, appropriate bonding between reinforcement and the filler for a complete load transfer from the matrix to filler.

Various processing methods have been employed for the preparation of 1D nanocomposites to achieve these goals like in-situ growth of nanotubes in matrix, powder processing including spark plasma sintering, colloidal processing, sol-gel processing, electrophoretic deposition etc. (mentioned in the later sections).

2.1.4.3. 2D nanocomposites

2D nanocomposites are defined as composites in which the reinforcements used are having any two dimensions confined in nano regime (≤ 100 nm). In terms of mechanical properties, geometrically, they are at benefit as they offer toughening mechanisms along two dimensions at reinforcement matrix interface. Layered silicates/clay minerals have been one of the oldest examples of 2D reinforcements. The layered silicate structure are present in the form of layered sheets separated by weak Van der Waals bonds forming a gap (or galleries) in between the layers where the cations are present which counterbalance the excess charge created due to isomorphous substitution of Si^{4+} by Al^{3+} from the tetrahedral sheets and Al^{3+} by Mg^{2+} from the octahedral sheets[82]. These layered silicate once used as reinforcement can increase tensile strength of polymers[40,83] and glass composites[84]. In polymers it also increase other multifunctional properties like Young's modulus[83], ion conductivity[85] etc.

A deeper insight of 2D nanomaterials to be used as reinforcements developed with the discovery of graphene by Novoselov et al.[86] Graphene exhibited similar electrical, thermal and mechanical properties as its 1D analogue (CNTs)[87,88]. 2D structure of graphene sheets provides them an edge over CNTs due to higher surface area[89] and less probability of entanglement (or agglomeration)[90] leading to better dispersion and hence comparatively better properties compared to CNTs. Graphene reinforced polymer composites show improved mechanical properties and thermal conductivity at very low concentrations[91,92]. Graphene majorly contributed to the enhancement of electrical conductivity of the composite matrix[89]. Graphene is also an effective reinforcement for enhancing the mechanical properties in several glass and ceramic matrices[93,94]. Porwal et al.[14] reported ~35% increase in the fracture toughness for graphene reinforced SiO_2 glass by using 2.5 vol% of concentration for graphene[14]. They have also been reported to improve the tribological properties of the Si_3N_4 composite by 60% with the reinforcement of 3 wt% of graphene oxide nanoplatelets.

2.1.4.3.1. Boron Nitride Nanosheets

Boron nitride nanosheets (BNNSs) are another potential candidates which are studied upon recently. They possess similar functional properties to BNNTs, while differing in geometrical properties, similar to those of graphene sheets having over

CNTs[14]. They are structural analogues of graphene with presence of alternation B and N atoms in place of C atoms in graphene. They can bear single layer or stack up to form multilayer systems. Though boron nitride thin films have been in existence for a while, achieving high quality single sheet of boron nitride still remains a typical task. Owing to the two-dimensional geometry, BNNSs provide higher specific surface area[96,97] and also lower tendency to entangle, and hence, lesser complicated methods are required for processing and dispersion of BNNSs. As reinforcement, the effect of toughening in BNNSs is observed along two dimensions compared to only one for BNNTs.

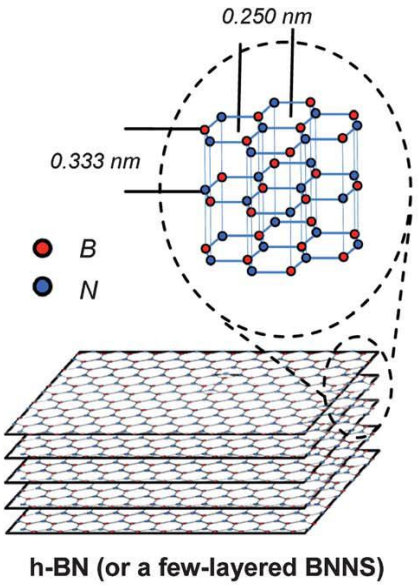

Fig. 2.6: Structure of 2D BNNS [95]

The methods to synthesise BNNSs are far more convenient and cost effective and give a better yield compared to BNNTs[63]. Boron nitride nanosheets are formed by forming a honeycomb network of borazine ($B_3N_3H_6$). These B-N bonds are covalent but have slight ionic nature with a bond length of 1.45 nm and the distance between centre of adjacent rings being 2.50 nm (Fig. 2.6)[95]. They also support the zig zag, arm chair and helical chirality.

The layers of BNNSs have weak Van der Waals forces in between them forming the interlayer distance being 0.333 nm. BNNSs have been used in several polymer matrices[98,99] as mechanical reinforcement showing good improvement in the elastic

modulus and tensile strength at small concentrations. Li et al. investigated that the bending modulus of the BNNSs is dependent on the thickness of the BNNSs due to the stacking faults layer by layer[100]. Lee et al.[101] reported the enhancement of toughness of Si_3N_4 composite by 24.7% by using 2 vol% concentration of boron nitride nanoplatelets. They also reported the increase in strength by 9.4% and tribological properties by 26.7% by using the same concentration. To the best of our knowledge, BNNSs have not been used in glass matrices and would be reported as a mechanical reinforcement for glasses in this work.

2.2. Processing of Glass Ceramic Composites

One of the greatest challenges for achieving target properties in composites is the good dispersion of the reinforcements. Considerable amount of work has been done and various methods have been devised for processing of glass ceramic matrix composites. Particularly for the processing of nanocomposites, high quality nanofillers dispersion very much affects the final properties of the nanocomposites as the nanofillers have the tendency to agglomerate due to high surface energy which deteriorates the properties of the bulk composite material. 2D nanofillers have better dispersions due to high surface area and they have geometrical aspects which supports lesser agglomeration than 1D nanofillers. Details of the processing methods have been described in the sections below.

2.2.1. Powder Processing

The most conventional method used for processing the glass ceramic methods is powder processing. It has been used for number of reinforcements like CNTs[102], BNNTs[8], graphene[7], boron nitride nanoplatelets or BNNS[101] for difference matrices like barium calcium aluminosilicate glass[8], alumina[5], zirconia[79], Si_3N_4[101], silica[14] etc. producing mixed results depending on the reinforcement of these nanofillers and the matrix. The basic methodology for the powder processing involves various steps[103,104]:

1) Natural or synthetic materials with desirable properties for the composites are selected.

2) These raw materials are processed through beneficiation process during which they are milled, washed and filtered to prepare them for densification purposes through sintering. The raw materials (fillers or matrix powder) can also be functionalized pre-milling which can enhance the interface interaction ultimately leading to increased strength of the composite.

3) The powder is then consolidated to form a bulk sintered sample.

The methodology may also include pre-processing of the precursors with the help of ultrasonication or mechanical mixing for achieving better dispersion of the fillers post sintering in the matrix. This processing methods has most commonly been used in preparation of 1D CNT nanocomposites with ceramics[105,106] and glasses[107]. Guo et al.[107] reported the preparation of 5 and 10 vol% CNTs in silica glass by powder processing leading to formation of dense samples increasing the electrical conductivity of silica glass by 14 orders of magnitude. Similarly preparation of BNNTs based nanocomposites have also been reported with barium calcium aluminosilicate glass by Bansal et al.[8] with milling of 4 wt% of BNNT in the glass matrix showing a uniform dispersion and the increase in the toughness of the glass by 35% compared to pure aluminosilicate glass. BNNTs have also been used in 3Y-TZP zirconia[79] by ball milling method. Graphene based nanocomposites produced by powder processing have been reported with silica[14], alumina[89] and silicon nitride[108]. Porwal et al.[14] reported uniform dispersion of graphene and graphene oxide nanoplatelets by their dispersion in Dimethylformamide (DMF) by sonication and then mixing them with silica glass achieving high dispersion and achieving high relative density of >99%. The dispersion of graphene oxide nanoplatelets dispersed in silica has been shown in Fig. 2.7.

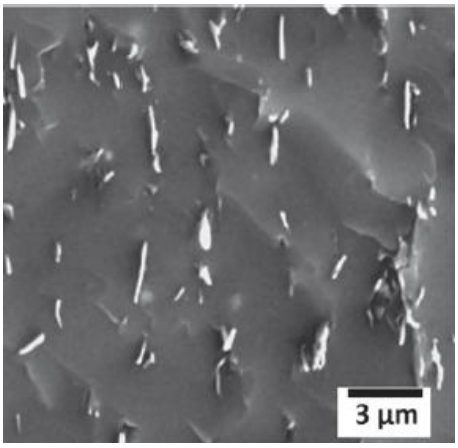

Fig. 2.7: Dispersion of 2.5 vol% of graphene in silica matrix by powder processing[14]

This processing method is relatively simpler and consumes less energy. The conditions applied during milling as well as the milling media and solvent used for dispersion play a crucial role to prevent the damage to the reinforcements as well as ensuring the uniform dispersion of reinforcement in the matrix. Due to these advantages, it is one of the most frequently used methods for processing of composites.

2.2.2. Colloidal Processing

Colloidal processing based composites involve a multiphase system in which either one or all the phases are in the form of continuous dispersions having variety of particle size ranging from nano- to micro-size, dispersions with small particles and large molecules. The interface between the dispersed phase and the dispersion medium is very important in determining the surface properties including surface charge, adsorption etc. Using colloidal processing, the key features which affect the properties of final composite are:

1) Particle size
2) Particle shape
3) Surface properties
4) Particle-particle interaction
5) Particle-dispersing medium interaction

Broadly, the colloidal dispersions were classified into: solid, liquid and gaseous, depending on phase of dispersed and dispersion medium. Generally, for glass and ceramics, mostly commonly, powders are suspended in liquid medium for colloidal processing. Colloidal dispersions may be lyophilic or lyophobic depending on the wettability or mixing capabilities of dispersed phase with dispersion medium, i.e. lyophilic colloidal suspensions are formed when the dispersed phase has affinity towards the dispersion medium and lyophobic if the dispersed phase repels the dispersion medium. During colloidal processing the particles have a tendency to aggregate due to Van der Waals forces therefore methods are applied to stabilize the suspension by creating repulsion between the particles. This can be achieved by electrostatic mechanism, i.e. by providing interaction between charged particles or polymeric mechanism by coating the particles with the polymer present in the dispersion to avoid aggregation. The opposite charge can be rendered on the dispersed phase by dispersing them in a polar dispersion medium. This process is called heterocoagulation.

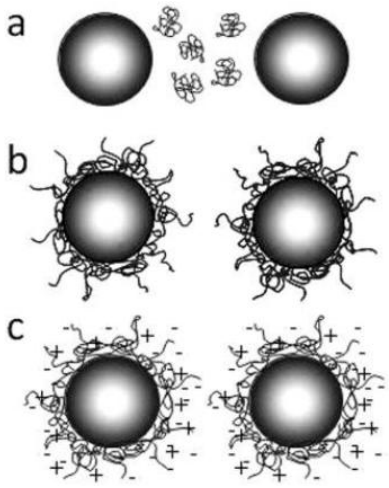

Fig. 2.8: Colloidal stabilization by polymers; a) depletion stabilization, b) steric stabilization, and c) electrostatic stabilization[109]

Polymers used for colloidal processing provide stability to the dispersion without being coagulated, by depletion stabilization (presence of polymer in dispersion), steric stabilization (presence of polymer attached to the surface of particle) and electrostatic stabilization (presence of polymer attached to the surface of particle so

providing like charge the particle surface leading to repulsion). The polymeric stabilizing mechanisms are explained in Fig. 2.8. However, the use of polymers in the composite formation may affect the properties of the consolidated sample on a macro scale and moreover it is not easy to completely remove this polymer on the later stages.

Colloidal processing methods have been used for ceramics[110] and polymers[111]. Perfect CNTs being inert in nature are not dispersed easily in the dispersing medium therefore treatment of CNTs with strong acids can lead to functionalization of CNT surfaces with hydroxyl or carboxylic acid groups. These treatments ensure the uniform dispersion of CNTs in lyophilic colloidal suspensions[112]. Wang et al. have also successfully produced graphene based ceramic nanocomposites where they prepared individual suspensions of graphene oxide and alumina with water and graphene oxide suspension was dropwise added to alumina suspension while magnetically stirring the alumina suspension ensuring the uniform dispersion of graphene in the resulting composite increasing the fracture toughness by 53% and increasing the electrical conductivity by 13 order of magnitude compared to pure alumina[113].

2.2.3. Sol-Gel Processing

The sol-gel processing is highly homogenous and maintains high purity of the composite. It is flexible process in terms of shaping the final composites as the precursors are liquids. In general, it comprises of four stages: sol formation, gelation, drying and densification[114]. The metal alkoxide precursors e.g. Tetraethylorthosilicate (TEOS) or Tetramethylorthosilicate (TMOS) hydrolyze and condense forming a colloidal sol used as a precursor for the preparation of silica glass. In the process, metal alkoxide is mixed with water in the presence of a catalyst (acidic or basic). Since the alkoxide and water are not miscible together, agents like ethanol are added to aid the mixing process.

As the liquid sol is condensed further, the solid phase starts to develop a network, converting it to gel form. The time taken by the gelation process depends on the chemistry of the solution. At this stage, the viscosity increases sharply and the gel further solidifies. During this phase, interstitial fluid and by-products of the hydrolysis enter into the pores of the gel. Hence it is called ‘wet’ gel at this phase where the cross

linking keeps increasing within the gel network. Sol-gel transformation after gelation becomes an irreversible process.

With the continual evaporation of liquid, the gel transforms to xerogel as it dries causing drastic volume shrinkage. It is quite critical stage as the capillary action of the drying process for the liquid can create stresses in the xerogel leading to cracking. Xerogel can be further densified using various sintering techniques. Sol-gel process can be combined with other processing methods like slurry and powder processing. Ye et al. reported the preparation of barium aluminosilicate (BAS) glass ceramic reinforced with 5-15 vol% of multiwalled CNTs (MWCNTs)[55]. They synthesized BAS glass ceramic by hydrolysis of alkoxides and they separately ultrasonicated the MWCNTs in ethanol. Finally, they prepared the mixture by ball milling them by ZrO_2 balls for 12 hours. This process helped in improvement of the mechanical properties to a great extent.

This process is most common for preparation of silica based composites for various application[115,116]. This processing method has also been used to prepare uniformly dispersed nanocomposites for CNTs[116,117] and graphene[92,118]. Watcharotone et al.[92] reported preparation of graphene-silica films to be used as transparent conductors. In their work, modified hummer's method was used for the exfoliation of graphene oxide sheets in a mixture of water and ethanol to which TMOS was added subsequently. This procedure leads to formation of highly stable suspension which was used to cast thin films on borosilicate glass or silicon. Evaporation of solvent lead to drying of the film and treatment with reducing environment of hydrazine monohydrate reduced graphene oxide to graphene.

2.2.4. Polymer Derived Ceramics

Polymer derived ceramics (PDC) processing technique enables the development of ceramic fibres, coating or layers which are stable at high temperatures with respect to decomposition, crystallization and phase separation. Preparation of PDCs does not require additives for thermal handling of precursors. They also exhibit advantage that they can be processed to obtain complex 3-D shapes. Moreover, these ceramics are high purity and supporting homogeneity. Polymer route uniquely provides the chance to process ternary and multinary ceramics.

The processing includes two major steps: 1) Evaporation: which includes preparation of pre-ceramic polymers from suitable monomers and cross linking of pre-ceramic polymer to form organic/inorganic network; 2) Pyrolysis process (conversion to ceramics) by use of moderate temperature (1000-1300 °C). Silicon based polymers (like polysilanes or polycarbosilanes etc.) are used to prepare complex shaped ceramics and powder. The pre-ceramic polymer used for thermal decomposition process should have sufficiently high molecular weight, rheological properties, solubility for providing shapes and latent reactivity required for curing and cross-linking. The cross-linking is a crucial step in which the polymeric precursors are cross linked forming an organic/inorganic network at low temperature (100-400 °C). The ceramization process involves thermolysis of organic groups at high temperature (600-1000 °C). This process results in amorphous covalent ceramics which could be crystallized at higher temperatures. PDC could be used for preparation of glass ceramic nanocomposites as preparation of nanofillers like CNTs, graphene, boron nitride nanotubes[119] is easy to be produced by pyrolysis of suitable liquid precursors.

Ji et al.[120] reported preparation graphene and silicon oxycarbide composites by using PDC technique. Composites were produced with up to 30 wt% loading by graphene oxide powder in polysiloxane which underwent cross linking and further during pyrolysis converted graphene oxide to graphene while polysiloxane to silicon oxycarbide at 1000 °C in argon for 1h. They were produced for application as anode in Li ion batteries and graphene-silicon oxycarbide composite produced by PDC showed higher discharging capability than pure graphene and pure silicon oxycarbide.

2.3. Sintering of Glass Ceramic Composites

Sintering can be defined as increasing the contact area between particulates by using relevant conditions like temperature, pressure and surrounding environment for transporting of the material to the pores and its surrounding[121]. Successful sintering procedures can lead to highly dense samples which is aim for uniformity in properties to be observed in all the sections of the sample. Basic methodology of sintering for consolidating the glass ceramics is presented in Fig. 2.9.

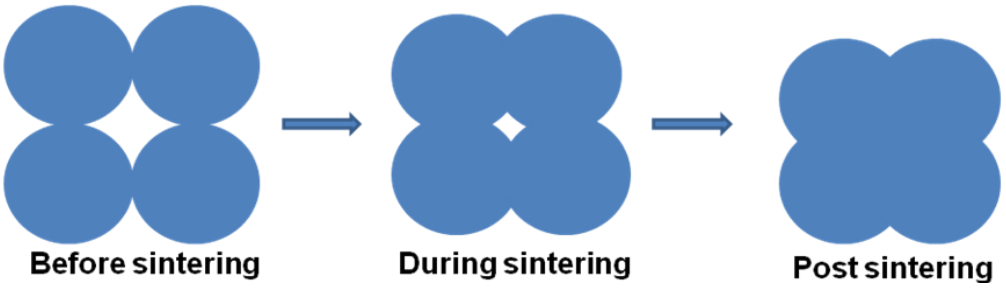

Fig. 2.9: Basic sintering methodology for densifying glass ceramics

2.3.1. Conventional Sintering Techniques

Conventional sintering techniques include methods like pressureless sintering. It involves use of high temperatures and prolonged sintering time as well as greater use of energy to achieve higher density composites. However, use of conventional sintering techniques lead to grain growth in ceramics and they also adversely affect the nanofillers used as reinforcements[122,123]. Other novel sintering methods have been developed by using lower temperatures and dwell time in order to overcome these drawbacks. Michalek et al. reported aqueous slip casting of alumina and 0.1 wt% MWCNTs[54] composites which were consolidated using pressureless sintering methods. They achieved 99.9% density with an application of 1500 °C temperature. Although not much damage was evident on the CNTs, no improvement in the mechanical properties like hardness or fracture toughness was observed either in the composite as compared to monolithic alumina matrix.

2.3.2. Two Step Sintering

Two-step sintering is a relatively simpler sintering technique with application of lower temperature to achieve higher density with slower grain growth in comparison to conventional sintering technique. In this method, sintering is carried out in two major steps in which the ceramics were sintered without applying pressure. In the first step, the powder sample was heated to a higher temperature to make the sample dense enough (>75%) to ensure good nucleation and initiation of crystal growth and then the temperature was decreased to achieve a fully dense sample without changing the grain size of the ceramic sample with constant heating rate cycle. This occurs due to the difference in kinetics of diffusion and migration of grain boundaries[124-126]. It has been

carried out for various oxide ceramic matrices like zirconia[127], alumina[128] etc. Chen et al.[124] reported the sintering of yttria stabilized zirconia by studying the shrinkage data by maintaining constant heating rate and obtained high density (~95%) tetragonal $(ZrO_2)_{0.97}(Y_2O_3)_{0.03}$ and cubic $(ZrO_2)_{0.92}(Y_2O_3)_{0.08}$ ceramics with nanocrystalline and sub-microcrystalline structures. Though, this technique is simpler yet uniformity in the densities of different phases of the matrix during transformation (if not controlled) can serve as a drawback. Also, the grain growth in the final stage of sintering is questionable for achieving highly dense samples[128].

2.3.3. Stress Assisted Sintering Techniques

To avoid the shortcomings of conventional techniques, other sintering methods were devised which took advantage of external compressive stresses in order to lower the sintering temperatures. Some of those techniques include: hot pressing, hot forging and hot isotactic pressing. Though these methods are used widely, the use of high temperature can lead to degradation of nano reinforcements and can lead to grain growth resulting in larger grain size.

2.3.3.1. Hot pressing

Hot pressing involves use of high pressure piston on the powder confined in a die while simultaneously applying high temperature on it to achieve pore-free highly dense samples. This is one of the most commonly used techniques. Uniformly distributed mixtures of fillers and matrix are one of the most necessary conditions to achieve defect-free superior quality composites. However, achieving uniform dispersion of nano reinforcement without agglomerating in the matrix remains a challenge till date. Boccaccini et al.[129] reported borosilicate glass composite reinforced with 10 wt% of MWCNTs by sol-gel process. They presented the comparative study of densification behaviour of the composite by using pressureless sintering and hot pressing. It was reported that while the cold pressing could not densify the sample to a great extent, hot pressing of the composite could lead to achieving high density with much lesser residual porosity observed. SEM of the porosity as observed for single step sintering, two step sintering and hot pressing are shown in Fig. 2.10.

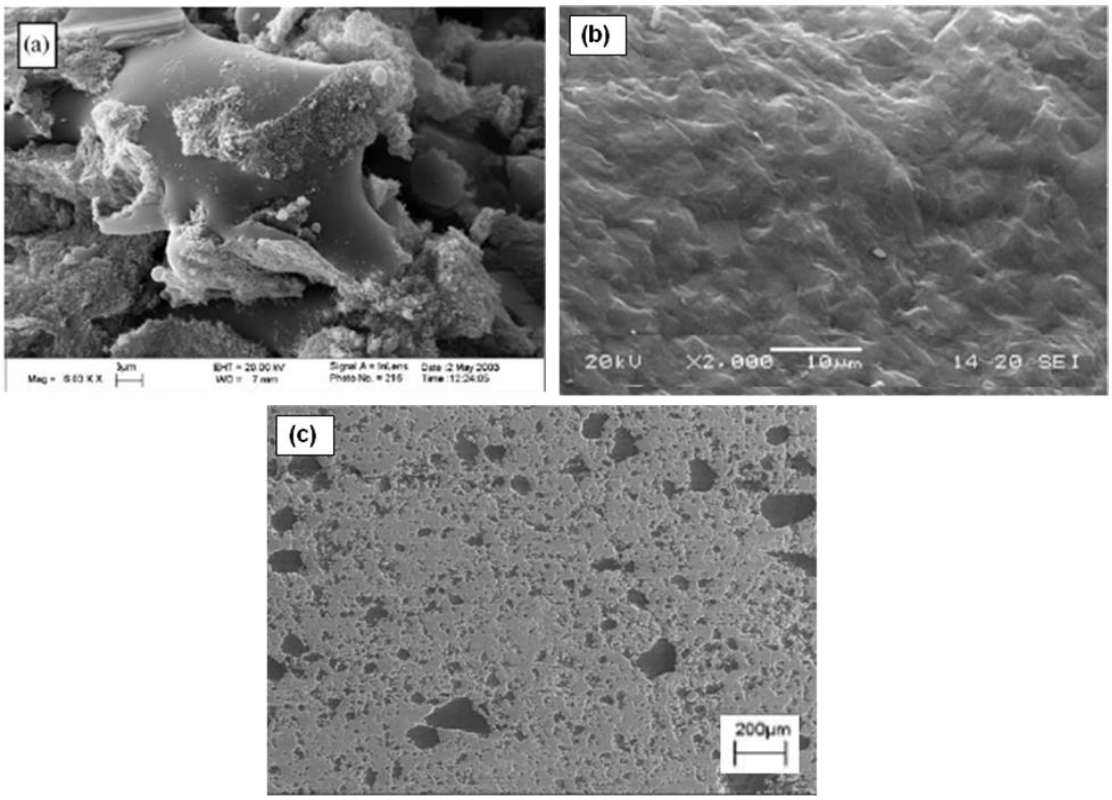

Fig. 2.10: Comparison of porosities observed in 10 wt% MWCNTs reinforced borosilicate glass composites by: a) single step sintering; b) two step sintering; c) hot pressing[129]

2.3.3.2. Hot Isostatic Pressing (HIP)

During hot isostatic pressing, the powder is constrained in a isolated membrane like structure and a high pressure gas, generally argon due to its inert nature so that it does not react with the powder, is employed for application of hydrostatic compressive stresses uniformly in all the directions[130]. Commercially, hot pressing and hot isostatic pressing are mostly used for preparation of ceramic composites[131]. The advantage of HIP is that it can be used to sinter complex shapes. Li et al. prepared bio-ceramics of partially stabilized zirconia (PSZ) with hydroxyapatite(HA) by HIP by applying 160 MPa pressure for 1 h while simultaneously applying a temperature of 1225 °C. HA did not suffer from much degradation and 97% theoretical density was observed for HIP sintered samples[132].

2.3.4. Field Assisted Sintering Techniques (FAST)

It is a powerful method also which has several technical and economical advantages over conventional sintering techniques as well as stress assisted sintering techniques. The advantages include fast heating rate, low dwelling period, no requirement for sintering aid, lower temperatures required and no pre-loading required. That makes it one of the most successful sintering methods in the field composite research.

2.3.4.1. Spark Plasma Sintering

Spark plasma sintering (SPS) uses the rapidly changing electric field for the sintering of ceramics and amorphous glasses. The use of high temperature can adversely affect the properties of the some reinforcements, e.g. CNTs and graphene. Also, longer sintering durations can lead to increase in the grain size for the glass and ceramic matrices therefore of rapid sintering by SPS really aids in the sintering of such composites without affecting the properties of the reinforcements or matrix. In this process, electric current affects the temperature which advances to Joule heating spread all over the specimen and is considered as the heat source. Concurrently, high pressure up to 1 GPa[133] is applied to sinter the sample by applying low temperatures. SPS possesses advantage of smaller holding time (3-10 min), lesser sintering temperature and high heating rate (~100 °C/minute) leading to greater hold on the microstructure of the glasses and ceramics. The key parameters governing the SPS are temperature, pressure and electrical parameters, e.g. voltage, frequency and power. The entire process is carried out in vacuum condition.

Many researchers have used SPS for densification of their composites achieving high densities[102]. It has been observed that in some cases in composites, the reinforcements align perpendicular to the direction of applied pressure[134], esp. in the case 2D reinforcements which promote the anisotropic properties of the composites. The reason for such anisotropy can be the geometry of the reinforcements. Centeno et al. confirmed such behaviour for graphene reinforced alumina composites[134] by Raman spectroscopy. They studied the Raman scans in both parallel and perpendicular directions to the applied pressure during SPS of the composite and found higher I_D/I_G ratio in perpendicular direction, i.e. 1.13 compared to parallel direction,

i.e. 0.83. The higher observation of edges of graphene sheets result in higher value of I_D peak and since graphene was aligned in the direction perpendicular to applied pressure, therefore higher value was obtained in compared to the direction parallel to applied pressure. The apparatus for carrying out SPS for composite samples is presented in Fig. 2.11.

Fig. 2.11: Spark plasma Sintering apparatus

2.3.4.2. Microwave Sintering Technique

Microwave sintering is another fast sintering process which uses low temperature and high speed sintering. In general, the kinetics of the microwave sintering technique is two-three folds higher when the conventional heating is replaced with microwaves[135]. During this process, the ceramic powders to be sintered are surrounded by the susceptors of microwaves, e.g. ferric oxide which transform the microwaves into heat. Since the specimen generates heat in itself, in contrast to conventional sintering techniques, the heating is rapid and selective thereby achieving high heating rates in shorter durations. It has a wide use in dental field as it takes nearly $1/12^{th}$ of time to sinter a dental ceramic compared to conventional sintering technique[136]. Additionally, it is an energy efficient technique as the heat loss is limited. This faster sintering process does not allow grain growth in high amount therefore it is one of the most important techniques for sintering of ceramics. The fast processing avoids formation of intermediate changes thus reducing the chances of their adverse effects in the final ceramic product.

Alumina-zirconia nanocomposites have been reported to have been sintered by microwave sintering[137]. Alumina reinforced with 5 vol% of zirconia achieved a density of 99% within 35 minutes. Uniform microstructure was observed while the grain growth was observed to be suppressed by rapid sintering process. The SEM of the microstructure observed for the sintered specimen is shown in Fig. 2.12.

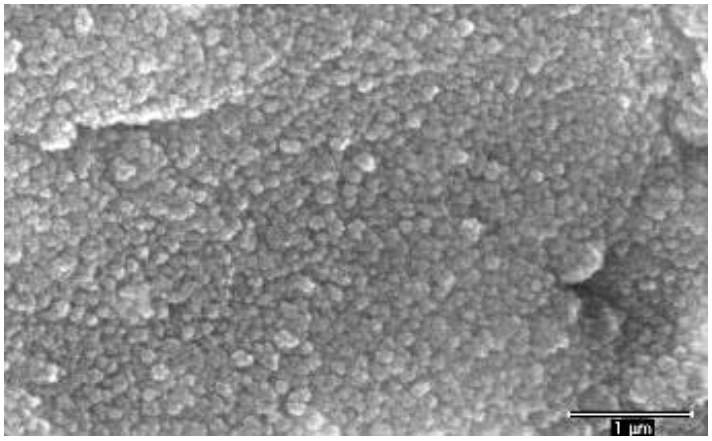

Fig. 2.12: SEM image of the fracture surface for alumina/zirconia nanocomposite

However, this technique suffers from some fundamental challenges. The microwave applicators used are conventional low frequency (2.4 GHz) ones. At room temperature, these applicators do not efficiently couple microwaves to ceramics and therefore poor microwave adsorption causes difficulty in initial heating of the samples. Also, thermal instability can accelerate catastrophic overheating of the samples affecting the properties of the composites. This process may generate non uniformities at high temperature leading to cracking of sample. Efforts have been made to overcome such drawbacks by using hybrid method in which microwave heating is collaborated with infrared source. Infrared source provides the pre-heating of the ceramics to their critical temperature after which microwave heating takes over and is sufficient[138].

Chapter 3 - Aim of the work

The main task of the thesis work deals with the study of reinforcement of glass ceramic composites to enhance their mechanical properties in comparison to monolithic glass ceramics. For this purpose, the work is mainly focused on boron nitride 1D and 2D reinforcements namely boron nitride nanotubes (BNNT) and boron nitride nanosheets (BNNS).

The tasks of the thesis work were broadly categorized into:

1) Characterization of the commercially obtained BNNT to study the morphology and structure of the BNNT. Detailed studies to understand the elemental analysis, purity, temperature dependence, density etc. for the commercially obtained BNNT. Necessary steps taken to make them more readily usable and yield maximum benefits in the composite matrix contributing to enhancement in the mechanical properties of nanocomposite matrix.

2) Synthesis and optimization of conditions to produce high quality BNNS by liquid phase exfoliation technique with high aspect ratio. Characterization of the morphology and properties of as-prepared BNNSs using Scanning Electron Microscope, Transmission Electron Microscope, X-Ray Diffraction, Thermo-gravimetric Analysis, Fourier Transform Infrared Spectroscopy, density analysis etc.

3) Preparation and processing of borosilicate glass (BS) - BNNT (BS-BNNT) as well BS and BNNS (BS-BNNS) composite powders by powder processing method and optimizing the conditions of Spark Plasma Sintering process for densification of the composite powders by reinforcing different concentrations of BNNTs and BNNSs.

4) Ceramographic preparation for the bulk composite samples and study of the mechanical properties of the bulk composite matrix. The mechanical properties

include the density, Young's modulus, micro-hardness, fracture mechanics, flexural strength, tribological properties etc.

5) Thorough investigation of the microstructure as well as the fracture micro-mechanics and micro-mechanisms developed in the matrices after the mechanical testing including observation of fractured surfaces after the testing using optical microscope, scanning electron microscope and other techniques.

Thesis work has mainly been divided into two independent chapters; one describing in detail about reinforcement of BNNT in borosilicate glass and their impact on the properties of the composites while the other dealing with preparation of BNNS and effect of their reinforcement in borosilicate glass.

Chapter 4- Boron Nitride Nanotubes Reinforced Borosilicate Composites

4.1. Materials

4.1.1. Borosilicate Glass

Commercially available borosilicate glass powder (BS; glass type GM27884: 55 wt% SiO_2–25 wt% BaO–10 wt% B_2O_3–10 wt% Al_2O_3; Schott NanoFine NF180, Germany) was used as the matrix for the glass composites. The glass transition temperature of the BS powder used was 665 °C, and the particle size (d_{50}) was 183 nm.

4.1.2. Boron Nitride Nanotubes (BNNTs)

Boron Nitride Nanotubes (BNNTs) with different morphologies were used as reinforcing materials. BNNTs were purchased from School of Materials Science and Engineering, Wuhan Institute of Technology in China. These BNNTs were prepared by self-propagation high-temperature synthesis (SHS) and further annealed using CVD process[139]. Two types of BNNTs were obtained differing in morphology, thereby used as reinforcements, namely, hollow cylindrical type (BNNT-C) and bamboo type (BNNT-B) with bamboo like knots in between. Wang et al.[139] (producers) reported the preparation of different types of BNNTs by employing a porous precursor prepared by SHS method. These precursors were synthesized by mixing B_2O_3, Mg, Fe_2O_3 and FeB in given ratios followed by heating the mixture in SHS reactor in argon atmosphere for 5-15 minutes at 700-800 °C. With the heat treatment, a bulk porous $B_{31}Fe_{17}(MgO)_{27}$ precursor was obtained which was crushed to debris and was annealed in a vertical annealing furnace with the heating temperature of 1000-1200 °C and heating rate 7 °C/minute for 6-12 hours and maintaining the flow of NH_3 or NH_3/N_2 between 0.5 to 10 l/minute in the chamber. The use of different temperatures and annealing times lead to formation of different types of BNNTs. The BNNTs obtained were of similar diameter, i.e. 10 nm ≤ d ≤ 100 nm but varied in lengths as BNNT-C (≥ 10 μm) were approximately double the length of BNNT-B (≥ 5 μm).

4.1.2.1. Purification of BNNTs

The as-received BNNTs were purified by leaching process during which BNNTs were treated with concentrated hydrochloric acid (HCl) and nitric acid (HNO_3) to remove the metallic impurities present in the BNNTs. BNNTs were suspended in ethanol using high sonication energy in order to break the agglomerates by shearing in the suspension. The suspension was allowed to stand after every hour of shearing to let the heavier agglomerates settle down and the supernatant containing the suspended BNNT in ethanol was separated. This process was repeated until all the BNNT were suspended in the solution and no agglomerates were to be found. The settled dust particles along with heavy metal impurities were discarded. The resulting supernatant contained suspended BNNTs which were filtered and the filtered BNNTs were re-suspended in 5M HCl solution at 90 °C for 5 hours with magnetic stirring. This process helped in the removal of residual iron present in the BNNTs. Iron (Fe) was present in the BNNTs as it acted as a catalyst during the BNNT growth process. Thorough stirring of the solution lead to chemical reaction between metal salts (Fe) present in the BNNTs with the acid to produce $FeCl_3$ salt which was soluble in hot water and made the colour of solution to turn green hence signifying removal of Fe from the BNNTs (as shown in Equation 4.1):

$$Fe + 3HCl \rightarrow FeCl_3(Green) + \frac{3}{2} H_2 \uparrow . \qquad (4.1)$$

The resultant solution was filtered using 0.22 μm Millex PTFE filter (Millipore Corp., Ireland) for separating the purified BNNTs from the $FeCl_3$ solution. This process was again repeated with 1M HNO_3 acid in order to remove the magnesium impurities in the form of magnesium nitrate salts.

The resulting purified BNNTs were filtered again using the PTFE filter and were further thoroughly washed with deionized water for neutralizing and washing out any traces of remaining acid present on the walls of BNNTs. The washing of BNNTs was carried out until neutral pH 7 was achieved. Energy Dispersive X-ray Spectroscopy (EDS; Tescan Lyra 3 XMU, Czech Republic) of the purified BNNTs was carried out to confirm the reduction in the amount of Fe content in BNNTs.

4.2. Powder Processing of BS-BNNT Mixtures

BS-BNNT composites were prepared with the as-received BNNTs with the concentrations of 0 wt%, 2.5 wt% and 5 wt% of BNNTs. BS-BNNT composites were also prepared after the purification process of the BNNTs with similar concentrations to see the effect of cleaning of BNNTs on the composite properties. The procedure followed for preparation of composites with BNNT-B and BNNT-C to prepare 0 wt%, 2.5 wt% and 5 wt% BS-BNNT composites as well as to prepare composites after BNNTs cleaning procedure with similar concentration were identical. In order to prepare BS-BNNT composites, BNNTs were suspended in ethanol with concentration of 1 mg/ml. The solution was ultrasonicated for 2-3 hours so as to break the agglomerated BNNTs with the shearing due to sonication until no sedimentation of BNNTs occurred after resting the suspension for certain time. The sediment represented the heavier agglomerates of BNNTs which settled down due to gravity. The well-dispersed BNNT suspension was added to quantitatively calculated amount of BS powder to prepare 0, 2.5 and 5wt % BS-BNNT composite slurries.

Fig. 4.1: Pulverisette planetary ball mill for preparation of composite slurries

The mixture of BNNTs and BS were milled by planetary ball mill (Pulverisette, Fritsch) shown in Fig. 4.1. for 12 hours using borosilicate glass balls (3 mm and 10 mm; Duran®, Ginzel s.r.o., Czech Republic) at 350 rpm. The powder to ball weight ratio used

was 1:20. Post milling, the slurries were dried in oven in ambient atmosphere at 100 °C for the removal of ethanol. The dried powders from slurries were collected, crushed and screened through 100-mesh sieve to obtain fine composite powders followed by heating the powders again at 300 °C for 3 hours to remove the traces of any trapped ethanol in the dried and crushed composite powders.

4.3. Sintering of Nanocomposites

The composite powders received after the drying process were consolidated into a disc shaped samples (HPD 25/1, FCT systems, Germany; carried out at Nanoforce Technology limited, UK) using SPS by placing the powder in graphite die with diameter of 20 mm. Graphite paper was inserted in the die to ensure no direct contact of the powder with the die as well as to guarantee electrical contacts between all parts. The dried and crushed composite powder was preloaded in the die with the help of a punch to bind the powder together using a pressing machine. This graphite die with pressed powder was loaded in SPS furnace. During SPS high electric DC currents were applied to achieve high temperatures with simultaneous application of high pressure. High heating rates applied along with the high pressure aid in reducing the temperature and sintering time for the powder. This in turn helped in maintaining the amorphous character of the glass powder without crystallizing. The composite powders for BS and BNNT-B (BS + BNNT-B) as well as BNNT-C (BS + BNNT-C) were sintered at 775 °C for a dwell time of 7 minute while applying 40 MPa pressure in vacuum. The heating and cooling rates used for the SPS process were 50 °C/minute. High heating rates and vacuum environment during SPS process avoided any damage to nano reinforcements during high temperature processing. The conditions of the sintering were slightly altered for each concentration in order to achieve highest relative density possible.

Fig. 4.2 shows the sintering profile of parameters for BS + 2.5 wt% BNNT-B which shows the rate of change of sintering temperature (in black), the average speed of the piston (in blue), the force applied by the piston on the composite powder present in the die (in green) and the displacement of piston with time (in red). Excess of graphite paper was removed from the surface of the dense samples prepared after SPS. The average speed of the piston gives an idea about the shrinkage rate of the sample.

The sharp peak for the shrinkage rate indicates viscous flow in BS + 2.5 wt% BNNT-B composite as a sintering mechanism.

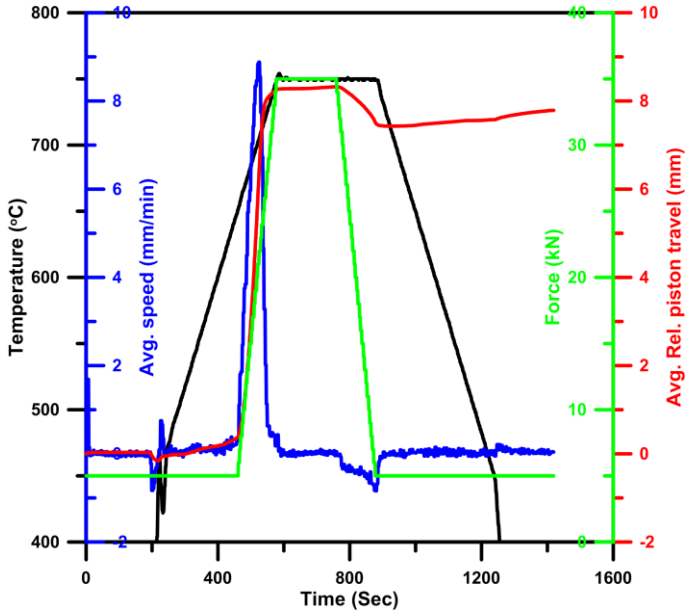

Fig. 4.2: Spark plasma sintering parameters profile for BS + 2.5 wt% BNNT-B showing rate of change of sintering temperature (in black), the average speed of the piston (in blue), the force applied by the piston on the composite powder present in the die (in green) and the displacement of piston with time (in red)

The disc samples were obtained with a diameter of 20 mm and with a thickness of ~3 mm. These disc samples were further machined into 2 mm × 3 mm × 20 mm dimensional bars and their surfaces were prepared by grinding and polishing for the mechanical tests.

4.4. Nanocomposites Characterizations

4.4.1 Zeta-potential Measurement

The zeta-potentials (Malvern Instrument-Nano ZS; carried out at Queen Mary University of London, UK) for the BNNT and BS powders were measured in ethanol by preparing a suspension of BNNT and BS in ethanol with concentration of 1 mg/ml by ultrasonication. Suspensions were prepared with the neutral pH (~7). Flow of liquid around the solid surface rendered surface charging which was neutralized by the

attracting the opposite charge ions present in the solvent forming an electric double layer (EDL). Zeta-potential helps to determine the strength and polarity of EDL. These zeta-potential studies helped to explain the interfacial bonding between the BNNTs and BS glass. The prepared suspension was filled in quartz cuvettes for measurement.

4.4.2. Density Measurements

Densities of the purified BNNT-B and BNNT-C were measured by helium pycnometer (AccuPyc II 1340 Pycnometer; carried out at Joint Glass Centre of the Institute of Inorganic Chemistry, Slovak Republic) with an accuracy of 0.0001 g/cm^3. Nearly 0.35 g of BNNT powder was used for the density measurements. An average of 20 measured values for the density was calculated and used.

For the measurement of the density of the bulk samples, the disc shaped samples prepared were grinded post-sintering to remove the excess graphite from the surface of the samples using 50-100 μm and 10-20 μm size diamonds embedded in metal matrix. The samples were further polished using diamond suspensions (DP suspensions P, Struers, Denmark) levelling down to ¼ μm suspension to remove any major cracks or holes present on the surface. The densities of the bulk sintered composite samples were calculated using Archimedes principle (Equation 4.2). An average of 3 measured values for the density was calculated and used.

$$\rho = \frac{m_1 \rho_0}{m_1 - m_2}. \qquad (4.2)$$

Where ρ is the density of the sample (g/cm^3), m_1 is the mass of the sample in air (g), ρ_0 is the density of water (g/cm^3), m_2 is the mass of the sample in water (g). The density of the BS powder used for the calculation of the theoretical density was 2.8 g/cm^3 (provided by the powder supplier).

4.4.3. Thermo-gravimetric Analysis

Thermo-gravimetric Analysis (TGA) measurements (carried out at Queen Mary University of London, UK) were carried out for the powdered BS and purified BNNT samples using Q500 TGA, Universal V4.5A TA Instruments (shown in Fig. 4.3), to understand the effect of temperature on the powdered samples in a given atmosphere. Approximately 15 mg of BS powder and 5 mg of purified BNNTs were loaded on the clean platinum pans respectively and were subjected to a temperature range up to 900 °C from room temperature with 40 ml/minute flow of N_2 and 60ml/min flow of air with an increasing heating rate of 20 °C/minute. The change in temperature was precisely measured with the help of a thermocouple. The increase in temperature resulted in loss/gain of weight signifying the thermal stability, decomposition, sublimation, absorption or desorption of molecules from the powder.

Fig. 4.3: Q500 TGA, Universal V4.5A TA Instruments thermo-gravimetric analysis apparatus

4.4.4. X-Ray Diffraction Studies

The X-Ray Diffraction (XRD) analysis of bulk sintered samples was performed using X'Pert diffractometer (Panalytical) using Co Kα radiation with a β filter in the secondary beam to analyze the crystallinity of the composite samples.

4.4.5. Scanning Electron Microscopy and Energy Dispersive X-Ray Studies

Field emission gun Scanning Electron Microscopy (SEM; Tescan Lyra 3 XMU, Czech Republic) integrated with Energy dispersive X-Ray studies (EDS) unit was used to study the structure and morphology of the purified BNNTs as well as pure BS powders and BS-BNNT composite powders produced. This technique was also used to analyze the fracture surfaces after the measurement of fracture toughness by chevron notch technique. The sample preparation for SEM for the powdered samples was done by placing minimal amount of powdered sample on the conductive carbon tape while spreading a thin layer of it on the carbon tape surface. However, for the preparation of bar samples, they were sonicated for 15 minutes in ethanol to remove any dust particles adhered to the surface and further dried in ambient atmosphere. These cleaned bar samples were carefully stuck to the holder with the help of carbon tape with precision. These samples were coated with a thin layer of carbon (avoiding any possible contamination to avoid any charging of the samples). Additionally, bar samples were well connected to the conductive carbon tape to avoid any space/air between causing charge development on the sample surface with the help of commercially available silver paste.

4.4.6. Elastic Modulus

The elastic modulus of the samples was measured using the impulse excitation resonance method using GrindoSonic Mk5i (J.W. Lemmens N.V., Belgium) on highly polished 2 mm × 3 mm × 20 mm bar shaped samples. An acoustic detector was used to detect the vibrations produced in the beams by tapping them with a light mechanical impulse. A mean value of 15 recorded measurement frequencies for each sample was considered. The measurements were recorded on the surface perpendicular to the direction of applied pressure during sintering. The averaged values of the frequencies (in GHz) were used to calculate the Young's modulus using Genemod software for each composite bar sample. The setup for the GrindoSonic Mk5i is shown in Fig. 4.4.

Fig. 4.4: GrindoSonic Mk5i setup for the measurement of the Young's modulus of bar samples

4.4.7. Vickers Hardness Measurements and Indentation Fracture Toughness

A computer-controlled micro-hardness tester (Zwick/Roell ZHU/Z2.5, Germany, with 9.8 N for 10 s dwell time; shown in Fig. 4.5.) was used for determination of Vickers micro-hardness and indentation fracture toughness of BS-BNNT glass composite bars with dimensions 2 mm × 3 mm × 20 mm.

Fig. 4.5: Computer-controlled micro-hardness tester (Zwick/Roell ZHU/Z2.5)

Vickers hardness measurement involves the use of pyramid shaped diamond indenter with the diagonals with an apical angle of 136°. The diagonals of the indent are measured by optical microscope after the force is applied on the sample's polished surface and removed. Average of the length of these diagonals help to determine the hardness of the sample using Equation 4.3, according to the standard (ENV 843-4:1994).

$$HVF = \frac{1.8544}{d^2} F \,. \tag{4.3}$$

Where, *HV F* is the Vickers hardness, *d* is the average length of the diagonals in μm measured by optical microscope and *F* is the applied force in N. Minimally, 10 measurements were carried out on each bar sample on the surface perpendicular to the direction of applied pressure during sintering. The indents were made in randomly selected regions which were well-separated and free from defects. A larger number of indentation tests were carried out during preliminary tests but offered no significant improvement in the scatter of data; therefore, indentation cracks and toughness values from 10 independent indentations were considered sufficient for this study.

The crack lengths observed at the corners of the indents were measured using confocal microscope (Lext OLS 3100, Olympus, Japan). The equation derived by Anstis et al.[140] and verified for glass matrix composite systems elsewhere[141] was used to calculate the indentation fracture toughness (K_{Ic}, $MPam^{1/2}$), as shown in Equation 4.4. Fig. 4.6. shows the scheme of the indent used for calculation of indentation fracture toughness.

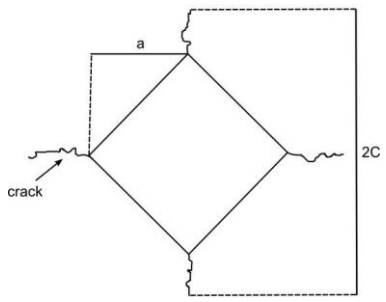

Fig.4.6: Schematics of the indent for calculating indentation fracture toughness

$$K_{Ic} = 0.0154 \times \left(\frac{E}{H}\right)^{1/2} \times \left(\frac{P}{C^{3/2}}\right). \quad (4.4)$$

Where E is Young's modulus (GPa), H is hardness (GPa), P is load (N), and C is average radial crack length (μm). To apply the equation, experimental Vickers hardness and elastic modulus values were determined for each BNNT reinforced borosilicate composite samples.

4.4.8. Fracture Toughness Measurements by Chevron Notched Beams

The fracture toughness for the BS glass and the composite samples was measured on polished bars with rectangular nominal dimensions of 2 mm × 3 mm. A chevron notch was introduced into the bars on the upper surface parallel to the direction of applied pressure during sintering with an angle of 90°. The chevron notch method is one of the most reliable techniques for the measurement of fracture toughness. The force required for the crack initiation is nearly half or two-third of the force required in chevron notch compared to other techniques for measurement of toughness and the crack propagation is stable and unstable crack propagation starts at maximum force. Additional advantages include higher reproducibility, less material required, no pre-cracking of the samples required etc.[142] The chevron notch was introduced using an ultrathin diamond blade with a thickness of 0.15 mm (Struers, Denmark) on a precision saw Isomet 5000 (Buehler, USA) according to ASTM standards (i.e. depth of notch is 0.2-0.25 times height of the specimen).

The samples were tested on a universal testing system, Instron 8862 (Instron, USA), by three-point bending with 16 mm span (shown in Fig. 4.7.), and at a crosshead speed of 1 μm/minute with the load cell capacity was 1 kN.

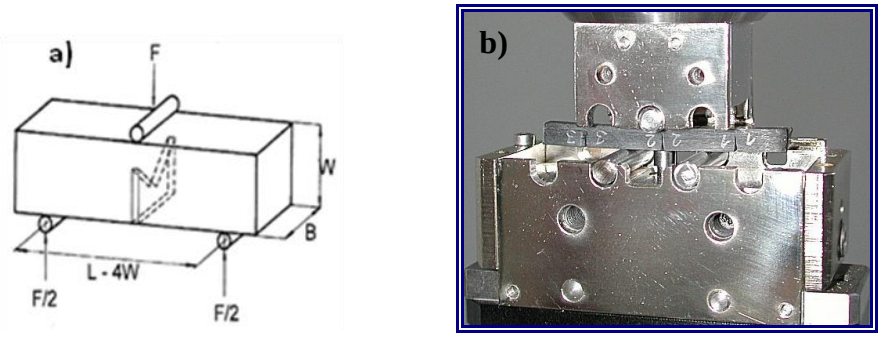

Fig. 4.7: a) and b) 3-point bending setup for the measurement of bulk fracture toughness

The bars were loaded in the same direction as applied pressure during SPS. Slow crack propagation was identified before reaching the maximum loading. The fracture toughness of the bars was calculated using Equation 4.7:

$$K_{Ic} = \frac{F_{\max} \cdot Y^*_{\min}}{BW^{1/2}}. \qquad (4.7)$$

Here K_{Ic} denotes the fracture toughness[142] (MPam$^{1/2}$), F_{max} is the maximum force determined from the load–deflection trace (N), Y^*_{min} is an index denoting minimum of geometrical compliance function Y^*_{min}[143], and B and W are the thickness and height of the sample respectively. At least three beams were tested for each composition.

4.4.9. Single Pass Scratch Resistance Tests

Scratch testing for the composites was analyzed to study the scratch resistance of the BNNT reinforced BS composites compared to the pure BS samples. UMT Multi-Specimen Test System (Bruker, USA; carried out at Institute of Materials Research, Slovak Academy of Sciences, Kosice, Slovak Republic) scratch tester (shown in Fig. 4.8.) was used to measure the single pass scratch test for the samples. Vickers indenter was used for the measurement with leading edge orientation with a constantly increasing force from 0.5 N to 2 N (with an accuracy of 0.25 mN) employing a constant speed of 0.1 mm/sec for the indenter displacement length of 2 mm on a sample glued to the sample holder. For the measurement, the samples were polished up till 1 µm dimension diamond suspension. 3 measurements were recorded for each set of sample.

The tangential and normal forces were continuously monitored along with coefficient of friction, indenter displacement, acoustic emission signals as well as penetration depth.

Fig. 4.8: UMT Multi-Specimen Test System used for the analyzing scratch resistance of the composite samples

Post measurements, these scratches were examined by confocal microscope and 3D profilometer (PLu neox, Sensofar-Tech, S.L., Spain) to analyze the profile as well as optical appearance of the scratches produced. Detailed study of these scratch grooves was further carried out using SEM and it was also used to measure the micro-damage mechanisms as well as to study the lengths at which the radial cracks and chipping initiated.

4.5. Results

4.5.1. Material Analysis

The BNNTs procured from Wuhan Institute of Technology were observed using SEM. The detailed SEM images showing the morphological differences of the BNNTs produced are given in Fig. 4.9.

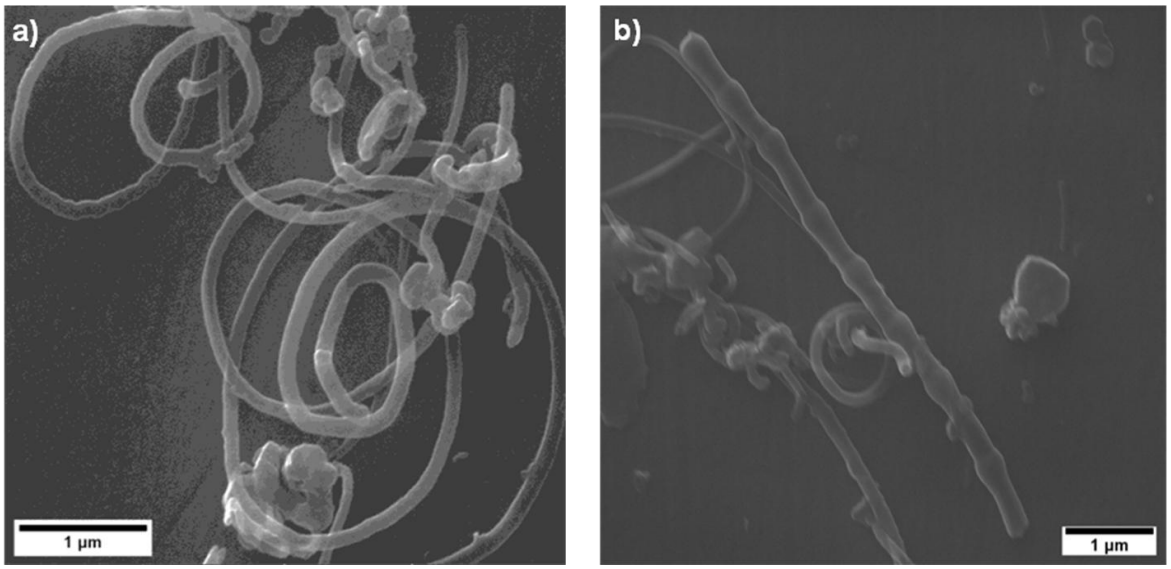

Fig. 4.9: a) Cylindrical boron nitride nanotubes; b) Bamboo like boron nitride nanotubes

TEM was performed on the BNNT-B and BNNT-C solution. It was observed that the elastic properties of the BNNTs were quite high (as observed in Fig. 4.10.). The black dots signify the residual Fe impurities left after cleaning process in the BNNTs.

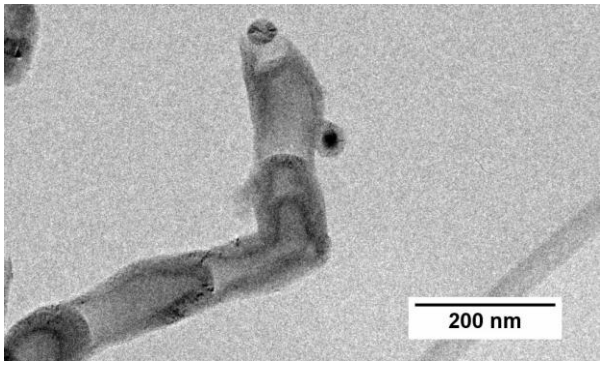

Fig. 4.10: TEM observed for suspended BNNT in ethanol

The zeta-potential of the BNNT and BS were measured to confirm the presence and quantify the electrostatic charge on the constituents while dispersed in the ethanol. A high development of negative charge was observed on BS powder (-21.3 mV) and BNNTs (-17.9 mV) in ethanol. It was observed that right after purification of BNNT through leaching process, the BNNT acquired a pH of 4.18 signifying the acidic character

of the BNNTs. In this case, the zeta-potential value for the BNNT was observed to be -0.578.

The densities of the purified BNNT-B and BNNT-C measured using helium pycnometer were 2.86 g/cm^3 and 2.37 g/cm^3.

Results of TGA for the BS and BNNT-C are presented in Fig. 4.11. The analytical graphs represent the change in the weight percent of the sample and derivative weight change (weight loss % per unit increase in temperature) while increasing the temperature from the room temperature to 900 °C.

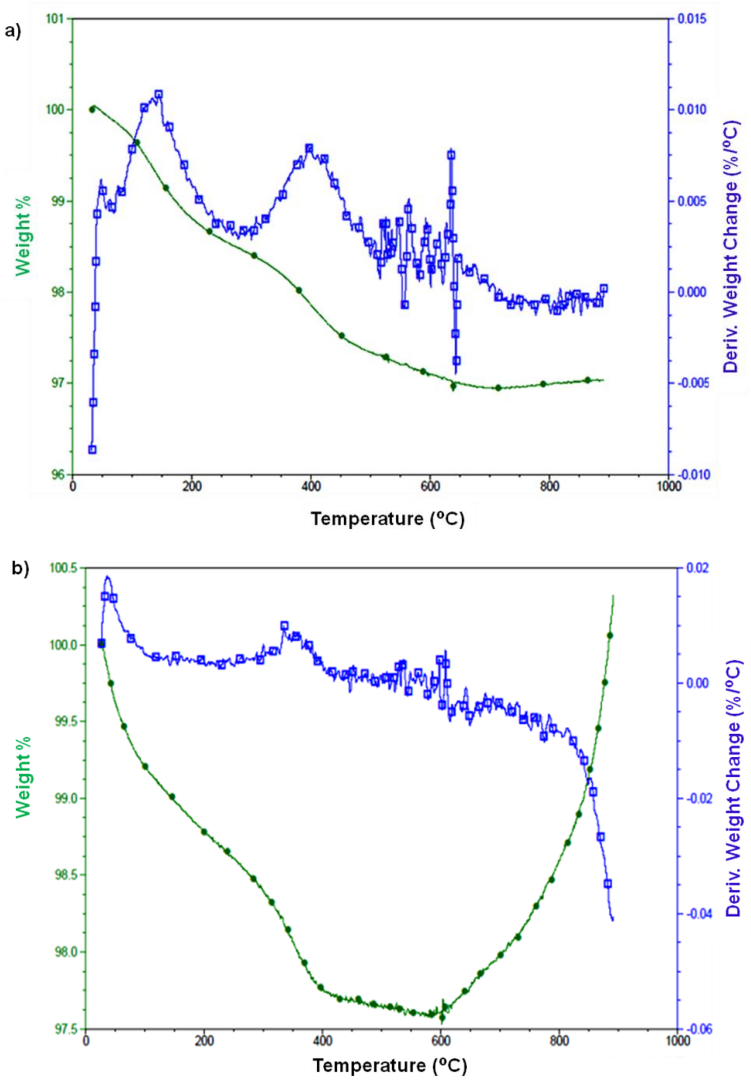

Fig. 4.11: Thermo-gravimetric analysis of; a) BS and b) BNNT showing their thermal stability

The EDS studies of the BNNTs were carried out before and after purification for the basic elemental analysis of the nanotubes to analyze and confirm the purity of the BNNTs. It was observed that there was a presence of nearly 54.6 wt% of Fe in the as-received BNNTs (Fig. 4.12.). The purification for the BNNTs carried out as mentioned in the experimental section 4.1.1.1 lead to an enormous reduction in the amount of these Fe impurities as can be observed in the Fig. 4.12. Fig. 4.12. shows the comparison between concentration of Fe and other impurities present in BNNT-C before and after the purification process.

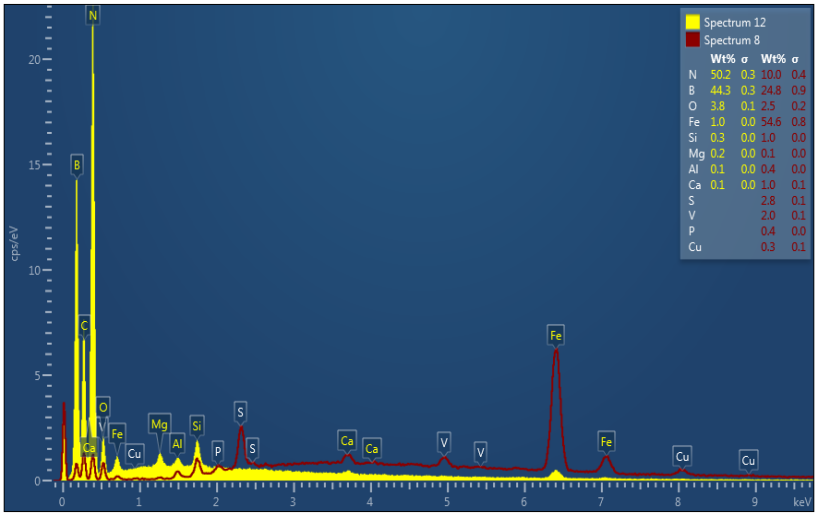

Fig. 4.12: Comparative EDS of as-received BNNT-C (red) and purified BNNT-C (yellow)

4.5.2. Microstructure Analysis for the Nanocomposites Prepared

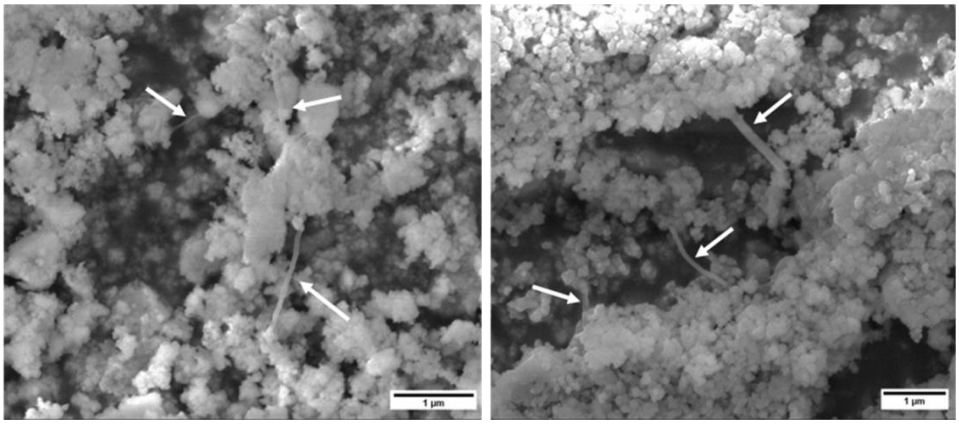

Fig. 4.13: SEM images of BS-BNNT composite powder with highly dispersed BNNTs (BNNTs indicated by arrows)

These as-received BNNTs were incorporated into the BS matrix with the concentrations of 0 wt%, 2.5 wt% and 5 wt% by ball milling method. The powders of the composites prepared were analyzed by SEM to observe the dispersion of BNNTs in the BS matrix. The SEM images of the composite powders showing the distribution of BNNTs are shown in Fig. 4.13. As shown in Fig. 4.13., the BNNT were found to be well distributed in the matrix. No significant damage was observed on the length or surface of BNNT after 12 hours of ball milling duration.

The relative densities of the bulk samples were measured using Archimedes principle and calculated according to the rule of mixture. The relative densities of the pure BS, as received BS-BNNT (2.5 wt%) and as-received BS-BNNT (5 wt%) are given in Table 4.1.

Table 4.1: Relative densities for 0 wt%, 2.5wt% and 5wt% of BS-BNNT using as-received bamboo like and cylindrical nanotubes

Relative density	**0 wt%**	**2.5 wt%**	**5 wt%**
BNNT-C	99.2 % (Pure borosilicate)	97.6%	97.2%
BNNT-B		98.1%	97.1%

New composite samples were prepared with the similar concentrations of purified BNNTs and the samples were further characterized. The densities of the bulk samples are given in Table 4.2.

Table 4.2: Relative densities for 0 wt%, 2.5 wt% and 5 wt% of BS-BNNT using purified bamboo like and cylindrical nanotubes

Relative density	**0 wt%**	**2.5 wt%**	**5 wt%**
BNNT-C	99.2 % (Pure borosilicate)	98.8%	97.8%
BNNT-B		98.5%	98.0%

XRD of the bulk samples prepared revealed the amorphous nature of the composite. Addition of 5 wt% of BNNTs also did not affect the amorphous nature of the glass.

4.5.3. Mechanical Properties of Bulk Nanocomposites

The value of indentation fracture toughness for the pure borosilicate glass sample, as-received BNNT-C reinforced borosilicate glass (0 wt%, 2.5 wt%, 5 wt%) and as-received BNNT-B reinforced borosilicate glass (0 wt%, 2.5 wt%, 5 wt%) are presented in Table 4.3 below. An increase of ~30% of indentation fracture toughness with 5 wt% reinforcement concentration of as-received BNNT was observed for the borosilicate composite samples.

Table 4.3: Indentation fracture toughness of as received BNNT reinforced BS glass composite

K_{Ic} (MPam$^{1/2}$)	0 wt%	2.5 wt%	5 wt%
BNNT-C	0.851 ± 0.027 (Pure borosilicate)	0.997 ± 0.065	1.099 ± 0.062
BNNT-B		0.933 ± 0.044	1.101 ± 0.069

For chevron notch beam fracture toughness ($K_{Ic,}$ MPa m$^{1/2}$) for composite samples formed by borosilicate glass reinforced with as-received BNNT-B and BNNT-C is given in Table 4.4.

Table 4.4: Fracture toughness by chevron notch measured for as received BNNT reinforced BS glass composite

K_{Ic} (MPam$^{1/2}$)	0 wt%	2.5 wt%	5 wt%
BNNT-C	0. 85 ± 0.03 (Pure borosilicate)	0.87 ± 0.05	0.66 ± 0.07
BNNT-B		0.91 ± 0.04	0.72 ± 0.08

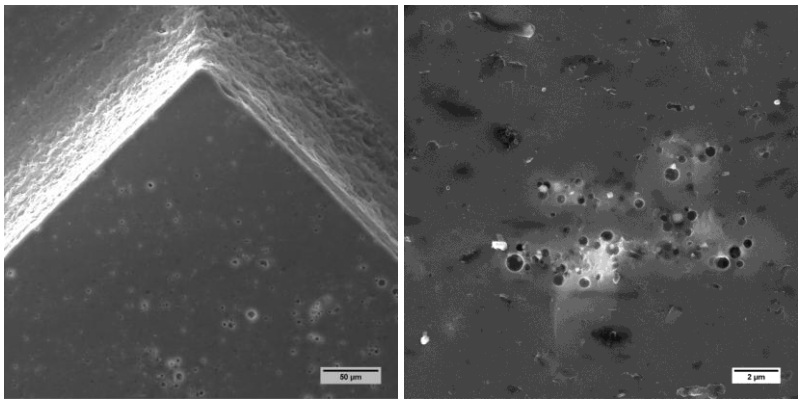

Fig. 4.14: Presence of holes in the fracture surfaces of BS-BNNT composites; a) notch tip and b) detail view of pores

The SEM images of the fracture composite sample prepared by the borosilicate and BNNT-C are given in Fig. 4.14. There were small bubbles like pores widely spread on the whole fracture surface for the composite sample prepared with as-received BNNTs.

After the purification process of BNNT and composites preparation with purified BNNTs, Young's modulus and the hardness values for these composites reinforced with purified BNNTs were measured and the values are given in Table 4.5 and graphically represented in Fig. 4.15. We observe a slight reduction in the values of Young's modulus as well as hardness with the increase in the concentration of BNNTs for both purified bamboo like and cylinder like BNNTs. There was a reduction of the values by approximately 7% in both cases compared to pure glass.

Table 4.5: Young's modulus and Vickers hardness for 0 wt%, 2.5 wt% and 5 wt% of BS-BNNT using purified bamboo like and cylindrical nanotubes

Material	Young's modulus (GPa)	Vickers Hardness HV 1 (GPa)
BS Pure	72.1 ± 0.4	6.24 ± 0.17
BS-2.5 wt% BNNT-C	69.4 ± 0.4	6.12 ± 0.27
BS-2.5 wt% BNNT-B	68.5 ± 0.8	6.01 ± 0.21
BS-5 wt% BNNT-C	68.0 ± 0.4	5.81 ± 0.16
BS-5 wt% BNNT-B	67.4 ± 0.7	5.86 ± 0.18

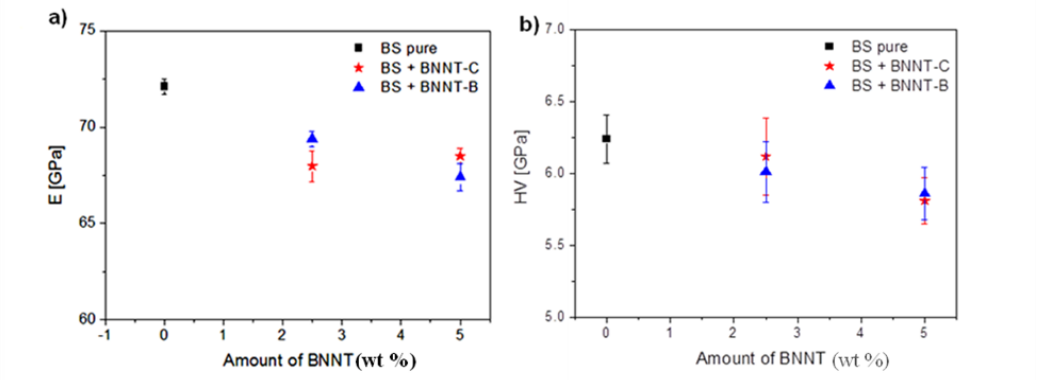

Fig. 4.15: a) Young's modulus and b) Vickers hardness for 0 wt%, 2.5wt% and 5 wt% purified BNNT-B and BNNT-C reinforced BS composites

The chevron notched fracture toughness of the composites prepared by purified BNNT-C and BNNT-B was measured in the similar way as for composites reinforced with as received BNNT-C and BNNT-B. The values of the fracture toughness for composites reinforced with purified BNNT-C and BNNT-B are given in Table 4.6 (as well as Fig. 4.16.).

Table 4.6: Fracture toughness by chevron notch measured for purified BNNT-C and BNNT-B reinforced BS glass composite

K_{Ic} (MPam$^{1/2}$)	0 wt%	2.5 wt%	5 wt%
BNNT-C	0. 85 ± 0.03 (Pure borosilicate)	1.02 ± 0.05	1.05 ± 0.08
BNNT-B		0.99 ± 0.03	1.06 ± 0.06

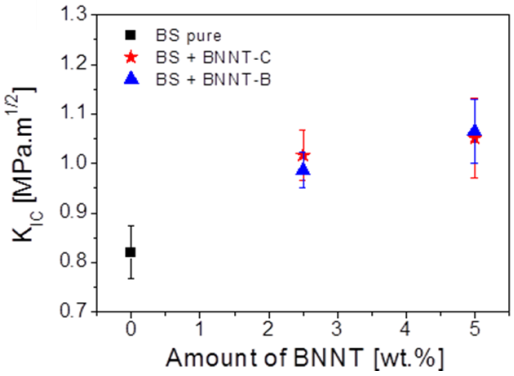

Fig. 4.16: Fracture toughness by chevron notch measured for purified BNNT-C and BNNT-B reinforced BS glass composite

For the observation of the toughening mechanisms, the tested beam's fracture surfaces were analyzed using SEM. Uniform dispersion and random alignment of BNNTs were observed throughout the surface therefore, it was believed that isotropic properties developed in the matrix. Also, the indents made during the indentation toughness were thoroughly observed by SEM. Fig. 4.17. depicts the significant toughening mechanisms observed in BNNTs reinforced BS composites.

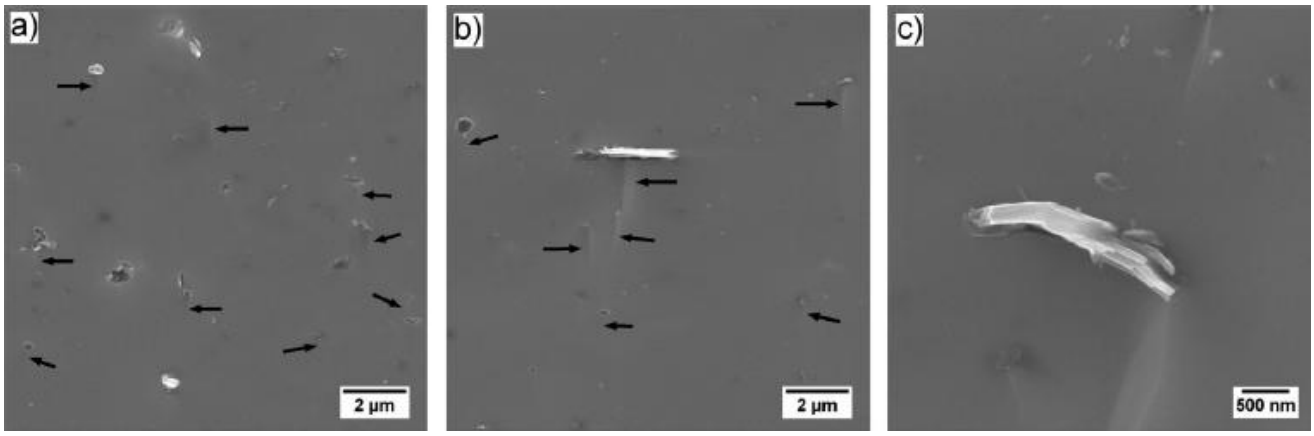

Fig. 4.17: SEM images for fracture surfaces showing pull-out of BNNTs, left behind cavities and the crack deflection around BNNTs (shown by arrows) in BS glass matrix reinforced by; a) 2.5 wt% BNNT-B; b) 2.5 wt% BNNT-C and; c) bundled up BNNT in BS glass matrix

4.5.4. Single Pass Scratch Resistance For the Composites

The results above did not show any major difference in the mechanical properties of the composites because of the use of different morphologies of BNNTs therefore we only tested BS glass reinforced with 2.5 wt% and 5 wt% of BNNT-C type composites to investigate the single pass scratch resistance of the composite samples compared to pure BS glass. The results of all the tested samples are given in Table 4.7.

Table 4.7: Scratch resistance for Pure BS and BS glass reinforced with 2.5 wt% BNNT and 5 wt% BNNT showing coefficient of friction (COF), transition displacement from micro-ductile to micro-cracking region, the lateral frictional force recorded between Vickers indenter and sample surface and normal applied by the indenter on the surface

Material	**COF**	**Transition (mm)**	**Friction force F_x (mN)**	**Normal force F_z (mN)**
BS Pure	0.264 ± 0.038	0.234 ± 0.015	59 ± 2.1	268 ± 5
BS + 2.5 wt% BNNT-C	0.279 ± 0.033	0.281 ± 0.023	77.6 ± 3.3	323 ± 4
BS + 5 wt% BNNT-C	0.276 ± 0.031	0.297 ± 0.024	80.7 ± 2.9	337 ± 7

The coefficient of friction (COF) of the sample increased slightly whereas we could observe a substantial increase in other important parameters like indenter displacement, normal and frictional forces with increasing amount of BNNT. These

parameters were determined by the optical observation of scratch grooves, the profile (depth) of the scratch groove and the transition area measured by acoustic emission (AE) signalling. Fig. 4.18. show the AE signals and COF measured with the distance travelled by indenter. The first peak of AE appears at 0.301 mm which is similar to the value determined using confocal microscope shown in Fig. 4.19.

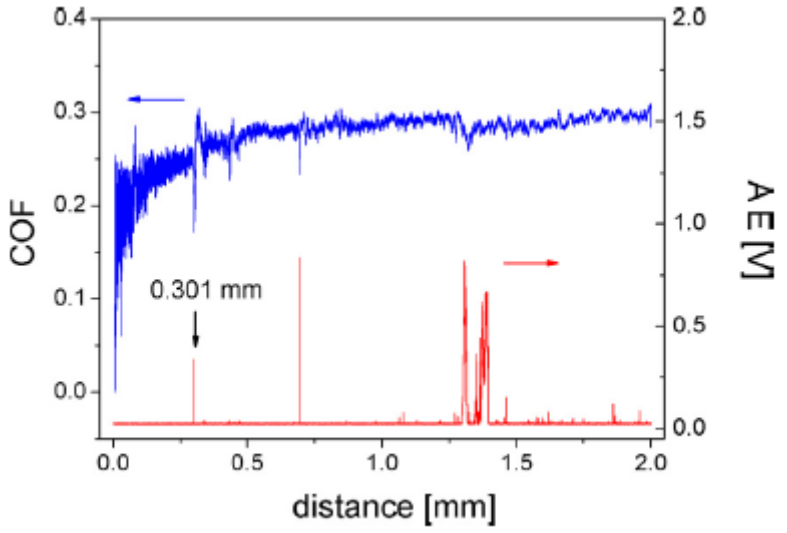

Fig. 4.18: Change of COF and AE with distance during scratch testing for BS – 2.5 wt% BNNT-C

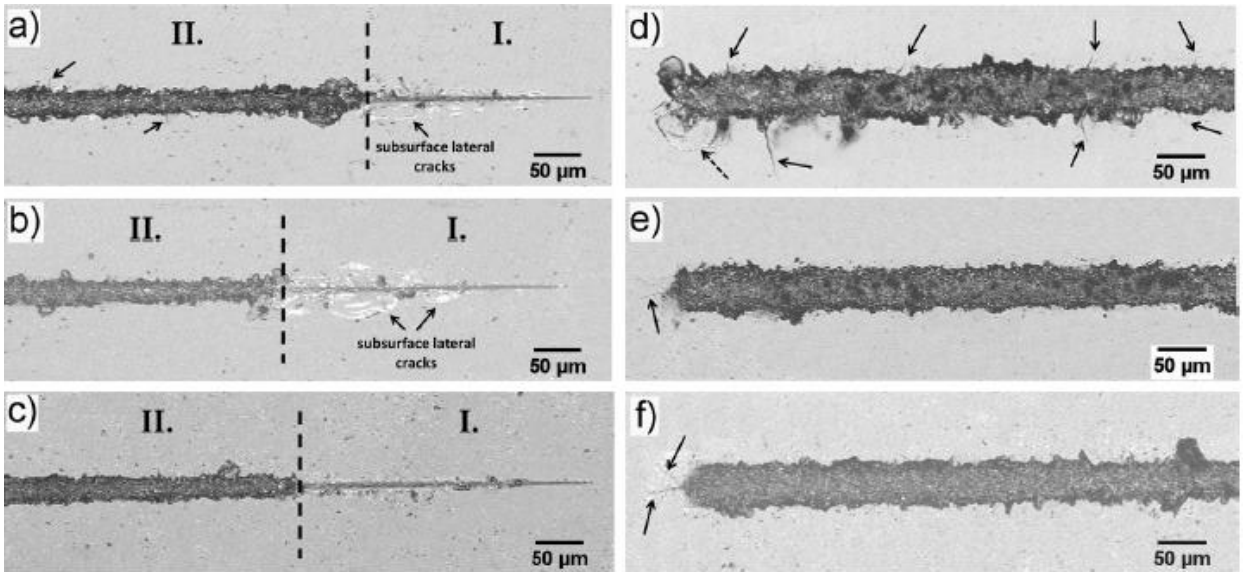

Fig. 4.19: Transition of scratch groove from micro-ductile to micro-cracking regime for a) pure BS glass, b) BS – 2.5 wt% BNNT-C, c) BS – 2.5 wt% BNNT-C. The scratch groove appearance on termination (at maximum load) for d) pure BS glass, e) BS – 2.5 wt% BNNT-C, f) BS – 2.5 wt% BNNT-C

4.6. Discussion

4.6.1. Material Analysis

The higher amount of like charge is necessary on the BS and BNNT in order to avoid agglomeration. The high charge presence on the constituents ensured lesser agglomeration (or more stability) and efficient miscibility of BNNTs and BS in ethanol. It was due to the higher like charges that the constituents experienced an electrostatic force of repulsion amongst them which promoted de-agglomeration. Therefore, ethanol was considered as a suitable dispersion medium for the composite formation as it would promote BNNTs to be exploited to their complete potential. Neutral pH (~7) was an important factor governing the charge presence on the components. As shown in the results that the value of zeta-potential generated on the BNNTs at acidic pH (4.18) was very low (-0.578), therefore, the BNNT would have much higher tendency to agglomerate due to low surface charge generation. The reason for this large difference in the values of zeta-potential is because in the acidic medium, H^+ ions gather around the nanotubes leading to neutralizing the negative potential developed on the surface of BNNTs. This has been commonly observed in the CNTs as well[144].

The density values observed for the BNNTs were close to value of bulk h-BN of 2.27 g/cm^3 [62]. A slightly higher densities of BNNTs compared to bulk h-BN were observed due to presence of residual metal impurities left after the purification process. The BNNT densities were also influenced by the inner structure of the BNNT, i.e. the cylindrical BNNT possessed lesser density than bamboo like BNNT.

During TGA measurements, it was found that the BS powder suffers a weight loss of about 3% with increasing the temperature to 900 °C as shown in Fig. 4.10(a). On the other hand, the BNNTs were also observed to have a weight loss of about 3% until 600 °C (Fig. 4.10. (b)), which may signify the sublimation of volatile impurities like ethanol or other solvent from the surface of BNNT and thereafter we observed an increase in the weight percent, which could be attributed to the increase of weight of BNNTs due to oxidation process carried out at high temperatures.

The EDS analysis revealed that the as-received BNNT had a large amount of Fe which might be present due to its use as a catalyst for the BNNT growth. The microstructural observation of the fracture surface revealed the presence of significant amount of small pores all over the surface, depicted in Fig. 4.14. We assume the presence of bubble like pores were due to these Fe impurities present in the BNNT which evaporated on sintering the samples, leaving the small pores behind. Several reports have been published about the use of Fe salts as a foaming agent[145]. Therefore, a need of purification of the BNNTs had arisen to remove the Fe and other impurities. In spite of using intensive acid purification measures repeatedly, complete removal of residual iron from the BNNT was found to be significantly difficult compared to CNTs using similar procedures[79].

4.6.2. Microstructure Analysis for the Nanocomposites Prepared

It was observed that the relative densities of the composites reduced with the increase in the concentration of the BNNTs (Table 4.1 and Table 4.2). The reason for this could be that besides the potential effect on crystallinity, the BNNT might obstruct the viscous flow of the amorphous glass during sintering as a solid impurity to inhibit the densification of the glass. It has been widely observed that fibre like reinforcements inhibit the densification process[6,53,57,146]. This might be the reason for the reduction of density of BS-BNNT composites with the increasing concentration of BNNT.

XRD revealed that the composites prepared were amorphous in nature. Use of high content of alumina (10 wt%) in the borosilicate glass composition aims to prevent the formation of cristobalite structure for the glass for high temperature processing. Despite, adding 5 wt% of BNNTs to the matrix, the amorphous nature of the composites was maintained. While using of reinforcements, in general, they act as a nucleation site which promote crystallinity[53] which is not seen for the present composites. A similar behaviour has been observed for CNTs reinforcement in silica where none or minimal amount of crystallinity was found[6]. The reason for such behaviour was subjected to the reduced mobility of silica network bound to the surface of nanotubes or because of the local stiffness of the nanotubes which did not allow the shrinkage of the matrix which is common while crystallization process. The BNNTs having similar structure to CNTs, also

affected the amorphous nature of the glass in a similar way. Du et al. also reported the hindrance of silica cristobalite transformation by the use BNNTs as reinforcements[71].

4.6.3. Mechanical Properties of the Bulk Nanocomposites

It was postulated that the presence the bubbles all over the surface, as can be seen in Fig. 4.14., was due to the presence of Fe impurities in the as-received BNNTs. This may be the key reason for lower values of bulk fracture toughness observed for as-received BNNTs reinforced BS nanocomposites compared to their indentation toughness observed. It was assumed that these bubble pores sites actually aided the crack propagation in the composite sample. On the other hand, in the case of indentation fracture toughness, specific areas where no or less pores were observed were selected judiciously and the indents were made with lower weights therefore no encounter with pores occurred leading to higher values of indentation fracture toughness.

The presence of small pores due to the residual Fe impurities left in the BNNTs after the purification process (though the dimensions of the pores were much smaller) also contributed to reduction of densities of the composite sample. This indicated that even a very minute concentration of Fe was enough to introduce porosity into the composite material. The porosity observed in the samples affected the reduction of Young's modulus and hardness of the composite samples as well, as shown in Table 4.5. Mukhopadhyay et al. observed similar reduction in the hardness of alumino-borosilicate glass ceramic by introducing CNTs into the matrix[57]. It must also be noted that the use of different kind of BNNTs did not have any significant effect on the values of Young's modulus and hardness.

We observed that the values of fracture toughness for as-received BNNT reinforced borosilicate composite samples were lower or equal to the values of pure borosilicate glass samples (shown in Table 4.4). However, the value of chevron notched beam fracture toughness for purified BNNTs reinforced BS composites increases from 0.85 to 1.05 for 5 wt% BNNT-C (Table 4.5). This showed that the removal of Fe impurities lead to the enhancement in the toughness of this composites. The linear

pattern of the values indicated the direct effect of BNNT concentration on the toughening of the amorphous matrix. These values observed were similar to that of the indentation fracture toughness. It has been reported that there is shear deformation under the indenter due to which the crack propagation is suppressed, which limits the crack propagation around indent resulting in higher toughness values observed[6]. However, in our composites, the values of the fracture toughness measured by indentation method and chevron notch method were in agreement so therefore, we can deduce that no shear deformation is observed for BNNT reinforced BS composites.

After the observation of fracture surface for purified BNNTs reinforced BS composites, it was seen that the BNNTs were found to be uniformly dispersed throughout the matrix (shown in Fig. 4.17.). This was also confirmed from the amount of pull-out which was regularly seen in the matrix. On the other hand, we could observe some BNNTs stuck together (about 3-4) in bundled form along their lengths which appeared to be one thick BNNT, shown in Fig. 4.17 (c). This result confirms that the use of amorphous glass matrix is beneficial for avoiding agglomeration of BNNT which is commonly observed in polycrystalline matrices on grain boundaries[57]. The pull-out lengths varied with the inner structure of the BNNTs. We observed shorter pull-outs for BNNT-B (up to 0.5 μm) in comparison to BNNT-C (up to 1.5 μm).

The interface bonding between the reinforcement and the matrix also plays a significant role affecting the mechanical properties of the composite. Weak interface helps in efficient pull-outs which due to friction produced between the reinforcement and matrix may lead to more energy dissipation than required ultimately increasing the toughness of the matrix. BNNT on the other hand, have been found to be strongly bonded with the amorphous glass matrices[71] which should have resulted in reduction of pull-out generally. On the contrary, even after strong bonding present between BNNT and the BS matrix, a significant amount of pull-outs were observed. The protrusions of the BNNTs from the matrix had rough surface and were of various thickness which signified that these BNNT were strongly adhered to the matrix surface. It was also confirmed as during the pull-out of BNNTs, some of the matrix material also got pulled out in the process.

In addition, since we were using multiwalled BNNTs, we observed addition phenomena called “sword-in-sheath” mechanism which is seen when there is strong bonding between matrix and the outer wall of multiwalled nanotube and due to inner weak bonding between the multiwalled nanotubes, the inner tubes move out extending the length of the nanotubes. It is believed that the BNNT-C displayed larger pull-out length compared to BNNT-B as they were pulled out intact while the BNNT-B were easily disconnected from the longer bamboo type nanotube links during pull-out. Tatarko et al. observed similar mechanism for BNNT influencing the toughening of 3Y-TZP ceramics[79]. In the literature, it has been shown for CNTs that the pull-out mechanism lead to negligible amount of energy dissipation[57]. This has been confirmed for BNNTs as well in this study as the pull-out of the BNNT-B and BNNT-C are varying but it does not lead to any significant change in fracture toughness values for both types of BNNTs.

Though pull-out being the major apparent toughening mechanism present, other toughening mechanisms present in the matrix were crack deflection (shown in Fig. 4.17.). Crack bridging was also found extensively in the crack openings. It was observed that the BNNTs were stretched being embedded in the matrix at both ends of the crack thickness in order to prevent the crack from opening further. It should be noted that the crack thickness for pure BS in the vicinity of the indent was ~ 450-490 nm whereas for the composite the crack thickness in the vicinity of the indent was ~220-290 nm which shows that the BNNT bridged the crack even on the maximum while stretching but not fracturing. This stretching has not been observed for any other nanotubes (including CNTs) where bridging is one of the significant mechanisms of toughening therefore this can be reported as a novel report of such toughening mechanism. All these toughening mechanisms lead to significant fracture toughness enhancement which proves that BNNT contributed directly in increasing the toughness of the amorphous BS glass matrix.

4.6.4. Single Pass Scratch Resistance For the Composites

The higher and wider AE peaks after longer indenter displacement (shown in Fig. 4.18.) signify the considerable amount of chipping which occurred due to higher

normal loading. The scratch grooves created were thoroughly studied through confocal microscope (as shown in Fig. 4.19.).

Fig. 4.19. (a-c) depicts the transition of micro-ductile (region I) to micro-cracking regime (region II) for pure glass as well as BNNT reinforced composites. It is clearly seen that the transition for composites occurred at longer indenter distance corresponding to higher normal and frictional loads compared to pure BS glass. Though, the transition distances did not increase linearly with the composition of the composites but were significantly higher than pure BS glass, i.e. ~0.28 mm for BS-2.5 wt% BNNT, ~0.30 mm for BS-5 wt% BNNT and ~0.23 mm for pure BS glass. The corresponding normal loads showed an increase of approximately 26% of scratch resistance for amorphous BS glass by addition of 5 wt% of BNNT (from ~268 mN for pure BS glass to ~337 nM for BS-5 wt% BNNT composite). In the scratch grooves observed for the samples by SEM, region I depicts the permanent plastic groove region. Fig. 4.19. (a) and (b) show the plastic sub surface cracking under the scratch plastic region for pure BS and BS-2.5 wt% BNNT whereas no such feature is observed for BS-5 wt% BNNT. These sub surface lateral cracking, shown in Fig. 4.18. (a), are commonly observed phenomena observed for amorphous glass scratches[147]. The region II is associated with the combination of lateral and radial cracking generated during Vickers indenter displacement above a critical load for a material, which leads to the chipping.

The radial cracks are common feature for micro-cracking regime and their presence and intersection is shown in Fig. 4.19. (d) by dashed arrows. The radial cracks generated in a curve manner perpendicular to the direction of scratch displacement (where we observe lateral cracking). The combination of radial and lateral cracks, lead to removal of material and hence we observed chipping of the samples. This chipping of the samples was a repeated process for the whole micro-cracking region and no other damages were observed for the samples. It was clearly seen from the comparison for different compositions in Fig. 4.19. that extensive chipping and longer lateral cracks lead to severe damage to pure BS glass in comparison to the composites prepared. For pure BS, some radial cracks were even observed in micro-ductile region where as these radial cracks were absent in the composites prepared where only small and fine

crack were observed at the end of scratch length where the composites suffered with much higher forces.

The overall scratch groove for BNNT reinforced BS glass was much smoother in comparison to pure BS glass. This study clearly indicated that introduction of BNNTs significantly improved the scratch resistance of BS glass compared to pure glass matrix.

Chapter 5- Synthesis of Boron Nitride Nanosheets and Boron Nitride Nanosheets Reinforced Borosilicate Composites

5.1. Materials

5.1.1. Borosilicate Glass

Commercially available amorphous BS glass powder (same as used for BNNTs) was used as glass matrix for the preparation of composites. The basic characteristics of the powder have been provided in section 4.1.1.

5.1.2. Preparation of Boron Nitride Nanosheets (BNNSs)

Boron nitride nanosheets (BNNSs) were used as another form of reinforcements in the BS glass matrix. Properties of BNNSs are described in details in section 2.1.4.3.1. Hexagonal boron nitride powder (h-BN; PT110, Momentive Ceramics Strongsville) was used for the preparation of BNNSs. Mean particle size (d_{50}) of commercially obtained h-BN powder was ~47 μm. The SEM image of the bulk h-BN powder is shown in Fig. 5.1. as provided by the manufacturer.

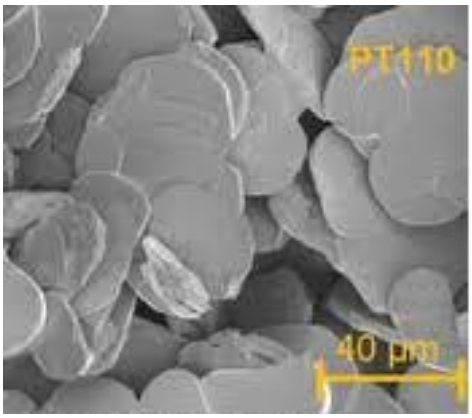

Fig. 5.1: Bulk h-BN powder with d50 particle size of ~47 μm manufactured by Momentive Ceramics Strongsville

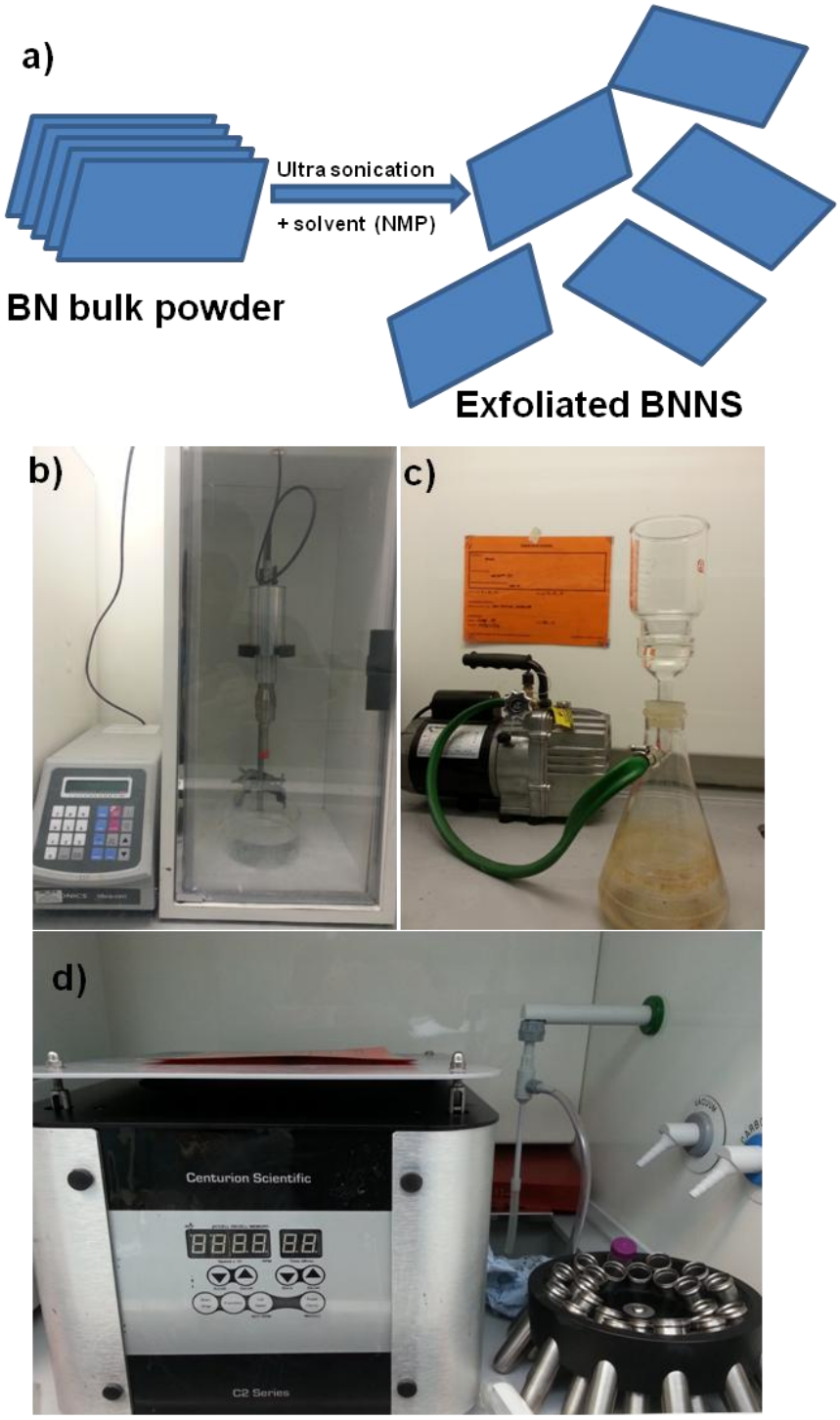

Fig. 5.2: Liquid phase exfoliation of BNNSs; a) schematics of exfoliation of BNNSs; b) Ultrasonication probe; c) Filtration unit; d) Centrifugation setup

BNNSs were prepared by the liquid phase exfoliation of h-BN powder. Exfoliation of h-BN precursor powder was carried out by dispersion of h-BN in a highly polar solvent, i.e. N-methyl-2-pyrrolidone (NMP) by a concentration of 100 mg/ml using a high power tip sonicator (CV33 flat probe sonic tip, 50 W, 25 kHz) for 24 hours. The

suspension was surrounded by an ice bath to prevent the oxidative degradation of NMP. Post 24 hours, the sonicated suspension was centrifuged (Centurion Scientific) at 500 rotations for 45 minutes to separate the supernatant containing lighter BNNSs which remained suspended while the heavier bulk h-BN powder settled down. The supernatant was separated from the settled bulk powder with the help of a pipette. A similar procedure has been used by Khan et al. for the exfoliation of graphene[148,149].

The supernatant containing suspended BNNSs was filtered by vacuum filtration process and the filtered BNNSs were collected and washed with ethanol and water repeatedly to remove the traces of residual NMP stuck on the BNNSs walls. This process was able to produce BNNSs with an average yield between 4-8%. Fig. 5.2. shows a methodology and typical setup employed for the preparation of BNNSs from the bulk h-BN powder by ultrasonic probe used with a pulsing of 5 sec on and 1 sec off and with an amplitude of 25% to prevent overheating of the tip, the filtration unit using nylon filters for separation of BNNSs from the solvent as well as the centrifugation setup for the separation of supernatant from the bulk powder by using 500 rpm for 45 mins.

NMP was considered favourable as a solvent for the liquid phase exfoliation purpose due to higher boiling point (~200 °C) which facilitates in using high power sonication tip without any harm to the dispersing solvent. Moreover, NMP being highly polar solvent aided in de-aggregation of BNNSs. The BNNSs prepared were characterized by SEM, TEM etc. for the detailed analysis of their morphology and structure.

5.2. Powder Processing of BS-BNNS Mixtures

For preparation of BS-BNNS composites, the BNNSs were suspended in approximately 100 ml of ethanol using ultrasonic probe for 2 hours to form a uniform suspension. The prepared suspension was found to be very stable even after keeping it stationary for a long time. This suspension was added to commercially available BS powder for the preparation of 0 wt%, 2.5 wt% (BS-BNNS (2.5 wt%)) and 5 wt% BNNSs (BS-BNNS (5 wt%)) reinforced BS glass in the nylon milling jar shown in Fig. 5.3. (a). These mixtures were ball milled with ethanol as a solvent for 6 hours at 350 rpm using 3 mm and 10 mm zirconia balls (YTZ® grinding media, Tosoh

Corporation, Japan), shown in Fig. 5.3. (b), using planetary mill. The powder to ball weight ratio used was 1:25. Different sizes of milling balls were employed to ensure uniform and fine mixing of the mixtures[150]. The slurries hence produced were dried in oven in ambient atmosphere at 100 °C to obtain composite powders. The dried powders were crushed and sieved through 250 mesh sieve. Thereafter, the fine powders were dried at 300 °C for removal of excess ethanol trapped in the composite powder for 24 hours.

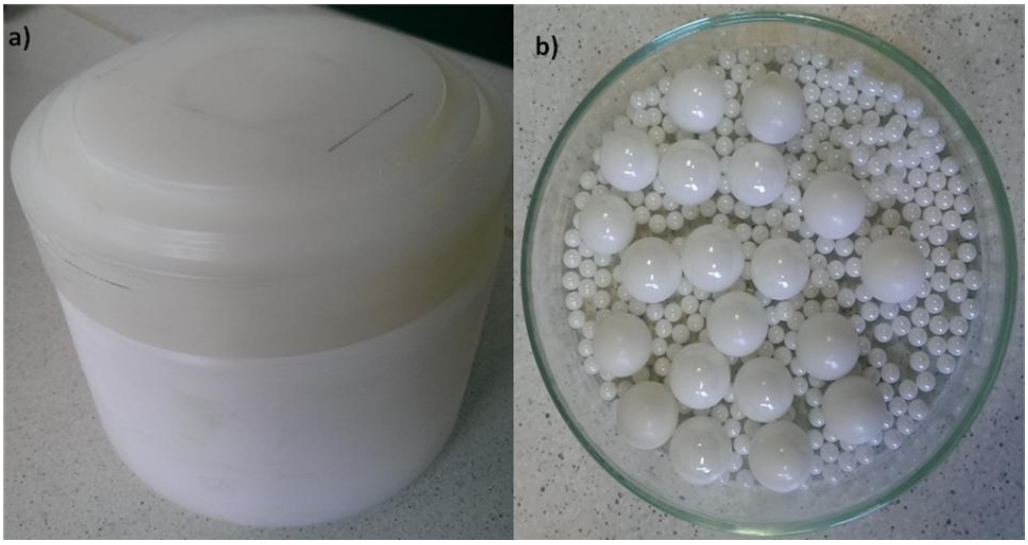

Fig. 5.3: Ball milling aids; a) Nylon ball milling jar; b) Zirconia balls with diameters of 3 mm and 10 mm

5.3. Sintering of BS-BNNS Nanocomposites

The BS-BNNS composites were processed and densified in the form of discs using the same methodology and conditions as that of BS-BNNT composites given in section 4.3. The SPS parameters profile of BS-BNNS (2.5 wt%) showing rate of change in temperature measured precisely by a thermocouple (shown in black), the average speed of the piston (shown in red), force applied by the piston (shown in blue) and the average relative piston travel (shown in green) with time is shown in Fig. 5.4.

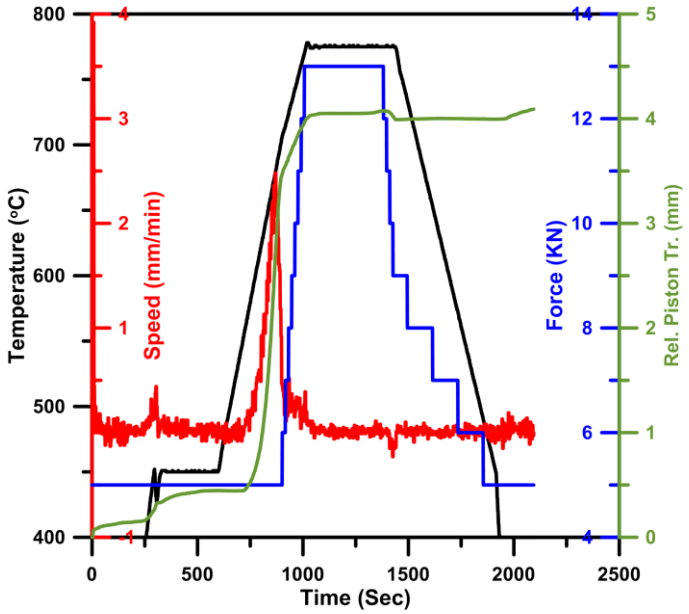

Fig. 5.4: Spark plasma sintering parameters profile for BS-BNNS (2.5 wt%) showing rate of change in temperature (black), the average speed of the piston (red), force applied by the piston (blue) and the average relative piston travel (green) with time

The bulk samples prepared by SPS were 20 mm in diameter. These samples were grinded by diamond wheels with 50-100 µm and 10-20 µm diamonds embedded in metal matrix. They were cut into beams by the linear saw (Buehler Isomet 5000). Further, the grinded beams were polished using diamond suspensions down to the level of 1 µm size of diamond particles to remove the visible defects observed with laboratory optical microscope. The setups required for the surface preparation of composite samples for the mechanical tests are given in Fig. 5.5.

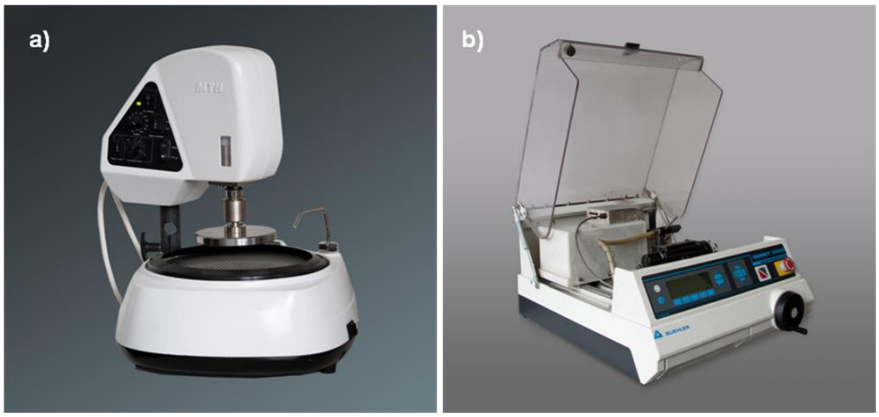

Fig. 5.5: Equipment required for surface preparation of samples; a) grinding and polishing wheel; b) Isomet 5000 saw for cutting of bars

5.4. Materials and Nanocomposite Characterizations

5.4.1. Scanning Electron Microscopy (SEM)

Field emission gun SEM (Tescan Lyra 3 XMU, Czech Republic) integrated with EDS unit was used to study the structure and morphology of produced BNNSs and BS-BNNS composite powders produced. For studying the morphology of BNNSs, a suspension of 0.1mg/ml of BNNSs in ethanol was prepared by ultrasonication. The suspension was drop casted on the surface of a carbon tape coated specimen holder and allowed to dry in ambient atmosphere, to remove the ethanol from the surface. The dried suspension was coated with a thin film of carbon. The sample preparation for the analysis of the composite powders and bulk bar samples after the mechanical tests were carried out following the same procedure as for BNNT.

5.4.2. Transmission Electron Microscopy (TEM)

Transmission Electron Microscopy (TEM) was carried out on JEOL JSM-2010 (Jeol, Japan) using the carbon grids for studying the morphology and structure of the BNNSs produced, shown in Fig. 5.6. For the sample preparation, a drop of suspension of BNNSs in ethanol (0.1 mg/ml) was drop casted on the carbon grid and allowed to dry in ambient atmosphere. High resolution analysis of the prepared BNNSs was carried out to study the crystal structure as well as the average thickness and length of the BNNSs produced. ImageJ analysis software was used for the statistical analysis of the thickness and length of the BNNSs.

Fig. 5.6: JEOL JSM-2010 Transmission electron microscope

5.4.3. Density Measurement for BNNS and Bulk Composite Samples

Density of the as produced BNNSs was measured by helium pycnometer (AccuPyc II 1340 Pycnometer) with an accuracy of 0.0001 g/cm^3. Nearly 0.25 g of BNNSs powder was used for the density measurements (carried out at Institute of Materials Research, Slovak Academy of Sciences, Košice, Slovak Republic). For the measurement of density of bulk bar samples, Archimedes principle was used.

5.4.4. Zeta-potential Measurement for BNNS

Neutral suspension (pH~7) of BNNSs in ethanol with a concentration of 0.1 mg/ml was prepared to measure the zeta-potential developed on the surface of BNNSs using Malvern Instrument-Nano ZS (carried out at Queen Mary University of London, UK). The procedure of sample preparation and measurement methodology was same as that for measurement of zeta-potential measurement for BNNT given in section 4.4.1.

5.4.5. TGA Studies for BNNS

TGA studies of BNNSs involved placing of 3 mg of BNNSs powder on a laboratory cleaned platinum holder and loading it to Q500 TGA, Universal V4.5A TA Instruments machine (carried out at Queen Mary University of London, UK). The effect of increasing the temperature from 0 °C to 900 °C on the weight of BNNSs present on the platinum holder was studied in ambient atmosphere under constant flow rate of N_2/air. This analysis could help us determine the oxidation behaviour of the material.

5.4.6. XRD Analysis for BNNS and Bulk Composite Samples

The XRD analysis of both the bulk sintered samples and the as produced BNNSs powder were performed using X'Pert diffractometer (Panalytical) using Co Kα radiation with a β filter in the secondary beam.

5.4.7. Young's Modulus for Composite Samples

The elastic modulus of the samples was measured using the impulse excitation resonance method using GrindoSonic Mk5i (J.W. Lemmens N.V., Belgium) on highly polished bar shaped samples using similar procedure as for BNNT reinforced composites.

5.4.8. Vickers Indentation for Composite Samples

Vickers indentation method (Zwick/Roell ZHU/Z2.5,Germany) with a mass of 1 kg (i.e. 9.8 N of load) was used to develop cracks in the BS and BS-BNNS nanocomposites to study the behaviour of the crack propagation in BNNSs reinforced composite matrix compared to pure BS glass.

5.4.9. Fracture Toughness Measurement by Chevron Notched Beams

Chevron notched bar samples were prepared for the measurement of fracture toughness. The notch was introduced into the beams with thin blades and the samples were measured using universal testing machine as in the case of BNNT reinforced composites using similar test conditions. The testing methodology is described in chapter 4 (section 4.4.8.).

5.4.10. Flexural Strength for Composite Samples

The flexural strength of the BS and composite samples bars was measured on highly polished bars (up to 1 µm diamond suspension), as the surface roughness plays a very important role in determining the accurate value of the strength. The bars were prepared with the nominal dimensions of 20 mm with chamfered edges to avoid the stress concentration on the sharp edges. The bars were loaded on the side perpendicular to the loading direction during SPS with a crosshead speed of 100 mm/min employing universal testing system, Instron 8862 (Instron, USA), on a 16 mm span. At least three specimens were measured for each composite concentration. The maximum force at which the bars were broken was recorded, which was used for the calculation of the flexural strength. The flexural strength of the sample bars was calculated using the following equation 5.4 according to the standard (EN 843-1:1995):

$$\sigma_f = \frac{3F_m \cdot l}{2bh^2} \ [MPa]. \qquad (5.4)$$

Here F_m denotes the maximum force (in N), l is the distance between the centres of outer support rollers in a three point bending set-up (in mm), b is the width, and h is

the thickness (dimension in crack propagation direction; expressed in mm) of the specimen.

5.4.11. Tribology Tests for Composite Samples

The wear behaviour of the BNNSs reinforced BS glass was analyzed by the help of DTHT 70010 tribometer (CSM Instrument, Switzerland) using non-lubricated ball-on-disc method (ASTMG99-03). The tests were performed on the sample using two types of balls, i.e. BS ball and alumina ball. The composite sample's surface were grinded and polished up to 1 μm diamond suspension to have mirror like surface (removing most of the defects observed by optical microscope). The specimens were glued to the holder and the tests were conducted with a normal force of 1 N by ball on the polished surface of the composite for both types of balls at room temperature employing a speed of 0.1 m/s for a track displacement of 500 m. The coefficient of friction was recorded continuously with respect to the distance moved by the balls on the wear tracks. The tracks were analyzed using confocal microscope (PLu neox, Sensofar-Tech, S.L., Spain) and the wear rate evaluated for the BS and BS-BNNS composite samples. Specific wear rate (equation 5.5) is defined as worn volume (V) per unit loading force (F_p) per unit sliding distance (L), i.e.

$$r = \frac{V}{F_p \cdot L}\left[\frac{mm^3}{Nm}\right]. \tag{5.5}$$

The worn volume is calculated by following equation 5.6:

$$V = A2\pi R\,[mm^3]. \tag{5.6}$$

Where A is the average of at least four values of the cross section area taken from different locations on the wear track observed by confocal microscope and R is the sliding radius of the ball on the disc (BS_R= 3 mm and $Alumina_R$= 7 mm). Specific wear resistance is also calculated by taking a ratio of specific wear rate for pure BS glass with specific wear rates of BS-BNNS composites for both 2.5 wt% BNNSs and 5 wt% BNNSs which determine the wear resistance improvement in the composites.

5.5. Results

5.5.1. Constituents Analysis Before Composite Preparation

The as-produced BNNSs were observed by SEM at a very high resolution. The BNNSs prepared, appeared to be transparent to the electrons as the thickness dimensions were in nanometers. The BNNSs observed by Tescan Lyra 3 XMU are shown in Fig. 5.7. These BNNSs were observed at a very high magnification of > 100 kx. Active shielding of the electrical signals was carried out in order to reduce the noise generated by the fluctuations of electrical signals at higher magnification during the analysis and recording of an image.

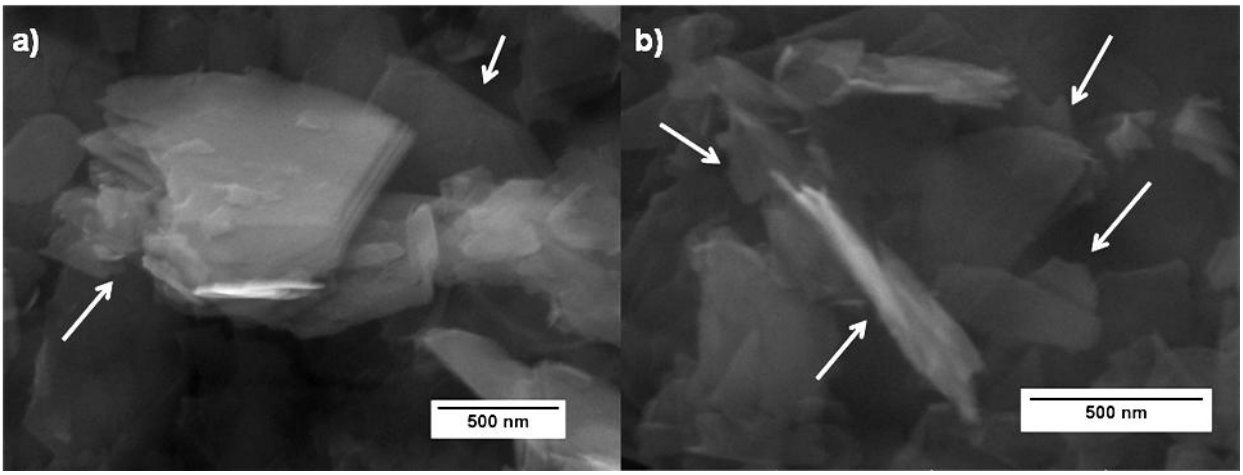

Fig. 5.7: SEM images showing; a) bunch of BNNSs stacked together; b) randomly scattered BNNSs placed in different orientation (marked by arrows)

TEM was used study the morphology and structure of BNNSs produced. Here as well, the BNNSs produced appeared completely transparent to the electron beam in low magnification due to extremely thin layers. The HRTEM images of the as produced BNNSs prepared by liquid exfoliation technique are presented in Fig. 5.8. (a). Observations of cracks in the BNNSs presented in Fig. 5.8. (b) were also encountered on several locations of the samples prepared.

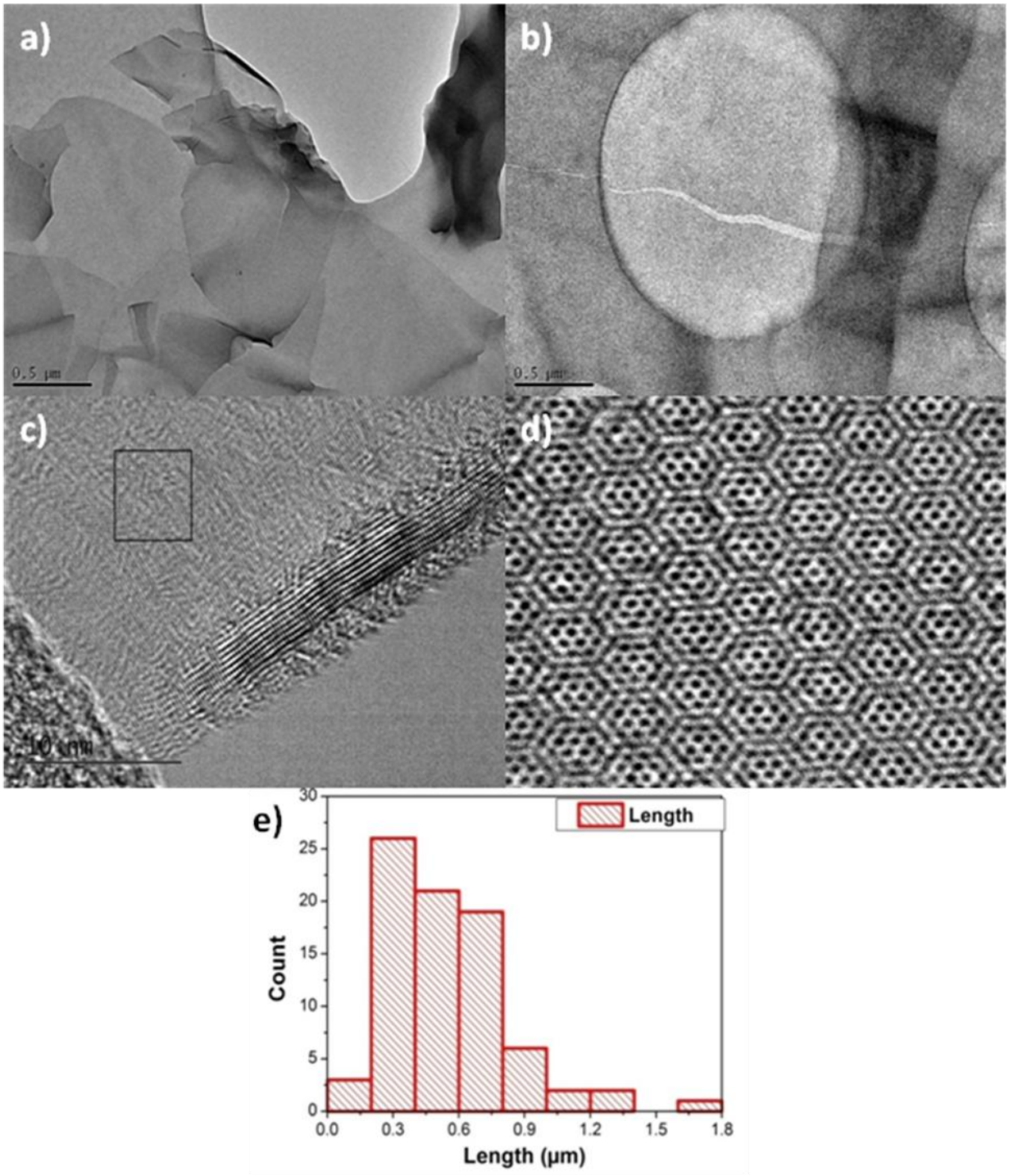

Fig. 5.8: (a) Low magnification TEM images of BNNSs; (b) Cracks observed in the BNNSs; (c) HRTEM showing fringes denoting curled BNNSs at edges; (d) Moiré patterns observed in BNNSs; (e) Statistic analysis of BNNSs along their length (longest dimension)

Fringes pattern was developed in BNNSs due to the curved edges of the stacked BNNSs (Fig. 5.8. (c)). These fringes were observed with the spacing distance between the fringes of 0.33 nm to 0.37 nm which is similar to the spacing of (002) plane of hexagonal BN crystal. In Fig. 5.8. (d), Moiré pattern is shown with the angle between the two stacking BNNSs was measured to be 12.5°. The length of the BNNSs was statistically analyzed by calculating an average of 100 different sheets shown in Fig. 5.8. (e) with an average size of 0.55 ± 0.29 µm along the longest dimension.

XRD measurements were carried out to investigate the crystalline behaviour of the BNNSs. The analysis of the BNNSs revealed that they were highly crystalline with ~99% pure phase. Co was used an anode for the formation of X-Rays, which detected a peak for BNNSs at 31.1°. The XRD analysis peak of BNNSs is shown in Fig. 5.9. (a). XRD was also conducted for BS - BNNS composites with BNNSs concentration of 0 wt%, 2.5 wt% and 5 wt% (Fig. 5.9. (b)).

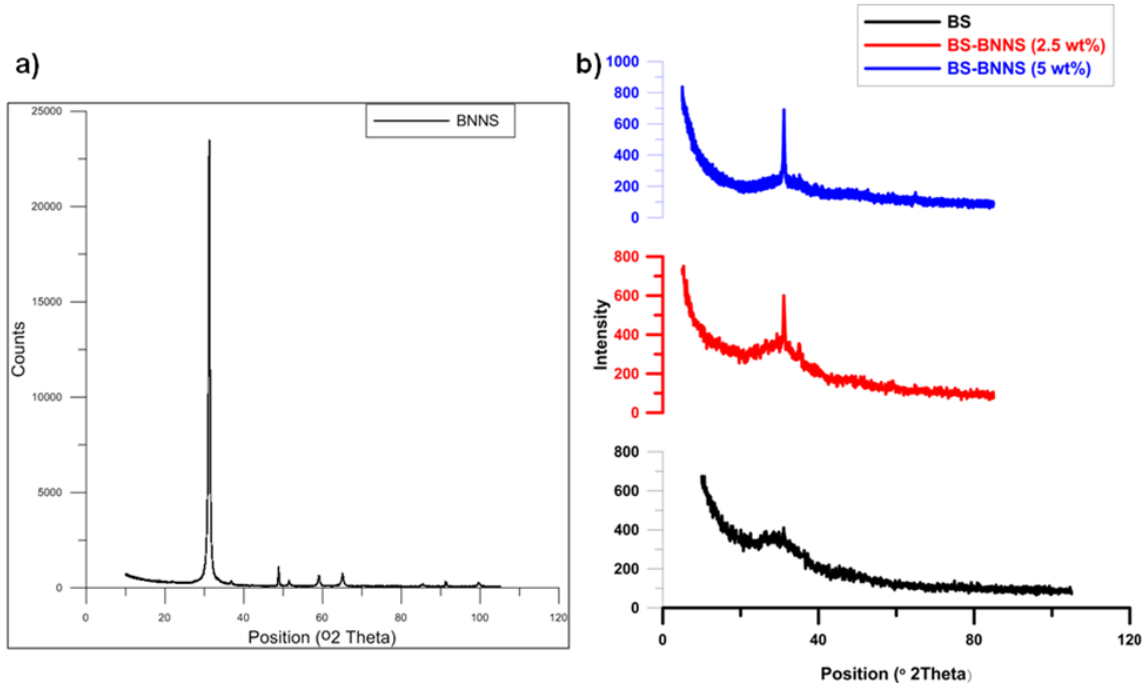

Fig. 5.9: XRD analysis of a) as produced BNNSs; b) BS and BNNSs reinforced BS with 2.5 wt% and 5 wt% concentration

The density of the boron nitride nanosheets were measured using helium pycnometer. After accounting the average of 20 values of measured densities, the density of BNNSs achieved was 1.8866 ± 0.0094 g/cm^3.

Along with other characterizations for BNNSs, the TGA was analyzed for as produced BNNSs. The recorded data for TGA is shown in Fig. 5.10. showing the rate of change of weight of BNNS with per degree increase in temperature in ambient air. The procedure of measurement for the TGA of BNNSs was similar as that of BNNT given in section 4.4.3.

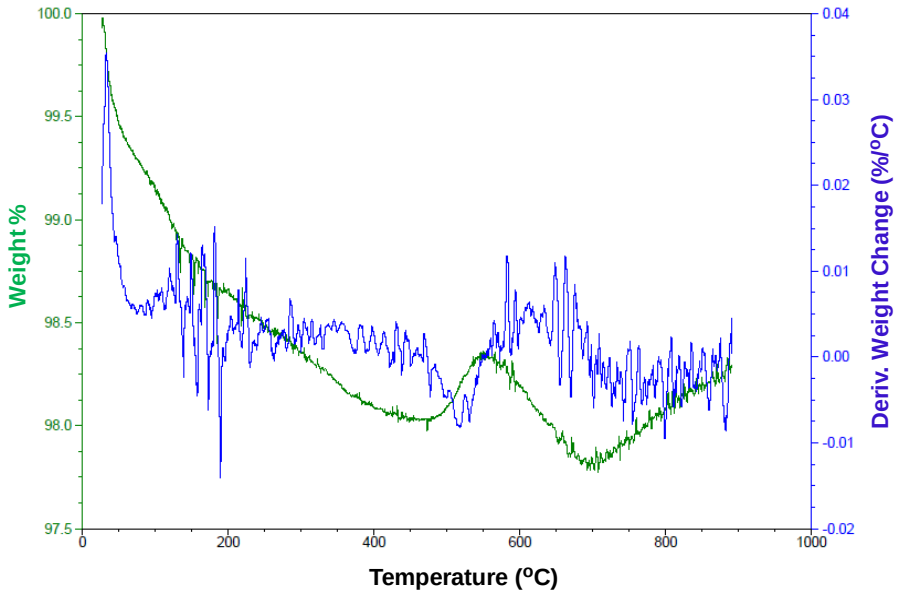

Fig. 5.10: TGA profile of as produced BNNSs

The plot for zeta-potential measurement for BNNS is provided in Fig. 5.11. The zeta-potential developed on BNNS in ethanol was measured to be -18.8 mV. It should be noted that the charge measured on the pure BS powder in ethanol was -21.3 mV as presented in section 4.5.1.

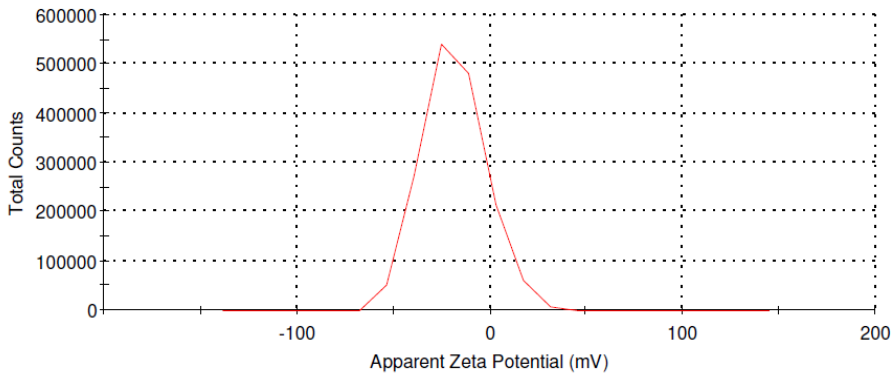

Fig. 5.11: Zeta-potential of BNNSs suspended in ethanol with concentration of 0.1 mg/ml

5.5.2. Microstructure Analysis

Post drying process for the composite slurry prepared by ball milling, the powder was analyzed using SEM. The SEM images of BS-BNNS powder composites after ball milling are presented in Fig. 5.12. The images show well dispersed BNNSs in the BS matrix. It was observed that the BNNSs prepared were not damaged due milling process after 6 hours.

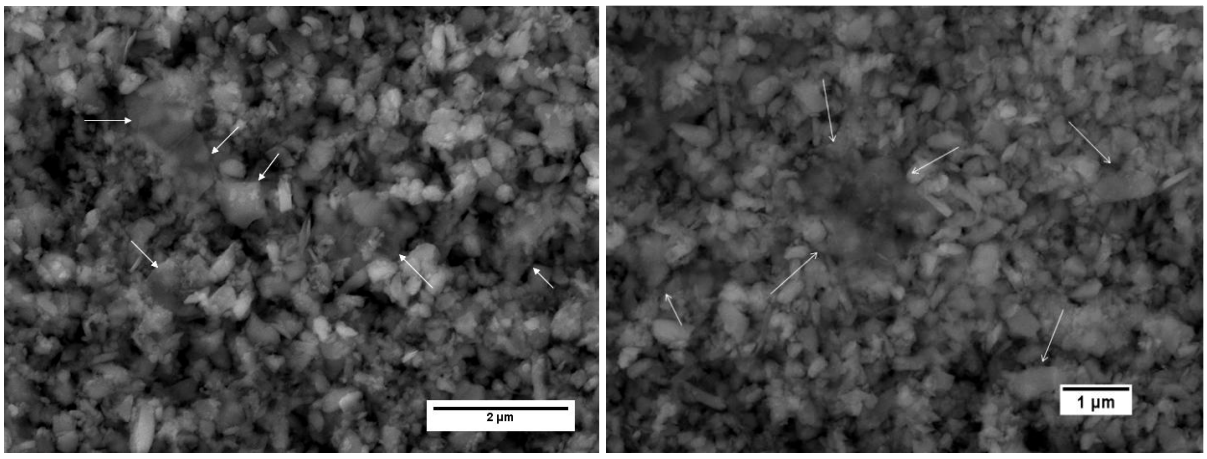

Fig. 5.12: Dispersion of BNNSs in BS composite after 6 hours of ball milling
(BNNSs shown by arrows)

The relative densities of the bulk samples were measured using Archimedes principle and were calculated according to the rule of mixture. The relative densities of the pure BS, BS-BNNS (2.5 wt%) and BS-BNNS (5 wt%) are presented in Table 5.1.

Table 5.1: Relative densities and Young's modulus of pure BS, BS-BNNS (2.5 wt%) and BS-BNNS (5 wt%) composites

Material	Relative density (%)	Young's modulus (GPa)
BS	98.50	71.9 ± 0.7
BS-BNNS (2.5 wt%)	98.78	74.0 ± 1.5
BS-BNNS (5 wt%)	98.80	73.3 ± 3.0

Table 5.1 also depicts the Young's modulus for BS as well as BS-BNNS composites. The change observed in the Young's modulus of the nanocomposites compared to BS glass was well in the scatter range.

5.5.3. Mechanical Properties

The fracture toughness of the BS-BNNS composite samples was measured using chevron notch technique. The value fracture toughness for the pure BS glass sample and BNNSs reinforced BS glass (0 wt%, 2.5 wt%, 5 wt%) are presented in Table 5.2 below. An increase in the fracture toughness for the BS composite samples with reinforcement concentration of 5 wt% of BNNSs is observed from the value of 0.76 $MPam^{1/2}$ to 1.10 $MPam^{1/2}$ showing an increase in the toughness by ~45%. Similarly, the values of the flexural strength are presented in Table 5.2 showed an increase of 45% in the flexural strength by reinforcing 5 wt% of BNNSs in BS matrix from 82.2 MPa to 119.0 MPa. The graphical representation of the almost linear increment of fracture toughness and flexural strength are presented in Fig. 5.13. Here, it should be noted that the use of 5 wt% of BNNT increased the fracture toughness of BS glass by ~30%.

Table 5.2: Fracture toughness and flexural strength of BNNSs reinforced BS glass composite

Sample	Fracture toughness (K_{IC})/MPa.$m^{1/2}$	Flexural Strength (σ_f)/MPa
BS	0.76 ± 0.05	82.2 ± 8.5
BS-BNNS (2.5 wt%)	1.01 ± 0.23	112.0 ± 13.8
BS-BNNS (5 wt%)	1.10 ± 0.11	119.0 ± 4.3

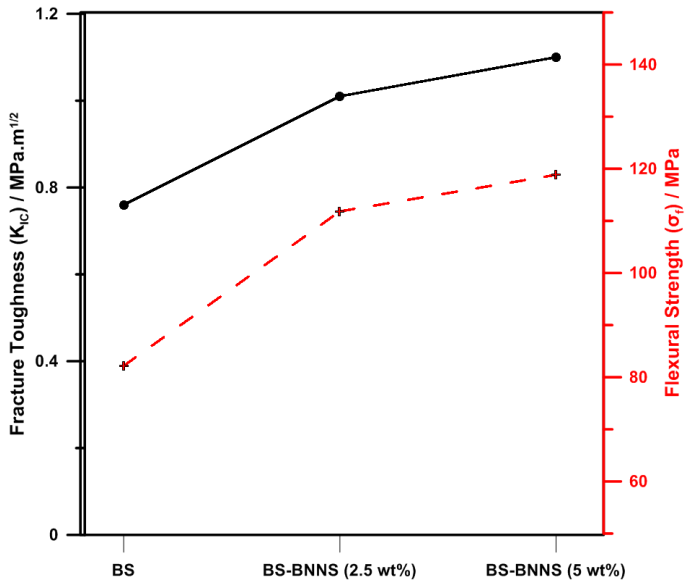

Fig. 5.13: Increase in the fracture toughness and flexural strength of BS-BNNS composites with increase BNNSs concentration

The dispersions of BNNSs in fracture surfaces of the broken specimens after testing were investigated using SEM. The BNNSs were found to be uniformly dispersed in all three concentrations of BNNSs reinforced composites. The dispersions can be seen in Fig. 5.14. The white arrows show the direction of applied stress during sintering of the specimens as well as direction of applied force for the measurement of fracture toughness. The BNNSs present in the composite matrix appeared to be thicker compared to the as produced BNNSs, shown in Fig. 5.8. (a), however, still being uniformly dispersed throughout the matrix. Fig. 5.14. also shows that the BNNSs were seen aligned to the direction perpendicular to direction of sintering of the specimens. The arrows depict the direction of applied force during sintering by SPS as well as during testing.

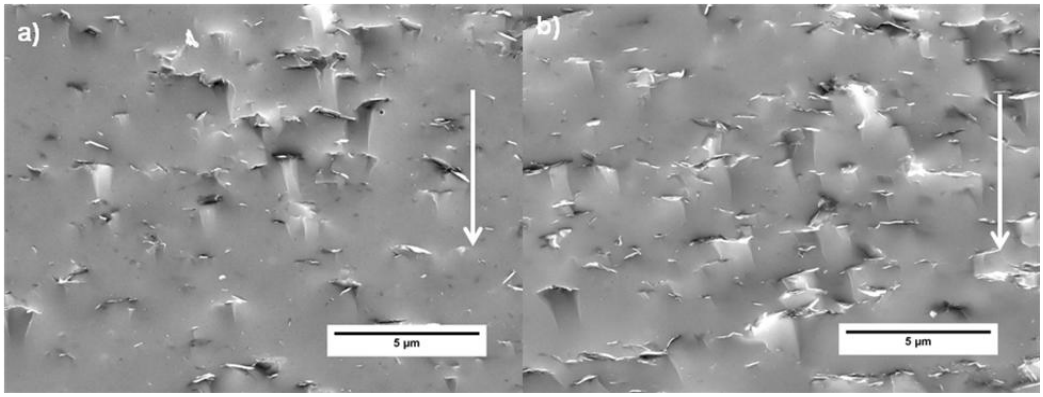

Fig. 5.14: Dispersion of BNNSs in BS for a) BS-BNNS (2.5 wt%); b) BS-BNNS (5 wt%) (arrows depicting applied force during fracture toughness measurement)

Fig. 5.15. shows the toughening mechanisms observed in BS-BNNS composite matrices. Fig. 5.15. (a) shows the pull-out of stacked layer of BNNSs from the matrix while the outer layer of the stack of BNNSs remained attached to the matrix. Fig. 5.15. (b) shows the crack behaviour observed in the pure BS glass which was relatively a straight path while Fig. 5.15. (c) depicts the crack deflection observed in BS-BNNS (2.5 wt%) composite. Fig. 5.15. (d) shows the crack bridging observed in BS-BNNS (5 wt%) composite.

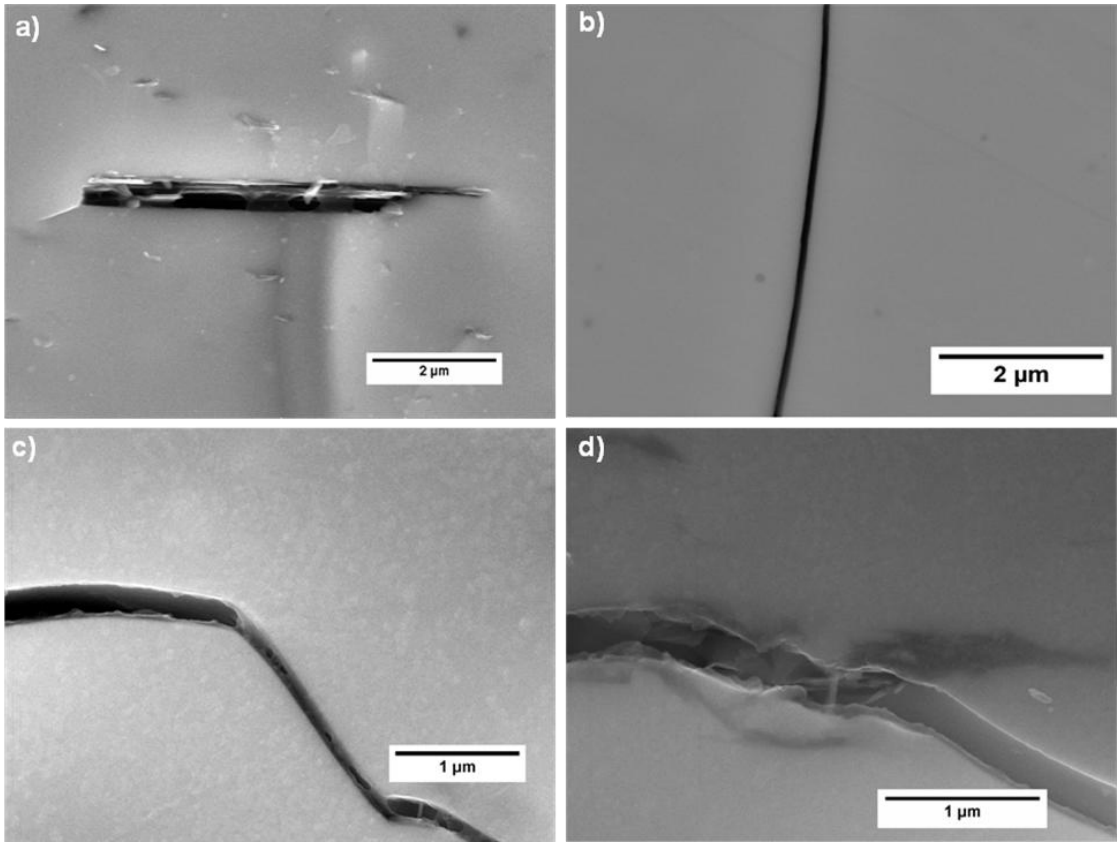

Fig. 5.15: Toughening mechanisms observed in BNNSs reinforced BS matrix a) Pull-out of inner layers of stack of BNNSs from BS matrix; b) straight crack in pure BS matrix; c) crack deflection observed in BS-BNNS (2.5 wt%) composite; d) crack bridging observed in BS-BNNS (5 wt%) composite

5.5.4. Wear Properties

Tribological tests were conducted for pure BS and BS-BNNS composites for 2.5 wt% BNNSs and 5 wt% BNNSs. These wear tests were conducted using two types of balls: BS and alumina. The Coefficient of Friction (COF), wear rate and normalized wear resistance are presented in Table 4.3 for the tribology tests performed by BS glass ball. It can be seen that with the increasing concentration of BNNSs up till 5%, the average COF decreases by 23 % for a sliding distance of 500 m. In fact, it was observed that there is a reduction of about 50 % of COF for initial 1 m of sliding track distance for BS-BNNS (5 wt%) composite compared to pure BS glass. The COF increased with the sliding distance as the surface roughness as well as the contact area for the BS ball increased with composite sample disc. For the initial phase of adding 2.5 wt% of BNNSs,

we noted an increase in COF from 0.78 for pure BS glass matrix to 0.83 for BS-BNNS (2.5 wt%).

Table 5.3: Values of COF, wear rate and wear resistance for Pure BS, BS-BNNS (2.5 wt%) and BS-BNNS (5 wt%) measured by tribological tests using BS ball

Sample	COF	Wear rate (mm^3/Nm)	Normalized wear resistance
BS	0.78 ± 0.16	12.95×10^{-4}	1
BS-BNNS(2.5 wt%)	0.83 ± 0.14	8.82×10^{-4}	1.47
BS-BNNS (5 wt%)	0.60 ± 0.09	4.93×10^{-4}	2.63

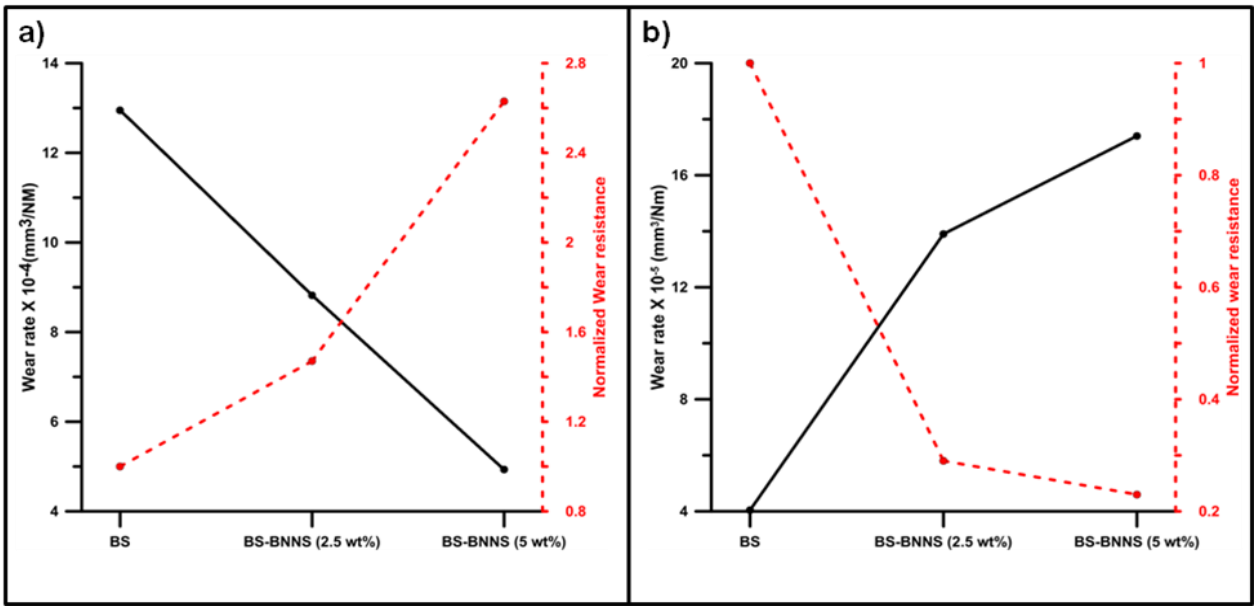

Fig. 5.16: Wear rate (black solid line) and wear resistance (red dashed line) for BS, BS-BNNS (2.5 wt%) and BS-BNNS (5 wt%) measured with; (a) BS ball; (b) alumina ball

The wear rates were measured after the completion of tests. There was a linear drop in the wear rate (as shown in Fig. 5.16. (a)) with the increasing concentration of BNNSs in the composite signifying the effective role of BNNSs in the matrix from 12.95×10^{-4} for pure BS glass to 4.93×10^{-4} for BS-BNNS (5 wt%). The wear resistance of the composites showed a marked increase of ~2.6 times by the introduction of 5 wt% of BNNSs compared to pure BS.

5.6. Discussions

5.6.1. Constituents Analysis Before Composite Preparation

During the SEM studies, it was observed that as ethanol was used as a solvent for the suspension, post the drying process of the ethanol suspension of BNNS on carbon tape, the suspended BNNSs came closer and then layered on each other randomly on the carbon tape as can be seen in Fig. 5.7. (a) and (b).

The ultra shearing of precursor boron nitride bulk powder by high frequency sonic waves lead to delamination of boron nitride nanolayers from the defect sites of the bulk powder and hence BNNS were produced (Fig. 5.8. (a)). The nanosheets after delamination from the bulk BN powder were broken to nanosheets of smaller dimensions due high power shearing by cracking, shown in Fig. 5.8. (b). The shearing process helped to break the non covalent bond between the bulk BN powder layers. The solvent played a very crucial role in the BNNSs synthesis process, as post-exfoliation interaction of highly polar solvent (NMP) with BNNSs formed, helped BNNSs to remain deagglomerated[151]. The spacing distance between the patterns of the fringes, seen in Fig. 5.8. (c), helped to deduce the number of layers of BNNSs present in the total stack. As per the calculation, the thickness of BNNSs varied from 4 to 30 layers. Fig. 5.8. (d) shows the Moiré patterns observed in the BNNSs due to overlapping of layers of BNNSs. The Moiré patterns were generated due to rotational misorientation due to overlapping of BNNSs at different angles.

The peak value of 2 theta observed for the XRD of BNNS and composite samples, i.e. 31.1° (Fig. 5.9.) differed from that given in the literature referred[74] due to the use of different anode material (Cu) in literature. The ratio of the crystal parameters c/a for the BNNSs was observed to be 2.66 which is slightly higher than standard h-BN value of 2.658 (JCPDS 340421). This suggests that there is expansion of basal planes by 0.08%. It was observed that the composites reinforced with BNNSs were completely amorphous except for crystalline peak of BNNSs at 2 theta value of 31.1°. The intensity of the given peak increased with the increasing concentration of BNNSs in BS glass matrix.

For TGA measurements, we observe a weight loss of about 2% up to ~450 °C (Fig. 5.10.) after which we see an increase in the weight which may be due to formation of some compounds formed due to presence of some residues in the BNNSs. The compounds, however, get completely decomposed at 650 °C. At this stage, the rise of weight may be subjected to oxidation of BNNSs.

Ethanol was considered as a favourable solvent for ball milling for preparation of BS composites reinforced with 2.5 wt% and 5 wt% BNNSs because of the high negative surface charge developed on BNNSs, i.e. -18.8 mV in ethanol (shown in Fig. 5.11.). The same surface charge in high magnitude on BS and BNNSs aided to avoid agglomeration of BNNSs resulting in good dispersion of BNNSs in BS glass matrix.

5.6.2. Microstructure Analysis

Higher densities achieved after the SPS (as shown in Table 5.1) clearly indicated that the BNNSs were well dispersed in the matrix. It has been observed that the agglomeration of reinforcements can play a distinct role in lowering of the density by the creation of pores[6,57,146]. These agglomerates can additionally lower the density of glass by hindering the viscous flow of glass during sintering thus acting as a hindrance to densify the composite completely[146].

No significant difference of Young's modulus was observed in composites compared to pure glass given in Table 5.1. This may be due to the presence of higher cohesion strength between BNNSs and BS. Due to high bonding strength between BS and BNNSs, composites behaved as pure glass until the glass approached peak load at which de-cohesion between the interface of BNNSs and BS took place. However, in the literature, a decrease of the Young's modulus is reported with the increasing concentrations of reinforcement. This is associated with a reduction in the relative density of the nanocomposite. Such behaviour has been reported for graphene composites[14] and CNT composites[152].

5.6.3. Mechanical Properties

As observed by SEM on the fracture surfaces, the reason for the thicker BNNSs could be the overlapping of BNNSs which occurred during the drying process of the slurry after milling. The uniformly dispersed BNNSs in ethanol come close and overlap when the solvent from the slurry evaporates. Porwal et al. also observed similar overlapping for increasing concentrations of graphene in alumina matrix from 0.2 vol% to 5 vol%[7].

The enhancement of fracture toughness of the composites was due to several toughening mechanisms observed in the matrix. It is difficult to judge the most pre-dominant toughening mechanism from the quantitative viewpoint in the matrices. The interfacial bonding between the matrix and the filler plays a crucial role in determining the filler's pull-out as the pull-out occurs when the shear stress is higher than the interfacial bonding between the filler and the matrix[94]. The applied stress provided energy to the BNNSs embedded in the matrix to pull-out and energy was utilized for breaking the bonding between the matrix and the BNNSs. The pulling out of BNNSs also lead to development of frictional forces at the interface between matrix and BNNSs, which helped in relaxation of stress experienced by the matrix which in turn enhanced the toughening of the composite[94]. It was observed that sometimes the bonding was so strong, that the outer layers of the stacking BNNSs, which were embedded in the matrix, were still left attached at the interface of BS and BNNSs while the inner BNNSs from the stack were pulled out breaking the weak inner Van der Waals forces in between the nanosheets analogous to sword-in-sheath mechanism observed in nanotubes. This observation, as shown in Fig. 5.15. (a), leads us to believe that BNNSs experienced strong bonding with the BS matrix.

For analyzing additional toughening mechanisms, matrix indentation was carried out to study the crack behaviour and its interaction with the BNNSs. Fig. 5.15. (b) shows the crack path for pure BS matrix in which the crack does not encounter any features inbuilt in the matrix perturbing its nature and growth. However, by introducing BNNSs into the matrix, the crack introduced after the indentation process encountered many features affecting its path. Fig. 5.15. (c) shows the crack deflection path of the propagating crack in the nanocomposites due to

interaction of the crack with the BNNSs reinforced in the BS matrix. Crack deflection can also be clearly seen in Fig. 5.14. (a) and (b). The coefficient of thermal expansion (CTE) of the BN is negative (-2.9 × 10^{-6} K^{-1} at 293 K along a axis)[153] while the CTE of the BS is 3.3 × 10^{-6} K^{-1}. CTE plays a very important role in determining the filler behaviour in the matrix. The CTE for BNNSs and BS indicate that during the cooling process, the BNNSs expanded while the BS matrix shrank. This leads to hoop compression stress on the expanding BNNSs in the matrix. Therefore, when the crack interacts with the BNNSs embedded, it is forced to deflect from its path around the 2D surface of BNNSs (clearly seen in Fig. 5.14. (a), (b) and Fig. 5.15. (c)). The tortuosity of the path of the crack around the BNNSs as well as generation of internal stresses inside the matrix contribute to the deformation energy dissipation and to the toughening of the BS composite.

Another toughening mechanism, commonly observed in the composites was crack bridging. During the process of crack propagation, the crack encountered BNNSs embedded in the matrix, which anchored the matrix and acted as a bridge, delaying the further opening of the crack. It was observed that the thickness of the crack after encountering of BNNSs reduced up to 55% of its previous thickness in the composite matrices. Even if we compared the opening of crack just nearby the indent for BS, we observed an opening ~350-400 μm while the opening of crack near the indent BNNSs reinforced BS observed was ~200-300 μm. The bridging ensures higher toughening of BNNSs reinforced BS composites. All the above mentioned toughening mechanisms effectively contribute to the increase in fracture toughness of BS-BNNS composites by 45%.

The rise in the flexural strength of the composites can be attributed effective transfer of elastic energy gained by the BS matrix to BNNSs embedded in the matrix due to favourable interfacial bonding between them. This contributes to the rise of ~45 % of flexural strength of composite compared to the pure matrix[31,55,57].

5.6.4. Wear Properties

During the testing of the wear properties, the reduction in the COF for the BS-BNNS (5 wt%) composite could be due to multi-layer of BNNSs stacked in the BS

composite matrix which acted as a lubricating surfaces for the composites thereby reducing friction on the surface during sliding. We observed a minor increase in the value of COF with increasing the concentration of BNNS in BS from 0 to 2.5 wt%. It could be due to the reason that 2.5 wt% of BNNSs might not be enough for the matrix to introduce the lubrication property to the matrix. However, over a certain critical concentration, friction started to decrease and therefore we observed a reduction in COF of BS-BNNS (5 wt%).

The drastic improvement in the wear resistance could be explained by the high loading concentration as well as uniform dispersion of BNNSs. With higher concentrations of BNNSs which were found to be uniformly dispersed, a well connected network of BNNSs was formed in the composites providing higher lubrication on the surface which aided in sliding and limiting friction[101]. Moreover, the 2D morphology of the BNNSs also created a lubricating layer on the surface limiting the damage caused due to wear testing[14]. The dramatic increase in the wear resistance could also be linked to the improved mechanical properties which were observed for BS-BNNS composites.

The hardness of the alumina ball is much higher than of BS ball as well as the BS matrix used in the composite, therefore, very low wear was observed the alumina ball after the completion of wear tests through alumina ball. It may be due to this reason, a negligible change in the COF of the composite with 5 wt% of BNNSs (0.84 ± 0.05) was observed compared to pure BS glass (0.86 ± 0.06) which is well in the scatter range. The higher hardness of alumina ball used a counterpart could also be the reason for increased wear rate and reduced wear resistance observed for the samples. We observe such high increase for wear rate in the BS-BNNS (5 wt%) composite as introduction of higher concentration of fillers resulted in comparatively softer material then pure matrix[7,14,79]. Fig. 5.16. (b) shows the change in the wear rate and wear resistance with increasing concentration of BNNSs measured using alumina ball as a counterpart[154]. Therefore, judicious selection of counterpart is quite necessary for the appropriate measurement of the tribological properties of these types of composites[154].

Chapter 6- Comparative Analysis

In this chapter, we would like to discuss about the role of BNNS and BNNT on BS matrix by comparing their effect as reinforcements. This chapter also presents the role of BNNT (from above work) in comparison to much studied CNT reinforced glass composites reported in the literature as well as role of BNNS (from above work) in comparison to graphene reinforced glass composites reported in the literature.

6.1. Comparison of the Effect of BNNS and BNNT as Reinforcements in BS Matrix

BNNS and BNNT are both made from the same source precursor of boron nitride therefore they possess similar functional properties in a broader aspect. However, from the mechanical reinforcement point of view, they exhibit different properties in terms of geometrical aspects as well as the available surface area.

As can be seen in chapter 4 and chapter 5, the BNNS offer better improvement in fracture toughness of BS glass (~45%) in comparison to increase offered by BNNTs (~30%) with 5 wt% concentration. Even the use of different morphologies of BNNTs, i.e. bamboo type and cylindrical shape, also did not contribute to any significant change in these properties.

The role of these reinforcements in the brittle matrices was to increase the toughness of the material so that the failure of the material was delayed in comparison to general catastrophic failure experienced in the pure glass matrix. As explained in earlier chapters, although the properties of the reinforcements are important, the interface between the reinforcement and the matrix plays a major role in determining the mechanical properties of the composites. The role of BNNS as a mechanical reinforcement was more pronounced in comparison to the BNNTs because of several factors as follows.

6.1.1. Surface Morphology

The BNNS possess comparatively rougher and uneven morphology of the surface compared to the BNNTs. BNNSs exhibit higher roughness compared to BNNTs due to presence of higher defect density on the surface of BNNSs. These defects were created during high energy shearing during the synthesis of BNNS which was required to peel the BNNS from the defect sites of bulk BN powder but it also affected the surface of produced BNNS. The uneven surface helped in better interlocking of BNNS and BS matrix at the interface during sintering process compared to comparatively smoother surface morphology of the BNNTs. The interlocking at the interface helped in efficient (and in ideal conditions, complete) load transfer from the matrix to reinforcement thereby improving the toughness of BS matrix.

6.1.2. Higher Surface Area

BNNS possess larger surface area in comparison to BNNT. It has been reported that the surface area calculated by Brunauer-Emmett-Teller (BET) method for a few layers of BNNS was ~927 m^2/g [96] and the surface area calculated by BET method for BNNTs was 200-300 m^2/g [97]. The advantage of higher value of surface area for BNNS was that it provides larger contact surface available to the matrix due to 2D structure (sheet structure). This enabled more interaction, both above and below the sheet, compared to lesser contact due to tubular structure of BNNT where matrix could not penetrate inside the tube. It also contributed to the better load transfer from the matrix to the BNNS improving the toughening of the matrix.

Table 6.1: Young's modulus (GPa) for BS-BNNT (2.5%, 5%) with cylinder and bamboo like BNNTs and BS-BNNS (2.5%, 5%) determined experimentally

Concentration	BNNT	BNNS
0%	72.1 ± 0.4	71.9 ± 0.7
2.5%	C- 69.4 ± 0.4	74.0 ± 1.5
	B- 68.5 ± 0.8	
5%	C- 68.0 ± 0.4	73.3 ± 3.0
	B- 67.4 ± 0.7	

The higher interfacial bonding in the BNNS compared to BNNT could be justified by the values of Young's modulus calculated for both the reinforcements as shown in Table 6.1. Although, there is no significant change in the Young's modulus for both cases still we see a reduction of 7% of Young's modulus for BNNT while for BNNS, the values of Young's modulus float in the same range as for pure BS glass signifying higher interfacial bonding present.

6.1.3. Geometrical Benefits

BNNSs having 2D geometry possess added advantage as compared to 1D geometry of the BNNTs. When the micro-crack propagation came in contact with the BNNSs, the toughening mechanisms were encountered in two dimensions around the nanosheets, i.e. along length and breadth (thickness dimension in nm). The crack was forced to deflect or move around the BNNS. The energy dissipation to overcome the barrier of BNNS for the crack propagation around the nanosheets or by pulling them out must be comparatively higher in comparison to the BNNTs. Crack deflection is the most effective toughening mechanism which is advantageous and responsible for higher values to fracture toughness for BNNS (Fig. 6.2.)

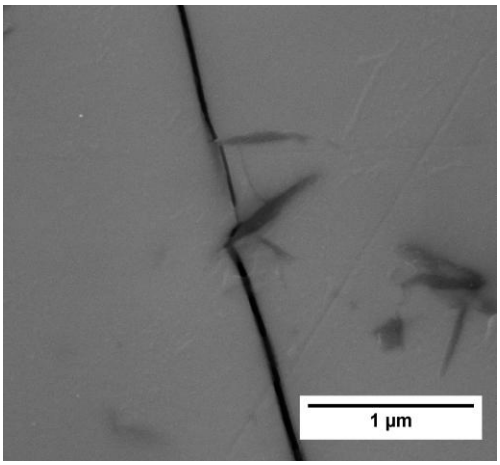

Fig. 6.2: Crack deflection observed in BS-BNNS (2.5 wt%)

6.1.4. Agglomeration

Nano reinforcements suffer from a severe drawback of agglomeration due to high surface energy and they cannot be utilized to full potential if they suffer from agglomeration therefore well dispersed phases of nano reinforcement are required. Geometrically, owing to the 2D structure, the BNNSs have far lesser tendency to agglomerate in comparison to BNNTs thereby improving the properties of BNNSs reinforced composite more than that of BNNTs reinforced glass.

Other than the above mentioned properties, the use of BNNSs as reinforcements is more cost effective as preparation of high quality BNNSs can be carried out by far more convenient methods compared to BNNT. BNNSs preparation methods also provide quantitatively much better final yield after preparation compared to BNNTs. Other than complicated fabrication methods, BNNTs have to be functionalized in order to prevent agglomeration though due to inert nature of BNNT, it is a difficult task. Therefore, use of BNNSs as reinforcements appears to be more beneficial compared to BNNTs.

6.2. Comparison of the Effect Reinforcing BNNT with CNT in BS Glass

BNNTs are analogous in structure and properties to CNTs. Many reports have been published regarding the effect of CNTs as a reinforcement on borosilicate glass[53,155,152] as a matrix. Boccaccini et al.[53] reported that with the reinforcing concentration of 10 wt% of multi walled CNTs in BS glass by powder processing and hot pressing, they experienced a reduction in the mechanical properties of the borosilicate matrix. They suggested the reason for this behaviour was the agglomeration of CNTs leading to ~9% residual porosity which was not infiltrated by the BS during sintering. They also experienced uneven distribution of the aggregates throughout the matrix due to which they also encountered different properties (large scatter) in different part of the samples. They recommended that the use of vigorous acid treatment could help functionalising the surface of CNTs and hence aid in better dispersion which could lead to higher densities achieved and thereby enhance the mechanical properties. However, one of the main drawbacks of this acid treatment is shortening of length of CNTs and creation of defects on the CNT walls.

On the other hand, in our work, it is reported that use of a smaller concentration (5 wt%) of BNNTs itself improved the fracture toughness of the composite by nearly 30%. The reason for this improvement was efficient dispersion methods carried out to avoid agglomeration of the BNNTs inside the matrix without any acid functionalization of BNNTs. In fact, functionalization of BNNT is very tedious task due to inert nature of BNNTs therefore it can be said that the BNNTs do not functionalize even after the acid treatment for purification which was confirmed by FTIR (not shown in the results). The improvement in the mechanical properties by reinforcing BNNT could also be attributed to better wetting of BNNT by BS due to better interaction at the interface leading to enhanced load transfer of the matrix to BNNTs thereby improving the toughness of the brittle BS glass matrix.

Boccaccini et al.[53] also reported a formation of cristobalite phase during the sintering of BS matrix by hot pressing. They attributed that CNTs were the reason of such behaviour as they acted as a nucleation site and also it lead to the shrinkage of the matrix which is pre-requisite for the formation of crystalline phase. No such behaviour was seen in case of BNNTs reinforced BS composites (section 3.6.2.) and high densities were achieved for BNNTs reinforced BS composites despite the presence of small pores all over the surface left due to residual Fe in the matrix. The uniform dispersion of BNNTs ensured uniform properties (less scatter) throughout the matrix. The random alignment of BNNTs supported isotropic properties developed throughout the tested samples.

Additionally, study of mechanical properties of BS glass reinforced with single walled CNTs (SWCNTs) have also been reported by Ghosh et al.[155] Their composite samples were prepared by melt quench technique and no porosity of the samples was seen for 2 wt% of SWCNT reinforced on BS glass. They reported an increase in indentation fracture toughness of about 11% for their samples due to cushioning effect of highly agglomerated SWCNT around the crack zone during testing. In comparison to these reported results, we observed an increase of ~17% with reinforcement of 2.5 wt% of BNNT-C. We assume that the improvement in the case of BNNTs reinforced composites is more in compared to similar concentration of SWCNTs because the BNNTs were well dispersed in the matrix and the interface interaction of BNNT with

matrix was much more pronounced in comparison to CNTs. These interfacial interactions helped in achieving much more toughening mechanisms in our samples.

Therefore BNNT can act as new form of reinforcements in place of CNT producing similar or higher improvement in the mechanical properties. They can specifically be used in high temperature, insulating and chemically resistant applications.

6.3. Comparison of the Effect Reinforcing BNNS with Graphene in Glass

BN bulk powder is slightly polar, they have dangling bonds, and due to slightly ionic nature have better bonding with the matrix compared to Van der Waals weak interface of graphene[156]. Studies on the use of 2D nanomaterials as a mechanical reinforcement for borosilicate matrix has been rather limited.

Graphene oxide nanoplatelets (GONP) have been used in silica matrix by Porwal et al.[14] to improve its mechanical properties like toughening and machinability. With reinforcing 2.5 vol% of GONPs, they observed an increase of fracture toughness by ~35%. We observe a similar improvement by ~33% in the fracture toughness of borosilicate glass by reinforcement of 2.5 wt% of BNNS while achieving similar density of the composites produced. However to experience such improvement, they have used commercially obtained GONPs and not graphene nanoplatelets because the oxide functional groups helped in better interaction of graphene with the silica matrix thereby avoiding the overlaps of the graphene itself. It helped in improvement of the toughening mechanisms observed. Colloidal processing method was used to prepare composite with better dispersion as they could not observe good dispersion in powder processing. We observe a good dispersion of BNNSs with powder processing itself. Fig. 6.3. depicts the dispersion observed in the present work for 2.5 wt% BNNS in BS glass produced by powder processing and dispersion of 2.5 vol% GONPs in silica matrix. The comparable dispersion could be a result of slightly ionic nature of BN which helped it to bind with the matrix covalently affecting the role of BNNS in BS glass.

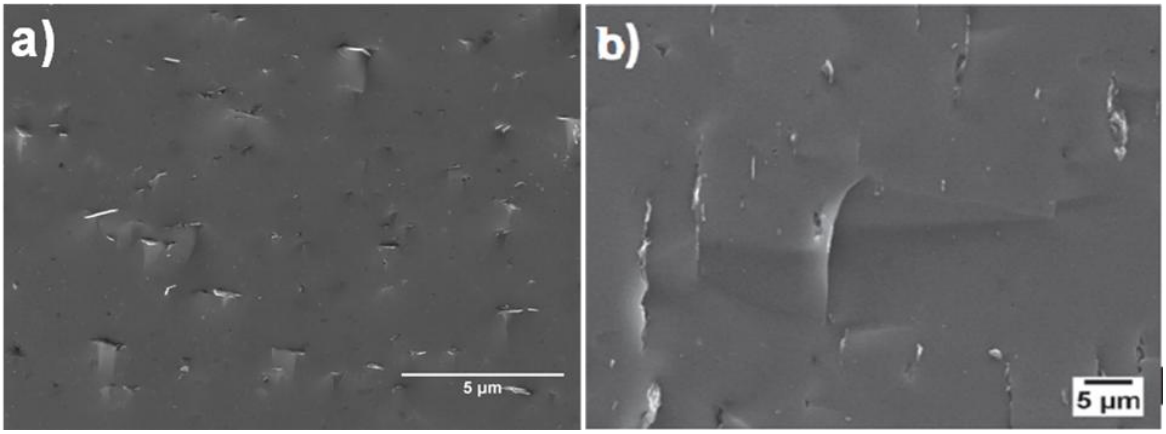

Fig 6.3: Dispersion of; a) BS-BNNS (2.5 wt%) produced by powder processing; b) Silica-GONP (2.5 vol%) produced by colloidal dispersion method by Porwal et al.[14]

Therefore, BNNS can conveniently replace graphene as a mechanical reinforcement for high temperature, insulating and chemically resistant applications for composites while significantly improving the mechanical properties of the composites prepared.

Chapter 7- Conclusion

In the present work, various issues dealing with preparation and processing of BNNT and BNNS reinforced BS glass composites were investigated as well as optimized to achieve the best results. These composites were characterized for their microstructural, mechanical and tribological properties. The effects of reinforcing different geometries of BN nanomaterial were studied. Interestingly, 1D (BNNT) and 2D (BNNS) geometry of BN materials showed different results despite having same/similar functional properties.

7.1. BNNT and BNNT Reinforced BS Glass Composites

BNNT with two morphologies, i.e. cylindrical type and bamboo like were used to reinforce amorphous BS glass with concentration 0 wt%, 2.5 wt% and 5 wt%. The present results clearly signify that increasing concentration of BNNT directly influenced the properties of BNNT reinforced BS composites.

The as-received standard quality BNNT did not improve the mechanical properties of bulk composites due to presence of small pores throughout the surface due to Fe impurities present in the BNNTs. Successful purification of BNNTs was carried out to remove the Fe impurities by acid washing leading to reduction of Fe impurities from ~54 wt% down to 1 wt%. The main results are summarized as follows:

1. Well dispersed BNNT-BS glass matrix composites were prepared using powder processing routes.

2. Highly dense samples were achieved using optimized condition for SPS with a density of ~98% by reinforcing 5 wt% of BNNTs. It was also observed that the increasing concentration of BNNTs lead to decrease in density compared to pure glass because of addition of second phase which acts as a hindrance for viscous flow of glass during sintering.

3. A unimportant decrease of ~7% was observed in the hardness and Young's modulus of the 5 wt% reinforced BNNTs composites compared to pure BS glass due to decrease in relative density.

4. The fracture toughness measured by Vickers indentation method and by chevron notched beam was quite similar showed an increase of ~30% for 5 wt% purified BNNT reinforcement compared to pure glass.

5. Pull-out, crack bridging, BNNT stretching and crack deflection were the main toughening mechanisms observed for prepared composite materials.

6. Shorter lengths of bamboo like BNNT (~0.5μm) were pulled out in comparison to cylindrical type BNNT (~1.5μm) as with the force, the bamboo links of the bamboo type nanotubes were easily disconnected from the joints.

7. Stretching of entangled BNNTs was uniquely observed as a strong toughening mechanism the matrix where the entangled BNNT were anchored on both edges of the crack opening ultimately leading to lesser opening width of the crack.

8. Sword-in-sheath mechanism was observed for BNNTs and the outer layer of the multiwalled nanotubes had a strong bonding interface with the matrix.

9. Efficient load transfer from the matrix to the BNNTs was observed leading to enhancement in fracture toughness of the glass composites.

10. Improvement in the scratch resistance (~26%) was observed for glass composites by incorporating ~5 wt% of BNNT in BS glass.

7.2. BNNS and BNNS Reinforced BS Glass Composites

1. BNNSs were successfully prepared using liquid exfoliation technique by delamination of the BNNS from the defect site producing BNNSs with the longest dimension of ~0.55 ± 0.29 μm.

2. BNNSs prepared were highly crystalline and the oxidation temperature for the BNNSs was ~650°C.

3. These BNNSs were used as reinforcement for BS glass and the well dispersed BNNSs based composites were prepared by powder processing and consolidated by spark plasma sintering with the concentrations of loading of BNNS as 0 wt%, 2.5 wt% and 5 wt%.

4. The density of the samples under the specific SPS conditions applied observed was quite high (i.e. > 98.5%) even after reinforcing 5 wt% of BNNS signifying limited agglomeration in the BNNSs dispersed in the matrix and the composite samples were observed to be completely amorphous except for the crystalline peak of BNNS observed.

5. No or negligible change in Young's modulus of the composite samples was observed in comparison to the pure BS glass which indicated the high bonding strength between the BS and BNNS interface making the composite behave as a monolithic glass in the initial phase before de-cohesion started to take place while reaching the final load.

6. Improvement in the fracture toughness by ~45% each for 5 wt% of BNNS reinforced BS composite (1.10 $MPa.m^{1/2}$) was observed in comparison to pure glass (0.76 $MPa.m^{1/2}$).

7. Toughening mechanisms like pull-out, crack bridging and crack deflection were the main observed for the characterized composite materials. The BNNSs were

observed to be aligned perpendicular to the direction of applied force during sintering and uniformly dispersed throughout the matrix.

8. Improvement in the flexural strength by ~45% each for 5 wt% of BNNS reinforced BS composite (~119 MPa) was observed in comparison to pure glass (~82 MPa).

9. Good interfacial bonding for BNNS and BS glass matrix was observed leading to efficient load transfer and ultimately contributing to improvement in the fracture toughness and flexural strength.

10. Improvement in the tribological properties of the BNNS reinforced BS glass composites were observed by using BS glass ball as a counterpart. A reduction of ~23% of coefficient of friction was observed by incorporating 5 wt% of BNNS in BS glass due to the lubrication effect of BNNSs present on the surface which aided in easy sliding of the counterpart.

11. The wear rate drops linearly by using BS ball as a counterpart with increasing concentration of BNNS from 0 wt% to 5 wt% reaching a minimum of 4.93×10^{-4} mm^3/Nm for BS-BNNS (5 wt%) in comparison to pure glass (12.95×10^{-4} mm^3/Nm) due to 2D morphology of the BNNS which were well connected and uniformly dispersed the matrix providing highly lubricated surface thus reducing the wearing of the composite disc during BS ball sliding.

12. The wear rate increases drastically by using the alumina ball due to much higher hardness of the counterpart than the matrix leading the weathering of the composite hence increasing the wear rate.

7.3. 1D and 2D Nanomaterials Reinforced Glass Composites

According to the results, we can conclude that 2D nanomaterial (BNNS) act as a better mechanical reinforcement in comparison to 1D nanomaterials (BNNT) due to larger surface area interacting with the matrix.

This is confirmed by nearly 45% increase in fracture toughness of 5 wt% BNNS reinforced glass composite in comparison to nearly 30% increase observed by reinforcing the same concentration of BNNTs in BS glass matrix. 2D reinforcement render their advantages along two dimensions, i.e. length and width while the 1D reinforcement only influence the properties of the composite along the length of the reinforcement.

We can also observe that the change in the Young's modulus though very less but comparatively is more in BNNT reinforced BS composite than BNNS reinforced BS composite as both the reinforcements though providing high bonding with the interface yet the interaction surface for 2D reinforcements is much more than for 1D reinforcements.

Therefore, due to these properties we confirm that 2D reinforcements act as more efficient reinforcement for the toughening of composites in comparison to 1D reinforcements.

Chapter 8- Future Work

BS-BNNT composites and BS-BNNS composites have shown promising results in comparison to much used CNT and graphene based glass composites as mentioned in the above sections. However, there is still a large scope for further investigations in these composites. Some of the future works that can be done in these fields are:

1. Effect of reinforcing higher concentrations of BNNTs and BNNSs in BS glass could be studied to find out the critical concentration up till which we can achieve the maximum improvement in the properties after which the properties start to deteriorate due to excessive agglomeration of BNNTs.

2. The quality and aspect ratio of BNNSs produced is an important factor governing the properties of the composites therefore preparation of high quality BNNSs is a critical task. More methods can be employed to prepare the BNNSs with lower thickness and more length. Additionally, investigation of composites reinforced with different aspect ratio of reinforcements (BNNS and BNNT) could be carried to study their effects on the properties of the composites. Similar studies have been carried out on graphene reinforced alumina composites[157].

3. Interfacial bonding between the reinforcements and the matrix plays a crucial role for the effective load transfer from the matrix to the reinforcements therefore functionalization of the BNNTs could be carried out in order enhance the interface bonding and increase in the mechanical properties of the composite.

4. Toughening mechanisms like crack deflection, pull-out, crack bridging etc. were observed in the matrix however individual quantification of effect of any particular toughening mechanism could be carried out using the methods proposed in the literature. Such quantifications have been reported for CNTs reinforced glasses[6] and BNNTs reinforced ceramics[79].

5. Testing of the wear properties of the BNNT and BNNS reinforced glass composites can be carried out in detail to find its applicability in various engineering applications. It is expected that these reinforcement would provide lubrication to the surface of the composites leading to decrease in the wear of the composites.

6. Thermal properties of the composites could be studied in order to use the composites for high temperature application. Also, the mechanical properties like fracture toughness and flexural strength can be carried out at higher temperatures to study the effect of temperature on the mechanical properties of the composites.

7. Since BNNTs and BNNSs are chemically inert, the effect of the chemical environment on the properties of the composites could be studied by studying the effect of acids, saline water, extreme conditions etc. on the mechanical properties of the composites.

8. BNNT and BNNS are highly insulation with a bandgap of 5-6 eV therefore effect of reinforcing different concentrations of these reinforcements on the electrical properties of the composites can be studied. With higher electrical properties these composites could be used electrical shielding applications.

9. Detailed analysis of the properties of BNNS reinforced composites could be carried out in direction parallel and perpendicular to the applied force during sintering. However, methods of achieve anisotropy in the BNNT reinforced BS composites could be carried out to observe any increase in the properties in one direction compared to isotropic samples.

10. Comparison of these reinforcements by incorporating them in more of glass and ceramic matrices with the present samples could be an interesting investigation. Moreover, hybrid composites are gaining limelight these days therefore hybrid composites by introducing two different kinds of reinforcements like BNNS and

graphene or BNNTs and CNTs rendering multifunctional properties to composites could be produced and examined.

References

1. Weiner, S.; Wagner, H. D., The material bone: Structure mechanical function relations. *Annual Review of Materials Science* **1998,** *28*, 271-298.
2. Park, S.; Seo, M. K., *Interface Science and Composites*. Elsevier Academic Press: **2011**.
3. Chawla K.K., , *Composite Materials: Science and Engineering*. Springer New York: **2012**.
4. Koichi, N., New design concept of structural ceramics—Ceramic nanocomposites. *The Centennial Memorial Issue of The Ceramic Society of Japan* **1991,** *99* (10), 974-982.
5. Porwal, H.; Kasiarova, M.; Tatarko, P.; Grasso, S.; Dusza, J.; Reece, M. J., Scratch behaviour of graphene alumina nanocomposites. *Advances in Applied Ceramics* **2015,** *114* (sup1), S34-S41.
6. Cho, J.; Inam, F.; Reece, M. J.; Chlup, Z.; Dlouhy, I.; Shaffer, M. S. P.; Boccaccini, A. R., Carbon nanotubes: do they toughen brittle matrices? *Journal of Materials Science* **2011,** *46* (14), 4770-4779.
7. Porwal, H.; Tatarko, P.; Grasso, S.; Khaliq, J.; Dlouhy, I.; Reece, M. J., Graphene reinforced alumina nano-composites. *Carbon* **2013,** *64*, 359-369.
8. Bansal, N. P.; Hurst, J. B.; Choi, S. R., Boron Nitride Nanotubes-Reinforced Glass Composites. *Journal of the American Ceramic Society* **2006,** *89* (1), 388-390.
9. Bernardo, E.; Nicolais, L., Glass Matrix Composite. In *Wiley Encyclopedia of Composites*, John Wiley & Sons, Inc.: **2011**.
10. Donald, I. W. In *Preparation, properties and applications of glass and glass-ceramic matrix composites*, **1995**; Trans Tech Publ: pp 123-144.
11. Fibre reinforcements. In *Fundamentals of Fibre Reinforced Composite Materials*, Taylor & Francis: **2005**; pp 19-81.
12. Brennan, J. J.; Nutt, S. R., SiC-Whisker-Reinforced Glass-Ceramic Composites: Interfaces and Properties. *Journal of the American Ceramic Society* **1992,** *75* (5), 1205-1216.
13. Moya, J. S., Layered ceramics. *Advanced Materials* **1995,** *7* (2), 185-189.
14. Porwal, H.; Tatarko, P.; Grasso, S.; Hu, C.; Boccaccini, A. R.; Dlouhy, I.; Reece, M. J., Toughened and machinable glass matrix composites reinforced with graphene and graphene-oxide nano platelets. *Science and Technology of Advanced Materials* **2013,** *14* (5), 1-10.
15. Crivelli-Visconti, I.; Cooper, G. A., Mechanical Properties of a New Carbon Fibre Material. *Nature* **1969,** *221* (5182), 754-755.
16. Sambell R. A. J., B. A., Phillips D. C., Bowen D.H., Carbon fibre composites with ceramic and glass matrices *Journal of Materials Science* **1972,** (7), 676-681.
17. Low, I. M., Ceramic Matrix Composites - Microstructure, Properties and Applications. Woodhead Publishing.**2006**
18. Boccaccini, A. R.; Kern, H.; Dlouhy, I., Determining the fracture resistance of fibre-reinforced glass matrix composites by means of the chevron-notch flexural technique. *Materials Science and Engineering: A* **2001,** *308* (1–2), 111-117.
19. Boccaccini, A. R., Glass and Glass-Ceramic Matrix Composite Materials. *Journal of the Ceramic Society of Japan* **2001,** *109* (1271), S99-S109.
20. Evans A. G., Zok F. W., Review The physics and mechanics of fibre-reinforced brittle matrix composites. *Journal of materials science* **1994,** (29), 3857-3896.

21. Brennan, J. J.; Prewo, K. M., Silicon carbide fibre reinforced glass-ceramic matrix composites exhibiting high strength and toughness. *Journal of Materials Science* **1982,** *17* (8), 2371-2383.
22. Dlouhý, I.; Chlup, Z.; Atiq, S.; Boccaccini, A. R., Fracture Resistance of Hybrid Glass Matrix Composite and Its Degradation Due to Thermal Ageing and Thermal Shock. In *Fracture Mechanics of Ceramics: Active Materials, Nanoscale Materials, Composites, Glass and Fundamentals*, Bradt, R. C.; Munz, D.; Sakai, M.; White, K. W., Eds. Springer US: Boston, MA, **2005**; pp 263-274.
23. Xu, H. H.; Eichmiller, F. C.; Antonucci, J. M.; Schumacher, G. E.; Ives, L. K., Dental resin composites containing ceramic whiskers and precured glass ionomer particles. *Dent Mater* **2000,** *16* (5), 356-363.
24. Chawla, N.; Chawla, K. K.; Koopman, M.; Patel, B.; Coffin, C.; Eldridge, J. I., Thermal-shock behavior of a Nicalon-fiber-reinforced hybrid glass-ceramic composite. *Composites Science and Technology* **2001,** *61* (13), 1923-1930.
25. Rouxel, T.; Lavelle, C.; Garnier, C.; Verdier, P.; Laurent, Y., Mechanical evaluation of SiC particle reinforced oxynitride glass and glass-ceramic composites. *Scripta Metallurgica et Materialia* **1994,** *31* (1), 15-20.
26. Hasselman, D. P. H.; Zdaniewski, W. A.; Swearengen, J. C.; Beauchamp, E. K., Effect of alumina dispersions on the thermal conductivity/diffusivity and thermal stress resistance of a borosilicate glass. *Journal of Materials Science* **1980,** *15* (2), 518-520.
27. Rawlings, R. D., Glass-ceramic matrix composites. *Composites* **1994,** *25* (5), 372-379.
28. Zhang, X.; Wang, Y.; Lu, J.; Zang, J.; Zhang, J.; Ge, E., Wettability and reactivity in diamond–borosilicate glass system. *International Journal of Refractory Metals and Hard Materials* **2010,** *28* (2), 260-264.
29. Kotoul, M.; Pokluda, J.; Šandera, P.; Dlouhý, I.; Chlup, Z.; Boccaccini, A. R., Toughening effects quantification in glass matrix composite reinforced by alumina platelets. *Acta Materialia* **2008,** *56* (12), 2908-2918.
30. Skorokhod, V. V., Layered Composites: Structural Classification, Thermophysical and Mechanical Properties. *Powder Metallurgy and Metal Ceramics* **2003,** *42* (9), 437-446.
31. Bansal, N. P., *Handbook of ceramic composites*. Springer: **2006**; Vol. 200.
32. Bennison, S. J.; Jagota, A.; Smith, C. A., Fracture of Glass/Poly(vinyl butyral) (Butacite®) Laminates in Biaxial Flexure. *Journal of the American Ceramic Society* **1999,** *82* (7), 1761-1770.
33. Seal, A.; Dalui, S. K.; Mukhopadhyay, A. K.; Phani, K. K.; Maiti, H. S., Mechanical behavior of glass polymer multilayer composites. *Journal of Materials Science* **2003,** *38* (5), 1063-1071.
34. Clupper, D. C.; Mecholsky, J. J., Toughening of tape cast Bioglass® by lamination with stainless steel 316L. *Journal of Materials Science Letters* **2001,** *20* (20), 1885-1888.
35. Clupper, D. C.; Mecholsky, J. J.; LaTorre, G. P.; Greenspan, D. C., Bioactivity of Bioglass®-steel and Bioglass®-titanium laminate composites. *Journal of Materials Science Letters* **2001,** *20* (10), 959-960.
36. Bangali, J.; Rane, S.; Phatak, G.; Gangal, S., Effect of ink organics on cambering of an Ag-metallized low temperature co-fired ceramics (LTCC). *Journal of Materials Science: Materials in Electronics* **2008,** *20* (5), 455-460.

37. Alias, R., 24 - Multilayer glass–ceramic composites for microelectronics: processing and properties A2 - Low, I.M. In *Advances in Ceramic Matrix Composites*, Woodhead Publishing: **2014**; pp 587-610.
38. Leighton, K.; Carberry, J.; Serafin, W.; Avery, T.; Templeton, D., Transparent Armor for the New Standard in Battlefield Performance. In *Advances in Ceramic Armor VII*, John Wiley & Sons, Inc.: **2011**; pp 27-41.
39. Gadkaree, K. P.; Chyung, K. C.; Taylor, M. P., Hybrid ceramic matrix composites. *Journal of Materials Science* **1988,** *23* (10), 3711-3720.
40. Gao, F., Clay/polymer composites: the story. *Materials Today* **2004,** *7* (11), 50-55.
41. Mark, J. E., Ceramic-reinforced polymers and polymer-modified ceramics. *Polymer Engineering & Science* **1996,** *36* (24), 2905-2920.
42. Wen, J.; Wilkes, G. L., Organic/Inorganic Hybrid Network Materials by the Sol−Gel Approach. *Chemistry of Materials* **1996,** *8* (8), 1667-1681.
43. Carroll, L.; Sternitzke, M.; Derby, B., Silicon carbide particle size effects in alumina-based nanocomposites. *Acta Materialia* **1996,** *44* (11), 4543-4552.
44. Galusek, D.; Galusková, D., Alumina Matrix Composites with Non-Oxide Nanoparticle Addition and Enhanced Functionalities. *Nanomaterials* **2015,** *5* (1),115-143.
45. Kamalian, R.; Yazdanpanah, A.; Moztarzadeh, F.; Ravarian, R.; Moztarzadeh, Z.; Tahmasbi, M.; Mozafari, M., Synthesis and characterisation of bioactive glass/forsterite nanocomposites for bone and dental implants. *Ceramics-Silikáty* **2012,** *56* (4), 331-340.
46. Galusek, D.; Sedláček, J.; Riedel, R., Al2O3–SiC composites prepared by warm pressing and sintering of an organosilicon polymer-coated alumina powder. *Journal of the European Ceramic Society* **2007,** *27* (6), 2385-2392.
47. Suzuki, T.; Kawakami, T.; Koyama, T.; Izaki, K.; Nakano, R.; Shitara, T.; Hakkei, K.; Hirai, T.; Niihara, K., Preparation of Fine Silicon Nitride Powders by Vapor Phase Reaction of Nitrogen Containing Organosilicon Compound with Ammonia. *Journal of the Ceramic Association, Japan* **1987,** *95* (1097), 91-95.
48. Mota, J.; Yu, N.; Caridade, S. G.; Luz, G. M.; Gomes, M. E.; Reis, R. L.; Jansen, J. A.; Walboomers, X. F.; Mano, J. F., Chitosan/bioactive glass nanoparticle composite membranes for periodontal regeneration. *Acta Biomaterialia* **2012,** *8* (11), 4173-4180.
49. Mishra, S.; Shimpi, N. G., Effect of the variation in the weight percentage of the loading and the reduction in the nanosizes of CaSO4 on the mechanical and thermal properties of styrene–butadiene rubber. *Journal of Applied Polymer Science* **2007,** *104* (3), 2018-2026.
50. Scotti, R.; Conzatti, L.; D'Arienzo, M.; Di Credico, B.; Giannini, L.; Hanel, T.; Stagnaro, P.; Susanna, A.; Tadiello, L.; Morazzoni, F., Shape controlled spherical (0D) and rod-like (1D) silica nanoparticles in silica/styrene butadiene rubber nanocomposites: Role of the particle morphology on the filler reinforcing effect. *Polymer* **2014,** *55* (6), 1497-1506.
51. Chu, K.; Kim, D.; Sohn, Y.; Lee, S.; Moon, C.; Park, S., Electrical and Thermal Properties of Carbon-Nanotube Composite for Flexible Electric Heating-Unit Applications. *IEEE Electron Device Letters* **2013,** *34* (5), 668-670.
52. Gojny, F. H.; Wichmann, M. H. G.; Fiedler, B.; Kinloch, I. A.; Bauhofer, W.; Windle, A. H.; Schulte, K., Evaluation and identification of electrical and thermal conduction mechanisms in carbon nanotube/epoxy composites. *Polymer* **2006,** *47* (6), 2036-2045.

53. Boccaccini, A. R.; Thomas, B. J. C.; Brusatin, G.; Colombo, P., Mechanical and electrical properties of hot-pressed borosilicate glass matrix composites containing multi-wall carbon nanotubes. *Journal of Materials Science* **2007,** *42* (6), 2030-2036.
54. Michalek, M.; Bodisova, K.; Michalkova, M.; Sedlacek, J.; Galusek, D., Alumina/MWCNTs composites by aqueous slip casting and pressureless sintering. *Ceramics International* **2013,** *39* (6), 6543-6550.
55. Ye, F.; Liu, L.; Wang, Y.; Zhou, Y.; Peng, B.; Meng, Q., Preparation and mechanical properties of carbon nanotube reinforced barium aluminosilicate glass-ceramic composites. *Scripta Materialia* **2006,** *55* (10), 911-914.
56. Mazaheri, M.; Mari, D.; Hesabi, Z. R.; Schaller, R.; Fantozzi, G., Multi-walled carbon nanotube/nanostructured zirconia composites: Outstanding mechanical properties in a wide range of temperature. *Composites Science and Technology* **2011,** *71* (7), 939-945.
57. Mukhopadhyay, A.; Chu, B. T. T.; Green, M. L. H.; Todd, R. I., Understanding the mechanical reinforcement of uniformly dispersed multiwalled carbon nanotubes in alumino-borosilicate glass ceramic. *Acta Materialia* **2010,** *58* (7), 2685-2697.
58. Fan, J.; Zhao, D.; Wu, M.; Xu, Z.; Song, J., Preparation and Microstructure of Multi-Wall Carbon Nanotubes-Toughened Al2O3 Composite. *Journal of the American Ceramic Society* **2006,** *89* (2), 750-753.
59. Chopra, N. G.; Luyken, R. J.; Cherrey, K.; Crespi, V. H.; Cohen, M. L.; Louie, S. G.; Zettl, A., Boron nitride nanotubes. *Science* **1995,** *269* (5226), 966-967.
60. Paine, R. T.; Narula, C. K., Synthetic routes to boron nitride. *Chemical Reviews* **1990,** *90* (1), 73-91.
61. Ishii, T.; Sato, T.; Sekikawa, Y.; Iwata, M., Growth of whiskers of hexagonal boron nitride. *Journal of Crystal Growth* **1981,** *52*, 285-289.
62. Golberg, D.; Bando, Y.; Tang, C.; Zhi, C., Boron nitride nanotubes. *Advanced Materials* **2007,** *19* (18), 2413-2432.
63. Golberg, D.; Bando, Y.; Huang, Y.; Terao, T.; Mitome, M.; Tang, C.; Zhi, C., Boron Nitride Nanotubes and Nanosheets. *Acs Nano* **2010,** *4* (6), 2979-2993.
64. Blase, X.; Rubio, A.; Louie, S.G.; Cohen M.L., Stability and Band Gap Constancy of Boron Nitride Nanotubes. *EPL (Europhysics Letters)* **1994,** *28* (5), 335-340.
65. Verma, V.; Jindal, V. K.; Dharamvir, K., Elastic moduli of a boron nitride nanotube. *Nanotechnology* **2007,** *18* (43), 1-6.
66. Suryavanshi, A. P.; Yu, M. F.; Wen, J. G.; Tang, C. C.; Bando, Y., Elastic modulus and resonance behavior of boron nitride nanotubes. *Applied Physics Letters* **2004,** *84* (14), 2527-2529.
67. Bettinger, H. F.; Dumitrica, T.; Scuseria, G. E.; Yakobson, B. I., Mechanically induced defects and strength of BN nanotubes. *Physical Review B* **2002,** *65* (4), 041406(1)-041406(4).
68. Boubakeur Essedik Belkerk; Amine Achour; Dongyan Zhang; Salah Sahli; Djouadi M.A.; Yap Y.K., Thermal conductivity of vertically aligned boron nitride nanotubes. *Applied Physics Express* **2016,** *9* (7), 075002 (1)- 075002 (4).
69. Chang, C. W.; Fennimore, A. M.; Afanasiev, A.; Okawa, D.; Ikuno, T.; Garcia, H.; Li, D.; Majumdar, A.; Zettl, A., Isotope Effect on the Thermal Conductivity of Boron Nitride Nanotubes. *Physical Review Letters* **2006,** *97* (8), 085901(1)- 085901(4).

70. Wei, X.; Wang, M.-S.; Bando, Y.; Golberg, D., Tensile Tests on Individual Multi-Walled Boron Nitride Nanotubes. *Advanced Materials* **2010,** *22* (43), 4895-4899.
71. Du, M.; Bi, J.-Q.; Wang, W.-L.; Sun, X.-L.; Long, N.-N., Microstructure and properties of SiO2 matrix reinforced by BN nanotubes and nanoparticles. *Journal of Alloys and Compounds* **2011,** *509* (41), 9996-10002.
72. Nigues, A.; Siria, A.; Vincent, P.; Poncharal, P.; Bocquet, L., Ultrahigh interlayer friction in multiwalled boron nitride nanotubes. *Nature Materials* **2014,** *13* (7), 688-693.
73. Lahiri, D.; Hadjikhani, A.; Zhang, C.; Xing, T.; Li, L. H.; Chen, Y.; Agarwal, A., Boron nitride nanotubes reinforced aluminum composites prepared by spark plasma sintering: Microstructure, mechanical properties and deformation behavior. *Materials Science and Engineering a-Structural Materials Properties Microstructure and Processing* **2013,** *574*, 149-156.
74. Wang, X.-B.; Weng, Q.; Wang, X.; Li, X.; Zhang, J.; Liu, F.; Jiang, X.-F.; Guo, H.; Xu, N.; Golberg, D.; Bando, Y., Biomass-Directed Synthesis of 20 g High-Quality Boron Nitride Nanosheets for Thermoconductive Polymeric Composites. *Acs Nano* **2014,** *8* (9), 9081-9088.
75. Zhi, C. Y.; Bando, Y.; Wang, W. L.; Tang, C. C.; Kuwahara, H.; Golberg, D., Mechanical and Thermal Properties of Polymethyl Methacrylate-BN Nanotube Composites. *Journal of Nanomaterials* **2008,** 642036(1)- 642036(5).
76. Lahiri, D.; Singh, V.; Benaduce, A. P.; Seal, S.; Kos, L.; Agarwal, A., Boron nitride nanotube reinforced hydroxyapatite composite: Mechanical and tribological performance and in-vitro biocompatibility to osteoblasts. *Journal of the Mechanical Behavior of Biomedical Materials* **2011,** *4* (1), 44-56.
77. Tatarko, P.; Grasso, S.; Porwal, H.; Chlup, Z.; Saggar, R.; Dlouhy, I.; Reece, M. J., Boron nitride nanotubes as a reinforcement for brittle matrices. *Journal of the European Ceramic Society* **2014,** *34* (14), 3339-3349.
78. Du, M.; Bi, J.-Q.; Wang, W.-L.; Sun, X.-L.; Long, N.-N., Influence of sintering temperature on microstructure and properties of SiO2 ceramic incorporated with boron nitride nanotubes. *Materials Science and Engineering a-Structural Materials Properties Microstructure and Processing* **2012,** *543*, 271-276.
79. Tatarko, P.; Grasso, S.; Chlup, Z.; Porwal, H.; Kasiarova, M.; Dlouhy, I.; Reece, M. J., Toughening effect of multi-walled boron nitride nanotubes and their influence on the sintering behaviour of 3Y-TZP zirconia ceramics. *Journal of the European Ceramic Society* **2014,** *34* (7), 1829-1843.
80. Yu, H.-H.; Wang, S.-R.; Yang, L.-Y., R-Curve Behavior of Si3N4/BNNT Composites. *Applied Composite Materials* **2013,** *20* (5), 947-960.
81. Xu, J.-J.; Bai, Y.-J.; Wang, W.-L.; Wang, S.-R.; Han, F.-D.; Qi, Y.-X.; Bi, J.-Q., Toughening and reinforcing zirconia ceramics by introducing boron nitride nanotubes. *Materials Science and Engineering a-Structural Materials Properties Microstructure and Processing* **2012,** *546*, 301-306.
82. Hofmann, U.; Endell, K.; Wilm, D., Kristallstruktur und Quellung von Montmorillonit. In *Zeitschrift für Kristallographie - Crystalline Materials*, **1933**; Vol. 86, 340-348.
83. Kojima, Y.; Usuki, A.; Kawasumi, M.; Okada, A.; Kurauchi, T.; Kamigaito, O., One-pot synthesis of nylon 6–clay hybrid. *Journal of Polymer Science Part A: Polymer Chemistry* **1993,** *31* (7), 1755-1758.

84. Liu, M.-Y.; Zhu, H.-G.; Siddiqui, N. A.; Leung, C. K. Y.; Kim, J.-K., Glass fibers with clay nanocomposite coating: Improved barrier resistance in alkaline environment. *Composites Part A: Applied Science and Manufacturing* **2011,** *42* (12), 2051-2059.
85. Vaia, R. A.; Vasudevan, S.; Krawiec, W.; Scanlon, L. G.; Giannelis, E. P., New polymer electrolyte nanocomposites: Melt intercalation of poly(ethylene oxide) in mica-type silicates. *Advanced Materials* **1995,** *7* (2), 154-156.
86. Novoselov, K. S.; Geim, A. K.; Morozov, S. V.; Jiang, D.; Zhang, Y.; Dubonos, S. V.; Grigorieva, I. V.; Firsov, A. A., Electric field effect in atomically thin carbon films. *Science* **2004,** *306* (5696), 666-669.
87. Porwal, H.; Grasso, S.; Reece, M. J., Review of graphene-ceramic matrix composites. *Advances in Applied Ceramics* **2013,** *112* (8), 443-454.
88. Geim, A. K.; Novoselov, K. S., The rise of graphene. *Nat Mater* **2007,** *6* (3), 183-191.
89. Fan, Y.; Wang, L.; Li, J.; Li, J.; Sun, S.; Chen, F.; Chen, L.; Jiang, W., Preparation and electrical properties of graphene nanosheet/Al2O3 composites. *Carbon* **2010,** *48* (6), 1743-1749.
90. He, T.; Li, J.; Wang, L.; Zhu, J.; Jiang, W., Preparation and Consolidation of Alumina/Graphene Composite Powders. *Materials Transactions* **2009,** *50* (4), 749-751.
91. Du, J.; Cheng, H.-M., The Fabrication, Properties, and Uses of Graphene/Polymer Composites. *Macromolecular Chemistry and Physics* **2012,** *213* (10-11), 1060-1077.
92. Watcharotone, S.; Dikin, D. A.; Stankovich, S.; Piner, R.; Jung, I.; Dommett, G. H. B.; Evmenenko, G.; Wu, S.-E.; Chen, S.-F.; Liu, C.-P.; Nguyen, S. T.; Ruoff, R. S., Graphene−Silica Composite Thin Films as Transparent Conductors. *Nano Letters* **2007,** *7* (7), 1888-1892.
93. Walker, L. S.; Marotto, V. R.; Rafiee, M. A.; Koratkar, N.; Corral, E. L., Toughening in Graphene Ceramic Composites. *ACS Nano* **2011,** *5* (4), 3182-3190.
94. Gao, C.; Liu, T.; Shuai, C.; Peng, S., Enhancement mechanisms of graphene in nano-58S bioactive glass scaffold: mechanical and biological performance. *Scientific Reports* **2014,** *4*,4712(1)-4712(10).
95. Lin, Y.; Connell, J. W., Advances in 2D boron nitride nanostructures: nanosheets, nanoribbons, nanomeshes, and hybrids with graphene. *Nanoscale* **2012,** *4* (22), 6908-6939.
96. Nag, A.; Raidongia, K.; Hembram, K. P. S. S.; Datta, R.; Waghmare, U. V.; Rao, C. N. R., Graphene Analogues of BN: Novel Synthesis and Properties. *Acs Nano* **2010,** *4* (3), 1539-1544.
97. Tiano, A. L.; Park, C.; Lee, J. W.; Luong, H. H.; Gibbons, L. J.; Chu, S.-H.; Applin, S. I.; Gnoffo, P.; Lowther, S.; Kim, H. J.; Danehy, P. M.; Inman, J. A.; Jones, S. B.; Kang, J. H.; Sauti, G.; Thibeault, S. A.; Yamakov, V.; Wise, K. E.; Su, J.; Fay, C. C. In *Boron Nitride Nanotube: Synthesis and Applications*, Conference on Nanosensors, Biosensors, and Info-Tech Sensors and Systems, San Diego, CA, **2014**
98. Zhi, C.; Bando, Y.; Tang, C.; Kuwahara, H.; Golberg, D., Large-Scale Fabrication of Boron Nitride Nanosheets and Their Utilization in Polymeric Composites with Improved Thermal and Mechanical Properties. *Advanced Materials* **2009,** *21* (28), 2889-2893.
99. Khan, U.; May, P.; O'Neill, A.; Bell, A. P.; Boussac, E.; Martin, A.; Semple, J.; Coleman, J. N., Polymer reinforcement using liquid-exfoliated boron nitride nanosheets. *Nanoscale* **2013,** *5* (2), 581-587.

100. Chun Li and Yoshio Bando and Chunyi Zhi and Yang Huang and Dmitri, G., Thickness-dependent bending modulus of hexagonal boron nitride nanosheets. *Nanotechnology* **2009,** *20* (38), 385707.
101. Lee, B.; Lee, D.; Lee, J. H.; Ryu, H. J.; Hong, S. H., Enhancement of toughness and wear resistance in boron nitride nanoplatelet (BNNP) reinforced Si3N4 nanocomposites. *Scientific Reports* **2016,** *6*, 27609(1)-27609(12).
102. Inam, F.; Yan, H.; Peijs, T.; Reece, M. J., The sintering and grain growth behaviour of ceramic–carbon nanotube nanocomposites. *Composites Science and Technology* **2010,** *70* (6), 947-952.
103. Reed, J. S., *Principles of Ceramics Processing*. 2nd ed.; John Wiley & Sons: New York, **1995**.
104. George Y. Onoda , L. L. H., *Ceramic Processing before Firing*. John Wiley & Sons: New York, **1978**.
105. Dusza, J.; Blugan, G.; Morgiel, J.; Kuebler, J.; Inam, F.; Peijs, T.; Reece, M. J.; Puchy, V., Hot pressed and spark plasma sintered zirconia/carbon nanofiber composites. *Journal of the European Ceramic Society* **2009,** *29* (15), 3177-3184.
106. Balázsi, C.; Shen, Z.; Kónya, Z.; Kasztovszky, Z.; Wéber, F.; Vértesy, Z.; Biró, L. P.; Kiricsi, I.; Arató, P., Processing of carbon nanotube reinforced silicon nitride composites by spark plasma sintering. *Composites Science and Technology* **2005,** *65* (5), 727-733.
107. Guo, S.; Sivakumar, R.; Kitazawa, H.; Kagawa, Y., Electrical Properties of Silica-Based Nanocomposites with Multiwall Carbon Nanotubes. *Journal of the American Ceramic Society* **2007,** *90* (5), 1667-1670.
108. Tapasztó, O.; Tapasztó, L.; Markó, M.; Kern, F.; Gadow, R.; Balázsi, C., Dispersion patterns of graphene and carbon nanotubes in ceramic matrix composites. *Chemical Physics Letters* **2011,** *511* (4–6), 340-343.
109. Moreno, R., Colloidal processing of ceramics and composites. *Advances in Applied Ceramics* **2012,** *111* (5-6), 246-253.
110. Gomes, C. M.; Rambo, C. R.; De Oliveira, A. P. N.; Hotza, D.; Gouvêa, D.; Travitzky, N.; Greil, P., Colloidal Processing of Glass–Ceramics for Laminated Object Manufacturing. *Journal of the American Ceramic Society* **2009,** *92* (6), 1186-1191.
111. Gong, X.; Liu, J.; Baskaran, S.; Voise, R. D.; Young, J. S., Surfactant-Assisted Processing of Carbon Nanotube/Polymer Composites. *Chemistry of Materials* **2000,** *12* (4), 1049-1052.
112. Poyato, R.; Vasiliev, A. L.; Padture, N. P.; Tanaka, H.; Nishimura, T., Aqueous colloidal processing of single-wall carbon nanotubes and their composites with ceramics. *Nanotechnology* **2006,** *17* (6), 1770-1777.
113. Wang, K.; Wang, Y.; Fan, Z.; Yan, J.; Wei, T., Preparation of graphene nanosheet/alumina composites by spark plasma sintering. *Materials Research Bulletin* **2011,** *46* (2), 315-318.
114. Dunn, B.; Zink, J. I., Molecules in glass: probes, ordered assemblies, and functional materials. *Acc Chem Res* **2007,** *40* (9), 747-755.
115. Zhou, J. C.; Chuang, M. H.; Lan, E. H.; Dunn, B.; Gillman, P. L.; Smith, S. M., Immunoassays for cortisol using antibody-doped sol-gel silica. *Journal of Materials Chemistry* **2004,** *14* (14), 2311-2316.

116. Lim, J.; Malati, P.; Bonet, F.; Dunn, B., Nanostructured Sol-Gel Electrodes for Biofuel Cells. *Journal of The Electrochemical Society* **2007,** *154* (2), A140-A145.
117. Hongbing, Z.; Wenzhe, C.; Minquan, W.; Zhengchan; Chunlin, Z., Optical limiting effects of multi-walled carbon nanotubes suspension and silica xerogel composite. *Chemical Physics Letters* **2003,** *382* (3–4), 313-317.
118. Cheng, W.-Y.; Wang, C.-C.; Lu, S.-Y., Graphene aerogels as a highly efficient counter electrode material for dye-sensitized solar cells. *Carbon* **2013,** *54*, 291-299.
119. Bechelany, M.; Bernard, S.; Brioude, A.; Cornu, D.; Stadelmann, P.; Charcosset, C.; Fiaty, K.; Miele, P., Synthesis of Boron Nitride Nanotubes by a Template-Assisted Polymer Thermolysis Process. *The Journal of Physical Chemistry C* **2007,** *111* (36), 13378-13384.
120. Ji, F.; Li, Y.-L.; Feng, J.-M.; Su, D.; Wen, Y.-Y.; Feng, Y.; Hou, F., Electrochemical performance of graphene nanosheets and ceramic composites as anodes for lithium batteries. *Journal of Materials Chemistry* **2009,** *19* (47), 9063-9067.
121. Walker, R. F., Mechanism of Material Transport During Sintering. *Journal of the American Ceramic Society* **1955,** *38* (6), 187-197.
122. Inam, F.; Yan, H.; Reece, M. J.; Peijs, T., Structural and chemical stability of multiwall carbon nanotubes in sintered ceramic nanocomposite. *Advances in Applied Ceramics* **2010,** *109* (4), 240-247.
123. Lin Hwang, G.; Chu Hwang, K., Carbon nanotube reinforced ceramics. *Journal of Materials Chemistry* **2001,** *11* (6), 1722-1725.
124. Chen, I. W.; Wang, X. H., Sintering dense nanocrystalline ceramics without final-stage grain growth. *Nature* **2000,** *404* (6774), 168-171.
125. Maca, K.; Pouchly, V.; Zalud, P., Two-Step Sintering of oxide ceramics with various crystal structures. *Journal of the European Ceramic Society* **2010,** *30* (2), 583-589.
126. Karel, M., Microstructure evolution during pressureless sintering of
bulk oxide ceramics. *Processing and Application of Ceramics* **2009,** *3* (1-2), 13–17.
127. Mazaheri, M.; Valefi, M.; Hesabi, Z. R.; Sadrnezhaad, S. K., Two-step sintering of nanocrystalline 8Y2O3 stabilized ZrO2 synthesized by glycine nitrate process. *Ceramics International* **2009,** *35* (1), 13-20.
128. Bodišová, K.; Galusek, D.; Švančárek, P.; Pouchlý, V.; Maca, K., Grain growth suppression in alumina via doping and two-step sintering. *Ceramics International* **2015,** *41* (9, Part B), 11975-11983.
129. Boccaccini, A. R.; Acevedo, D. R.; Brusatin, G.; Colombo, P., Borosilicate glass matrix composites containing multi-wall carbon nanotubes. *Journal of the European Ceramic Society* **2005,** *25* (9), 1515-1523.
130. Hu, C.; Li, F.; Qu, D.; Wang, Q.; Xie, R.; Zhang, H.; Peng, S.; Bao, Y.; Zhou, Y., 8 - Developments in hot pressing (HP) and hot isostatic pressing (HIP) of ceramic matrix composites A2 - Low, I.M. In *Advances in Ceramic Matrix Composites*, Woodhead Publishing: **2014**; 164-189.
131. Bordia, R. K.; Camacho-Montes, H., Sintering: Fundamentals and Practice. In *Ceramics and Composites Processing Methods*, John Wiley & Sons, Inc.: **2012**; 1-42.
132. Li, J.; Liao, H.; Hermansson, L., Sintering of partially-stabilized zirconia and partially-stabilized zirconia—hydroxyapatite composites by hot isostatic pressing and pressureless sintering. *Biomaterials* **1996,** *17* (18), 1787-1790.

133. Grasso, S.; Yoshida, H.; Porwal, H.; Sakka, Y.; Reece, M., Highly transparent α-alumina obtained by low cost high pressure SPS. *Ceramics International* **2013,** *39* (3), 3243-3248.
134. Centeno, A.; Rocha, V. G.; Alonso, B.; Fernández, A.; Gutierrez-Gonzalez, C. F.; Torrecillas, R.; Zurutuza, A., Graphene for tough and electroconductive alumina ceramics. *Journal of the European Ceramic Society* **2013,** *33* (15–16), 3201-3210.
135. Oghbaei, M.; Mirzaee, O., Microwave versus conventional sintering: A review of fundamentals, advantages and applications. *Journal of Alloys and Compounds* **2010,** *494* (1–2), 175-189.
136. Ma, Z.; Liu, Y., Sintering of Ceramics-New Emerging Techniques ed A. *Lakshmanan (Rijeka, Croatia: In Tech) chapter* **2012,** *21*.
137. Menezes, R. R.; Kiminami, R. H. G. A., Microwave sintering of alumina–zirconia nanocomposites. *Journal of Materials Processing Technology* **2008,** *203* (1–3), 513-517.
138. Clark, D. E.; Sutton, W. H., Microwave Processing of Materials. *Annual Review of Materials Science* **1996,** *26* (1), 299-331.
139. Wang, J.; Zhang, L.; Zhao, G.; Gu, Y.; Zhang, Z.; Zhang, F.; Wang, W., Selective synthesis of boron nitride nanotubes by self-propagation high-temperature synthesis and annealing process. *Journal of Solid State Chemistry* **2011,** *184* (9), 2478-2484.
140. Anstis, G. R.; Chantikul, P.; Lawn, B. R.; Marshall, D. B., A Critical Evaluation of Indentation Techniques for Measuring Fracture Toughness: I, Direct Crack Measurements. *Journal of the American Ceramic Society* **1981,** *64* (9), 533-538.
141. Dlouhy, I.; Reinisch, M.; Boccaccini, A. R.; Knott, J. F., Fracture Characteristics of borosilicate glasses reinforced by metallic particles. *Fatigue & Fracture of Engineering Materials & Structures* **1997,** *20* (9), 1235-1253.
142. Boccaccini, A. R.; Rawlings, R. D.; Dlouhý, I., Reliability of the chevron-notch technique for fracture toughness determination in glass. *Materials Science and Engineering: A* **2003,** *347* (1–2), 102-108.
143. Bluhm, J. I., Slice synthesis of a three dimensional "work of fracture" specimen. *Engineering Fracture Mechanics* **1975,** *7* (3), 593-604.
144. de la Cruz, E. F.; Zheng, Y.; Torres, E.; Li, W.; Song, W.; Burugapalli, K., Zeta potential of modified multi-walled carbon nanotubes in presence of poly (vinyl alcohol) hydrogel. **2012**, *7*, 3577-3590.
145. Rabiei, A.; Murakami, T.; Akagi, T.; Kasai, E., 8th International Conference on Porous Metals and Metallic FoamsDevelopment of Porous Iron based Material by Slag Foaming and its Reduction. *Procedia Materials Science* **2014,** *4*, 27-32.
146. Ning, J. W.; Zhang, J. J.; Pan, Y. B.; Guo, J. K., Fabrication and mechanical properties of SiO2 matrix composites reinforced by carbon nanotube. *Materials Science and Engineering a-Structural Materials Properties Microstructure and Processing* **2003,** *357* (1-2), 392-396.
147. Le Houérou, V.; Sangleboeuf, J. C.; Dériano, S.; Rouxel, T.; Duisit, G., Surface damage of soda–lime–silica glasses: indentation scratch behavior. *Journal of Non-Crystalline Solids* **2003,** *316* (1), 54-63.
148. Khan, U.; Porwal, H.; O'Neill, A.; Nawaz, K.; May, P.; Coleman, J. N., Solvent-exfoliated graphene at extremely high concentration. *Langmuir* **2011,** *27* (15), 9077-9082.

149. Khan, U.; O'Neill, A.; Porwal, H.; May, P.; Nawaz, K.; Coleman, J. N., Size selection of dispersed, exfoliated graphene flakes by controlled centrifugation. *Carbon* **2012,** *50* (2), 470-475.
150. Jankovic, A., Variables affecting the fine grinding of minerals using stirred mills. *Minerals Engineering* **2003,** *16* (4), 337-345.
151. Haar, S.; El Gemayel, M.; Shin, Y.; Melinte, G.; Squillaci, M. A.; Ersen, O.; Casiraghi, C.; Ciesielski, A.; Samorì, P., Enhancing the Liquid-Phase Exfoliation of Graphene in Organic Solvents upon Addition of n-Octylbenzene. *Scientific Reports* **2015,** *5*, 16684(1)-16684(9).
152. Thomas, B. J. C.; Shaffer, M. S. P.; Boccaccini, A. R., Sol-gel route to carbon nanotube borosilicate glass composites. *Composites Part a-Applied Science and Manufacturing* **2009,** *40* (6-7), 837-845.
153. Yates, B.; Overy, M. J.; Pirgon, O., The anisotropic thermal expansion of boron nitride. *Philosophical Magazine* **1975,** *32* (4), 847-857.
154. Kovalčíková, A.; Kurek, P.; Balko, J.; Dusza, J.; Šajgalík, P.; Mihaliková, M., Effect of the counterpart material on wear characteristics of silicon carbide ceramics. *International Journal of Refractory Metals and Hard Materials* **2014,** *44*, 12-18.
155. Ghosh, S.; Ghosh, A.; Das, S.; Kar, T.; Das, P. K.; Banerjee, R., Enhanced mechanical properties of single walled carbon nanotube-borosilicate glass composite due to cushioning effect and localized plastic flow. *AIP Advances* **2011,** *1* (4), 042133(1)-042133(5).
156. Pakdel, A.; Zhi, C.; Bando, Y.; Golberg, D., Low-dimensional boron nitride nanomaterials. *Materials Today* **2012,** *15* (6), 256-265.
157. Porwal, H.; Saggar, R.; Tatarko, P.; Grasso, S.; Saunders, T.; Dlouhý, I.; Reece, M. J., Effect of lateral size of graphene nano-sheets on the mechanical properties and machinability of alumina nano-composites. *Ceramics International* **2016,** *42* (6), 7533-7542.

List of Publications

International Conferences

1. **Richa Saggar,** Harshit Porwal, Peter Tatarko, Ivo Dlouhý, Michael J. Reece. Boron Nitride Nanosheets Reinforced Glass Matrix Composites, Material Science Engineering (MSE 2014), September 23 – 25, 2014, Darmstadt, Germany. (Oral)

2. **Richa Saggar,** Harshit Porwal, Peter Tatarko, Ivo Dlouhý, Michael J. Reece. Boron Nitride Nanosheets Reinforced Glass Matrix Composites, Material Science and Technology 2014 (MS&T'14), October 12 – 16, 2014, Pittsburgh, PA, USA. (Oral)

3. **Richa Saggar,** Harshit Porwal, Peter Tatarko, Ivo Dlouhý, Michael J. Reece. Boron Nitride Nanosheets Reinforced Glass Matrix Composites, 17th International Conference on the Strength of Materials (ICSMA 17), August 9 – 14, 2015, Brno, Czech Republic. (Poster)

Journals

1. **Saggar R**., Porwal H., Tatarko P., Dlouhý I., Reece M.J., Boron Nitride Nanosheets Reinforced Amorphous Glass Composite, Advances in applied ceramics 2015, 115 (S1), S26-S33.

2. Tatarko, P.; Grasso, S.; Porwal, H.; Chlup, Z.; **Saggar, R**.; Dlouhy, I.; Reece, M.J., Boron nitride nanotubes as a reinforcement for brittle matrices. Journal of the European Ceramic Society 2014, 34 (14), 3339-3349.

3. Porwal H., Tatarko P., **Saggar R**., Grasso S., Mani M.K. , Dlouhý I. , Dusza J, Reece M.J., Tribological properties of silica–graphene nano-platelet composites, Ceramics International 2014, 40 (8), 12067–12074

4. Porwal H., **Saggar R.,** Tatarko P., Grasso S., Saunders T., Dlouhý I., Reece M.J., Effect of lateral size of Graphene nanosheets on the mechanical properties and machinability of alumina nanocomposites, Ceramics International 2016, 42(6) 7533-7542